U.PORTO
FACULDADE DE CIÊNCIAS
UNIVERSIDADE DO PORTO

PhD

PhD

3.º CICLO

FCUP
2013

U.PORTO

Statistical studies of planet frequency: understanding planet formation

Annelies Mortier

FC

U.PORTO
FACULDADE DE CIÊNCIAS
UNIVERSIDADE DO PORTO

Statistical studies of planet frequency: understanding planet formation

Annelies Mortier

Tese de Doutoramento apresentada à
Faculdade de Ciências da Universidade do Porto,
Departemento de Física e Astronomia

2013

PhD

PhD

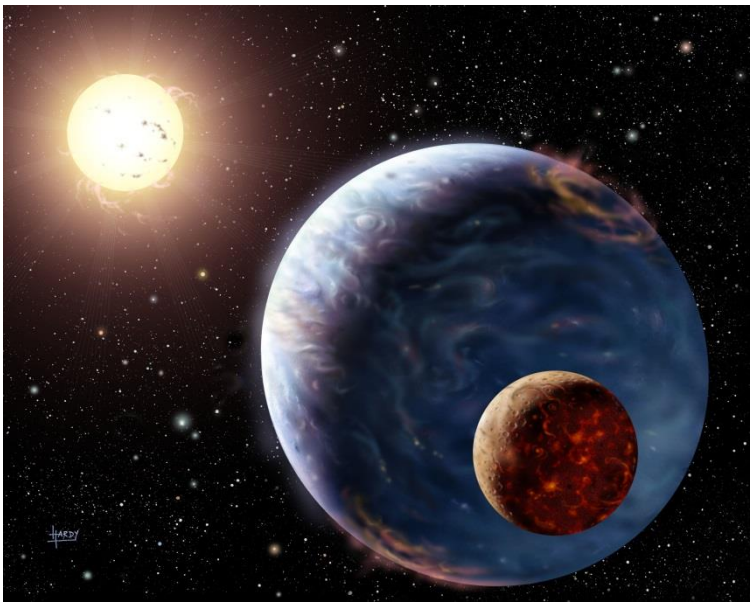

Statistical studies of planet frequency: understanding planet formation

Annelies Mortier
Doutoramento em Astronomia
Departamento de Física e Astronomia
2013

Orientador
Nuno M.C. Santos,
Professor Associado Convidado,
Faculdade de Ciências

Annelies Mortier

Statistical studies of planet frequency: understanding planet formation

Tese submetida á Faculdade de Ciências
da Universidade do Porto para obtencão
do grau de Doutor em Astronomia.

Defesa pública: 20 de dezembro de 2013

O júri de doutoramento:

Presidente:	Prof. José Luis Campos de Oliveira Santos
Orientador:	Doutor Nuno Miguel Cardoso Santos
Outros vogais:	Doutor David Montes Gutierrez
	Doutor Alexandre Carlos Morgado Correira
	Doutor Mário João Pires Fernandes Garcia Monteiro

To everybody out there,

following their dreams.

Non scholae,

sed vitae.

Acknowledgments

This thesis is the result of three beautiful years as a PhD-student in Porto. Writing it would not have been possible without the support, guidance, and help of many people and I would like to take the opportunity here to thank them.

First off, I would like to acknowledge the support of CAUP for giving me the PhD fellowship resulting from the Starting Grant (agreement number 239953) awarded by the European Research Council/European Community under the FP7 to Nuno Santos.

Of course, I owe a great deal of gratitude to my supervisor. Nuno, you have been an amazing supervisor. You have given me more opportunities than I could have dreamed of and really taught me how to be an independent researcher. You were always available and smiling whenever I bursted in your office, patiently answering my never-ending stream of questions and showing me how to be more political in this scientific world.

The planet team in CAUP is an extraordinary fun team to work in. This young and dynamic group of people always made me comfortable to speak my mind and ask for help. Over the years I have worked with most of you and all of you have contributed in making me the researcher that I am today. Sergio, Vardan, and Elisa, I would like to specifically thank you as my unofficial co-supervisors for working with me, teaching me the tricks of the stellar parameter game, helping me on numerous occasions, and also for proof-reading this thesis. I could not have done it without you.

CAUP has been a tremendous place to work in over the past three years. Several office mates have come and gone always making our office a lively place to be in. Diana, Mahmoud, Maria, Lisa, João, Gerasim, Andrew, Carlos, thanks for all the nice moments we had together. Diana, thanks for translating my abstract in Portuguese and for helping me, together with Mahmoud, to bind my thesis. I would also like to thank the administrative people of CAUP, helping me with all sorts of issues I had. Elsa, Paulo, Manuel, Argentina, I'll never forget the big smiles on your faces whenever I just stepped into your office. To everybody in CAUP, a big thank you for making these three years an unforgettable experience.

In our little world of astronomy, collaborations are inevitable. I got the opportunity to work

with several people in different institutes. Thanks to Alessandro, Garik, João, Joanna, Fernando, and everybody else I forget here. To all the people in Chile, thanks for making my observing trips always so smooth, even when the airline lost my luggage. Isa and Ewine, although you were not directly involved in my PhD, I owe you for introducing me to astronomical research and standing by me during my first baby steps.

Living in a foreign country is not always easy, but thanks to some crazy colleagues and friends, I've alway felt at home. Vardan, Mahmoud, Diana & João, Pedro, Maria, Vasco, Elisa, Simon, Barbara, Elsa & Filipe, Arlindo, thanks for dinners, beer, wine, football, dancing. Alexandra, thanks for the amazing desserts at the Christmas dinners, and for the recipe of the perfect chocolate cake.

Finally, I would like to thank my family and friends back home for always supporting me, ook wanneer het niet altijd even makkelijk is door de afstand. Mama en papa, merci om mij altijd de vrijheid en de kansen te geven om mijn eigen weg te gaan in dit leven. Pietertje, uw enthousiasme en wetenschappelijke interesse werken altijd aanstekelijk. En tenslotte, ook een hele dikke merci voor het mooiste sterretje in mijn leven. Hanzj, je maakt het altijd makkelijk wanneer het moeilijk is.

Abstract

In this thesis I present the results of the work done during my PhD. It revolves mainly around the frequency of giant planets as a function of various stellar parameters, like the stellar metallicity and mass. Understanding these correlations and their significance helps in narrowing down the theories of planet formation and evolution.

FGK dwarfs that host giant planets are found to be more metal-rich than stars that are not orbited by a giant planet. Dedicated planet searches are thus performed with metal-poor stars to understand how rare exactly giant planets are around these stars. In Chapter 2, I report on the results of a study of two such metal-poor samples that were searched for planets. By studying the detection limits in the data, I quantified the frequency of giant planets, and in particular hot Jupiters, around these metal-poor stars.

I found that giant planets are indeed rare around metal-poor stars, but that their frequency may be higher than what is expected from a purely exponential relation with metallicity. Chapter 3 reports on the results of a Bayesian study of a large volume-limited planet-search sample of FGK dwarfs. Different functional forms are tested to describe the giant planet frequency around FGK dwarfs. For metal-poor stars both a constant as an exponential dependence is investigated. The possible dependence of mass is also explored. Comparing these models with a Bayesian analysis revealed that none of them was statistically significant or could be ruled out.

Chapter 4 describes the giant planet frequency around evolved stars. An appropriate line list is tested for deriving stellar parameters of evolved stars. With these precise stellar parameters, the giant planet frequency around evolved stars is explored. For giant stars (with $\log g < 3.0$), it appears that there is no dependency on metallicity. Subgiants still show an increasing trend.

The last part of this thesis is about precise and accurate stellar parameters for transit hosts. For transiting planets, the stellar density can be directly derived using the transit light curve. This density will provide an independent measurement of the surface gravity which is not well constrained using spectroscopy. I show that this difference in surface gravity mostly has an effect on the derivation of the stellar, and thus planetary, radius.

Resumo

Nesta tese apresento os resultados do trabalho desenvolvido durante o meu doutoramento. Este trabalho é essencialmente sobre a frequência de planetas gigantes como função de vários parâmetros estelares, tais como a metalicidade e a massa da estrela. A identificação destas correlações assim como a intrepretação do seu significado ajuda a limitar as teorias de formação e evolução estelar.

As estrelas anãs FGK que albergam planetas gigantes são mais ricas em metais do que as que não são orbitadas por um planeta gigante. Assim, têm sido feitas buscas dedicadas a estrelas pobres em metais para compreender exactamente quão raros são os planetas gigantes à volta destas estrelas. No Capítulo 2, apresento os resultados de um estudo sobre duas dessas amostras de estrelas pobres em metais, para as quais se procuraram planetas. Estudando os limites de detecção nos dados, quantifico a frequência de planetas gigantes, em particular de planetas quentes com massa tipo Júpiter que orbitam estas estrelas pobres em metais.

O resultado deste estudo é que os planetas gigantes à volta de estrelas pobres em metais são de facto raros, mas a sua frequência pode ser maior do que se esperaria quando nos baseamos numa relaçao com a metalicidade puramente exponencial. No Capítulo 3 são apresentados os resultados de um estudo Bayesiano sobre uma grande amostra de estrelas añas FGK, limitada em volume, que são usadas para procura de planetas. Várias fórmulas funcionais são testadas para descrever a frequência de planetas gigantes à volta de estrelas anãs FGK. Para estrelas pobres em metais são investigadas tanto uma dependêcia constante como exponencial. É também explorada uma possível dependência da massa. Comparando modelos com uma análise Bayesiana revela que nenhum deles era estatisticamente significante ou que pudesse ser descartado.

O Capítulo 4 descreve a frequência de planetas gigantes à volta de estrelas evoluídas. Uma lista apropriada de riscas espectrais é testada na derivação de parâmetros estelares para estrelas evoluídas. A frequência de planetas gigantes em torno de estrelas evoluídas é explorada a partir destes parâmetros estelares precisos. Para estrelas gigantes (com $\log g < 3.0$), parece não haver uma dependência com a metalicidade. Estelas sub-gigantes ainda apresentam uma tendência crescente.

A última parte desta tese é sobre parâmetros estelares precisos e exactos para estrelas com trânsitos. Quando os planetas transitam as suas estrelas, a densidade estelar pode ser directamente calculada usando a curva de luz do trânsito. Esta densidade irá providenciar uma medida independente da gravidade superficial, que não é bem restringida através da análise espectroscópica. Eu mostro que esta diferença na gravidade superficial têm efeito especialmente no cálculo do raio estelar e, consequentemente, no cálculo do raio do planeta.

Samenvatting

Dit proefschrift bundelt de resultaten van het gedane werk tijdens mijn doctoraat. Het gaat vooral over de frequentie van reuzenplaneten als functie van verschillende stellaire eigenschappen, zoals het metaalgehalte en de massa. Inzicht in deze correlaties en het belang ervan helpen bij het verbeteren van de theorieën van planeetvorming en evolutie.

Dwergsterren met spectraalklasse F,G of K die een reuzenplaneet hebben, blijken metaalrijker te zijn dan dergelijke sterren zonder reuzenplaneet. Er bestaan dus toegewijde missies op zoek naar planeten rond metaalarme sterren om te begrijpen hoe zeldzaam reuzenplaneten precies zijn rond deze sterren. In hoofdstuk 2 rapporteer ik de resultaten van een studie van twee dergelijke missies. Door het bestuderen van de detectielimieten in de data, kon ik de frequentie van reuzenplaneten en in het bijzonder van hete Jupiters rond deze metaalarme sterren bepalen.

Ik vond dat reuzenplaneten inderdaad zeldzaam zijn rond metaalarme sterren, maar ook dat de frequentie hoger zou kunnen zijn dan wat verwacht mag worden van een zuiver exponentiële relatie met metaalsterkte. Hoofdstuk 3 beschrijft de resultaten van een Bayesiaanse studie van een groot volume-beperkt sample van dwergsterren van type F, G, of K waarbij gezocht wordt naar planeten. Verschillende functiebepalingen worden getest om de frequentie van reuzenplaneten rond F, G, of K dwergsterren te omschrijven. Voor metaalarme sterren wordt zowel een constante als een exponentiële relatie onderzocht. Het mogelijke verband met de massa wordt ook bekeken. Door deze functies onderling te vergelijken aan de hand van een Bayesiaanse analyse bleek dat geen van hen statistisch significant is.

Hoofdstuk 4 beschrijft de frequentie van reuzenplaneten rond geëvolueerde sterren. Een adequate lijst van spectraallijnen wordt bekeken om de stellaire eigenschappen van geëvolueerde sterren te bepalen. Met deze precieze stellaire eigenschappen wordt de reuzenplaneet-frequentie rond geëvolueerde sterren onderzocht. Voor rode reuzen (met $\log g < 3.0$) blijkt er geen relatie te zijn met metaalsterkte. Sterren die zich in de fase tussen dwergen en rode reuzen bevinden vertonen nog steeds een positieve correlatie met metaalsterkte.

Het laatste deel van dit proefschrift gaat over juiste en nauwkeurige stellaire eigenschappen

van sterren waarbij een planeet ontdekt is via de transitmethode. Met de data van zo een transit-moment, kan de dichtheid van de ster direct afgeleid worden. Deze dichtheid kan een onafhankelijke bepaling van de zwaartekracht van de ster geven, welke niet goed kan worden afgeleid met behulp van spectrumanalyse. Ik laat zien dat dit verschil in waardes van de zwaartekracht vooral een effect heeft op de berekening van de straal van de ster en dus ook op de straal van de planeet.

Contents

List of Figures

Chapter 1

Introduction

Are we alone? This is a question that mankind has been asking itself for centuries. In modern exoplanet research, the foundations are laid to answering this question. As more and more extrasolar planets are found (see e.g. `www.exoplanet.eu` - Schneider et al. 2011), insight is gained in the mechanisms behind planet formation and evolution. With improving technical abilities, Earth-sized planets start being detected around other stars (e.g. Dumusque et al. 2012) and their planet atmospheres studied (e.g. Swain et al. 2013).

After decades of attempting to detect an extrasolar planet, the first planets were detected in 1992 (Wolszczan & Frail 1992). By measuring the stellar pulses, it was found that the pulsar PSR1257+12 is orbited by at least 2 objects of planetary mass. However, these planets would not be able to contain life as the radiation coming from the pulsar is deadly. Additionally, these planets would be so-called second generation planets, formed after the destruction of the pulsar's progrenitor by a supernova.

In 1995, the very first planet around a solar-type star was detected (Mayor & Queloz 1995). 51Pegb turned out to be a Jovian planet with a minimum mass $M_p = 0.5\,\mathrm{M}_{Jup}$. In contrast to the Solar System planets, 51Pegb was found to orbit very close to its host star ($a = 0.05\,\mathrm{AU}$). This discovery of a *hot Jupiter* came as a surprise. It seemed that the configuration of our Solar System was not the only possibility for planetary systems. Furthermore, it changed planet formation theories. Since massive planets are not expected to form in-situ at close distances from their star (there is not enough building material at close distances), the existence of hot Jupiters was evidence for planet migration theories (Lin et al. 1996).

Since these first discoveries, the search for extrasolar planetary systems accelerated and today, more than 1000 planets have been detected[1], with thousands more candidates from the Kepler mission (Batalha et al. 2013). Extrasolar planets thus appear to be very common in our

[1] for an updated number, see the Extrasolar Planet Encyclopaedia `www.exoplanet.eu` (Schneider et al. 2011)

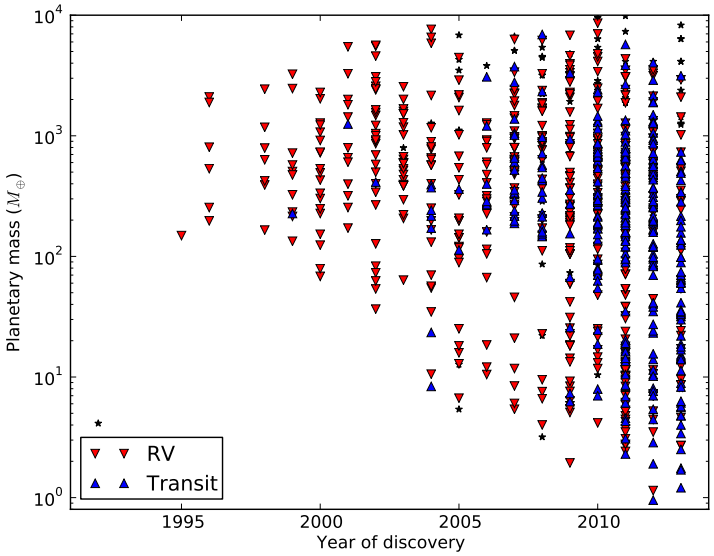

Figure 1.1: Planetary mass (in Earth mass) is plotted versus the year of discovery for all known exoplanets in the Extrasolar Planet Encyclopaedia. Planets detected with the radial velocity technique are plotted by red downward triangles and planets detected with the photometric transit method by blue upward triangles. Planets detected with other methods are denoted with black stars.

Universe. Fig. 1.1 shows the planetary mass (in Earth mass) of all known exoplanets versus the year of discovery. From this figure, it can be seen that the amount of discoveries grows exponentially. Not only are more planets found on a daily basis but also each year, lower mass planets are detected thanks to better equipment and larger data sets.

The variety in planetary properties is also striking. As mentioned before, there is the existence of hot Jupiters such as 51Pegb (Mayor & Queloz 1995), HD189733b (Bouchy et al. 2005), or HAT-P-36b (Bakos et al. 2012). Other surprising discoveries entail very eccentric planets such as HD80606b with $e = 0.93$ (Moutou et al. 2009) or HD43197b with $e = 0.83$ (Naef et al. 2010), circumbinary planets (e.g. Kepler16b, Kepler34b - Pierens & Nelson 2013), planets with extremely low periods such as CoRoT-7b with $P = 0.85$ days (Léger et al. 2009) or 55Cnce with $P = 0.74$ days (Endl et al. 2012), and even evaporating planets (e.g. KIC12557548b - Brogi et al. 2012). By using this huge diversity of different exoplanets, more complex theories of the formation and evolution of planetary systems are formulated.

Paramount to the process of reviewing the models of planet formation and evolution is the information coming from the stars that are orbited by planets. In this thesis I will mainly focus on this subject, namely the giant planet frequency as a function of stellar parameters and how that affects planet formation theories. In the following sections, I will first (Section 1.1) outline in a brief way the different detection methods that are used to search for exoplanets and which

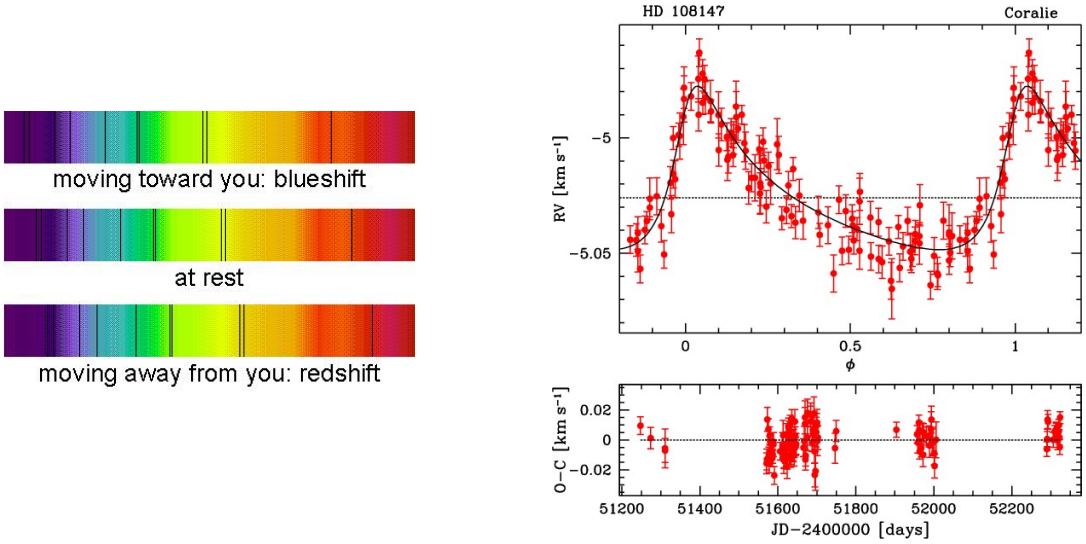

Figure 1.2: Left panel: illustration of the Doppler shift, measured through spectral lines. Right panel: Example of the phase-folded radial velocity curve for HD108147b (Pepe et al. 2002a).

information we can extract from each method, as well as their difficulties and drawbacks. In Section 1.2 I will give an overview of the current planet formation theories. I will highlight the importance of precise stellar parameters, how they relate to planet properties and how this can help us to improve theoretical planet formation models in Section 1.3. Finally, I will outline the contents of this work in Section 1.4

1.1 Planet detection methods

Different techniques can be used to detect an exoplanet. Each technique has its advantages and disadvantages, and each technique will characterize the planet differently. Six main techniques are used these days to detect planets. However, only two of them have proved to be very successful, the radial velocity and the photometric transit technique. Together, these two techniques have detected over 90% of all known exoplanets, as can be seen from Fig. 1.1.

1.1.1 Radial velocity

Radial velocity is the stellar velocity along the line-of-sight. This can be measured through the Doppler shift in the spectral lines of a star's spectrum ($\Delta\lambda/\lambda = v/c$ where v is the radial velocity and c the speed of light). Light coming from a star moving toward the Earth will be Doppler shifted to bluer (shorter) wavelengths, while a star moving away from the Earth will emit light shifted to redder (longer) wavelengths (see left panel of Fig. 1.2).

When a star is orbited by one or more planets, these planets will gravitationally pull on the star and make it move around the center of mass. This creates a periodic wobble in the star's radial velocity. An example of a phase-folded radial velocity curve is given in the right panel of Fig. 1.2 that shows the RV curve of HD108147b (Pepe et al. 2002a). In the case of an eccentric orbit, the radial velocity has the following dependence with time (see Appendix A.1 for more definitions and formulae):

$$RV(t) = \gamma + K[\cos(\varpi + \nu(t)) + e\cos\varpi]$$

The amplitude K of this periodic signal depends on the planetary mass M_p, the distance of the planet from its star (or period P), the stellar mass M_*, the eccentricity e of the orbit, and the inclination i of the orbit:

$$K = \frac{M_p \sin i}{\sqrt{1-e^2}} \left(\frac{2\pi G}{P M_*^2}\right)^{1/3},$$

with G the gravitational constant (Cumming et al. 1999). A higher stellar mass or a larger planetary period will reduce the amplitude K. On the other hand, a more massive planet will increase the amplitude of the signal. The amplitude of the periodic signal induced by a planet is only about a couple meters or even centimeters per second. As a reference, the radial velocities induced on the Sun by Jupiter, Saturn, Neptune, and Earth are 12.4, 2.75, 0.28, and 0.09 m/s, respectively. High precision measurements are thus needed to detect planets this way. High-resolution spectrographs, like HARPS (La Silla, Chile, Pepe et al. 2002b), CORALIE (La Silla, Chile, Queloz et al. 2000), and HIRES (Keck, Hawaii, Vogt et al. 1994) are used for dedicated planet searches or planet confirmations.

The period and eccentricity can be determined from modelling the periodic signal in the radial velocity curve. However, the inclination i cannot be determined. The radial velocity method will thus only determine the mimimum mass of the planet $M_p \sin i$. Furthermore, the precision and accuracy of this minimum mass relies on the precision and accuracy of the stellar mass.

While the inability to determine the inclination is an important limitation to the radial velocity method, it is statistically not that important. Assuming that inclination angles are randomly (isotropically) distributed in space, edge on-systems (with inclinations closer to 90 deg) are much more frequent than face-on systems. Consequently, the probability that $\sin i > 0.5$ is about 87% (see Lovis & Fischer 2011, and references therein). This is of course assuming an isotropic prior distribution. Several works have been trying to understand and quantify the posterior distribution (e.g. Ho & Turner 2011; Lopez & Jenkins 2012), but no

consensus has been reached.

The shifts in the spectral lines (and thus the radial velocity) have to be derived with very high precision (at 5000 Å, a radial velocity of 5 m/s induces only a wavelength shift $\Delta\lambda \sim 8{\cdot}10^{-5}$ Å). Using the cross-correlation function (CCF), information from several lines can be used in one averaged line to determine the radial velocity (more details can be found in Baranne et al. 1996). This simple and robust way of measuring RV was turned into a more efficient method by including weights to each spectral line (Pepe et al. 2002a, for more information).

There are several stellar limitations to the RV detection method, such as oscillations, granulation, rotation, spots, or pulsations (e.g. Nardetto et al. 2008; Boisse et al. 2011; Dumusque et al. 2011, and references therein). These astrophysical processes change the shape of the spectral lines. This variation in the line profile will lead to a different RV measurement than the one coming from the Doppler shift. These additional shifts can thus mimic a signal that can be misinterpreted as coming from a planet.

Effects coming from stellar oscillations and granulations are easily to get around using clever observational strategies, as described in Dumusque et al. (2011). Other astrophysical processes are not that easy to factor in. Higher stellar rotation ($v \sin i$) will make the spectral lines appear wider and blend with neighbouring spectral lines, resulting in a lower precision for the RV measurements (Bouchy et al. 2001). Fast rotating stars are usually early-type young stars, since their angular momentum is increased by still accreting material from the surrounding disk (Bouvier et al. 1997). For this reason, planetary searches are usually focused on slow rotators, minimizing the effect of the stellar rotation on the spectral lines.

Even with all these precautions, a careful treatment of the radial velocities is still necessary. Several indicators and tools have been developed to investigate RV signals possibly coming from activity, such as the bisector, V_{span}, the Na I index, SOAP-T, or V_{asy} (Queloz et al. 2001; Boisse et al. 2011; Gomes da Silva et al. 2012; Oshagh et al. 2013; Figueira et al. 2013).

1.1.2 Photometric transit

When a planet crosses its star, the starlight is dimmed and an eclipse occurs. This dimming can be detected as a dip in the photometric light curve (see Fig. 1.3 for an illustration and a real observational example). When the planet passes behind the star, a secondary eclipse occurs, resulting in a less deep drop in the light curve as the reflected light from the planet is blocked.

The shape of the light curve is influenced by the stellar and planetary radius. The larger the planet, the more light it will block from the star. Similarly, for a larger star, a planet will block out less light. Furthermore, the inclination and the semi-major axis of the planetary

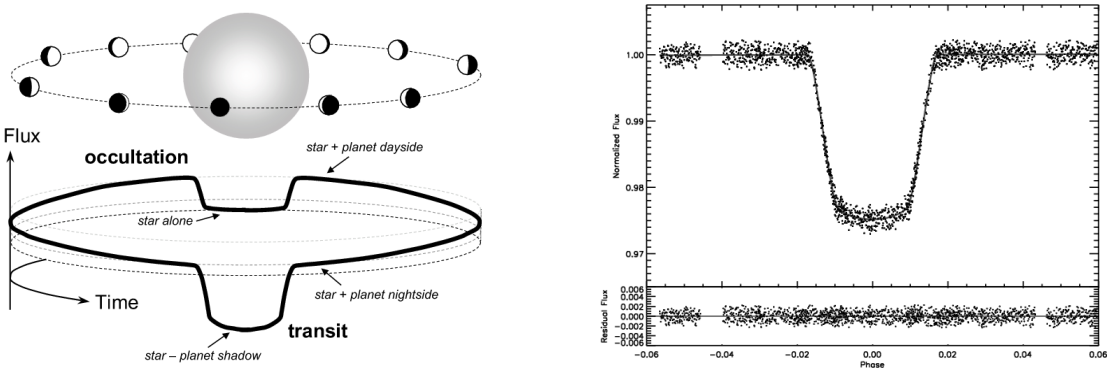

Figure 1.3: Left panel: illustration of the transit technique (Winn 2011). Right panel: Example of the transit light curve for HD189733b (Sing et al. 2009), with residuals in the bottom panel.

orbit are important in the light curve analysis. In the simplified case of a circular orbit, the following definitions are valid (a more detailed description is found in Winn 2011):

$$\begin{aligned} \text{Transit depth:} \quad & \frac{\Delta F}{F} = \left(\frac{R_p}{R_*}\right)^2 \\ \text{Transit duration:} \quad & T_{dur} = \frac{2R_*}{v} = 13h\frac{R_*}{R_\odot}\sqrt{\frac{a}{\mathrm{AU}}\frac{M_\odot}{M_*}} \\ \text{Probability of transit:} \quad & P(i > \theta) = \frac{R_*}{a} \end{aligned}$$

In these equations, F is the photometric flux, R_p the planetary radius, a and i the semi-major axis and inclination of the orbit, v the velocity of the planet, R_* the stellar radius, and M_* the stellar mass.

From these equations, it can be seen that a transit light curve only determines ratios: the radius ratio R_p/R_* and the reduced stellar radius R_*/a. Precise stellar radii are thus crucial to characterize exoplanets detected with the photometric transit technique. A transit light curve gives no information on the mass of the planet. However, the analysis of the light curve can determine the inclination of the orbit. When combining transit data with radial velocity data, the true planetary mass can thus be derived.

When analyzing a transit light curve, one should take into account the fact that a stellar disk is brighter in the center than on the edges. This effect is referred to as limb darkening. This effect makes the light curve rounded at the bottom and influences the steepness of the dip. The limb darkening of a star is connected with the stellar's temperature and its atmosphere's opacity (Winn 2011). Several laws can be used to describe the limb darkening effect on the transit light curve (e.g. Claret 2004; Southworth 2008).

A good alignment of the system and high precision photometric measurements are obviously necessary for the photometric transit technique to work. In the beginning of planetary searches, this technique did not reveal many results. However, over the last few years, large space surveys, CoRoT and Kepler, and several ground missions such as WASP, HATNet, and OGLE have been observing thousands of stars, searching for transit signatures, exponentially increasing the amount of exoplanets found by the transit method (see Fig. 1.1). Over 200 planets have been confirmed from these efforts, with thousands more expected from Kepler candidate planets (e.g. Fressin et al. 2007; Hartman et al. 2012; Batalha et al. 2013; Moutou et al. 2013; Triaud et al. 2013).

As for the radial velocity technique, the photometric transit method is not immune to errors. Many situations, other than a planet crossing the star, can create a dip in the light curve and thus a false positive. Common false positives entail grazing eclipses from binary systems, dwarf stars passing in front of a giant star, or the transit of low-mass stars (due to the radius-mass degeneracy in the transit analysis). Understanding the rate of false positives in the presently large amounts of data of light curves is very important, but contradictory numbers currently exist in literature (Brown 2003; Morton & Johnson 2011; Santerne et al. 2012; Fressin et al. 2013).

For the confirmation of transiting planet candidates, radial velocity follow-up observations are needed. However, due to faint targets or high activity stars, RV follow-up is not always possible. Another technique, based solely on the light curves is therefore developed. When multiple planets are present around a star, the timing of the transits will not be regular, but vary a little. Apart from the confirmation of planets, this transit timing variation (TTV) can also be used to detect additional planets in a system. Kepler19c was detected this way (Ballard et al. 2011). It can also be used to rule out high mass companions (Montalto et al. 2012).

1.1.3 Other methods

The work in this thesis only makes use of planets detected with the radial velocity and photometric transit technique. However, I will shortly describe the other techniques that are used for exoplanet detection.

Direct imaging

The only direct way of detecting an exoplanet is by using direct imaging. The name speaks for itself as the technique consists of taking an image of the exoplanet. Taking a time series of snapshots will help in determining the planet's orbit characteristics as the rotation of the

planet around the star will be visible.

It is a promising technique with a simple idea behind it but it has many challenges. A planet is much fainter in comparison with its host star. In optical wavebands, a star is $10^6 - 10^9$ times brighter than a planet. Additionally, a planet is most often close to its star. For example, at a distance of 10 pc, the Sun and Jupiter would be separated by only 0.5 arcsec (Traub & Oppenheimer 2011). This makes the planet "disappear" in the stellar light. Conventional imaging techniques are thus not adequate and more complex methods are needed to process the image of the exoplanet.

The technique is also limited by seeing, an effect coming from the atmospheric turbulence. This can be partially overcome by using adaptive optics (Angel 1994). Given these challenges in directly detecting exoplanets, only about 35 planetary systems[2] were discovered this way (e.g. Chauvin et al. 2005; Marois et al. 2008; Lagrange et al. 2010; Kalas et al. 2013).

The planets found by this technique are all high mass planets on very wide orbits since these types of planets are the easiest to detect by direct imaging. The lightest planet found this way is Fomalhaut b, with a mass of only 2 Jupiter masses (Kalas et al. 2013). Furthermore, several stellar companions have been found using this technique with masses around the planet/brown dwarf boundary[3], making it difficult to distinguish whether these objects are planets or stars (e.g. Chauvin et al. 2005; Carson et al. 2013).

Additionally, directly imaged planets have challenged formation theories. The first directly detected exoplanets could not be explained by the standard core-accretion theory (Pollack et al. 1996). Gravitational instability seems to better explain the existence of these heavy planets on wide orbits (e.g. Chauvin et al. 2005; Delorme et al. 2013). More information on both formation theories can be found in section 1.2.

Astrometry

For the astrometry technique, the orbital motion of the star, projected in the sky, is measured. When a planet is present around a star, the star will wobble in the sky, because the star rotates around the center of mass of the system (see section 1.1.1). This technique is the oldest planet detection technique around. It is a useful technique because it can provide the full orbital geometry and thus measure the true mass directly. Since astrometry only measures the angular displacement, other techniques are needed in complement to characterize the planet.

To this date, there are no confirmed planet detections with the astrometry method though several planets have been confirmed with the technique (e.g. Han et al. 2001; Benedict et al.

[2]according to the Extrasolar Planet Encyclopaedia `www.exoplanet.eu`

[3]The International Astronomical Union has adopted a mass of 13.6 Jupiter masses to distinguish between planets and brown dwarfs, although this value is arbitrary and highly debated.

2002, 2010; Reffert & Quirrenbach 2011). The upcoming ESA mission Gaia (to be launched in November 2013) will provide precise astrometry data that can be used to detect planets (Sozzetti 2010).

Pulsar timing

Pulsars are small remnants of a star that has exploded as a supernova. As they rotate, the pulsars emit radio waves with an extreme regularity. The presence of a planet creates a time delay in these regular pulses. This method is so sensitive that it is able to detect very small planets, much smaller than any other method can. The very first exoplanets were discovered this way (Wolszczan & Frail 1992).

However, there are several disadvantages to this method. First of all, since a pulsar is formed as a result of a supernova explosion, planets are not expected around these neutron stars, unless they are second generation planets. This decreases the probability of finding a planet this way. Another disadvantage is the fact that pulsars emit high-energy radiation, making life, as we know and define it, on these planets impossible.

Gravitational microlensing

Light from a distant background star is bent by gravity when a star passes between the observer and the background star. The star then acts as a lens. If the lensing star is orbited by a planet, the lensing effect will be even larger as the gravitational field of the planet also contributes.

Unfortunately, this effect can only be observed once per star and the necessary alignment of the system for the method to work is highly improbable. Furthermore, the targets are usually faint, especially compared with the bright background star, making follow-up observations with other methods very complex. Most planets detected this way (about 20 in total, e.g. Sumi et al. 2010; Han et al. 2013) orbit stars residing between the Sun and the Galactic Center, making the probability of a detection higher due to the larger amount of background stars.

1.2 Planet formation

In spite of all the exoplanets discovered at this point, the theory of planet formation and evolution is still not fully understood. The first planet formation theories were based on the structure and composition of the Solar System (SS), since that was the only known planetary system for a long time. The SS consists of 4 solid and 4 gaseous planets with cores (2 gas giants and 2 icy giants) residing on coplanar circular orbits. These eight planets are complemented with several smaller bodies (dwarf planets, moons, comets, Kuiper Belt).

Due to the first discoveries of hot Jupiters (e.g. Mayor & Queloz 1995; Butler et al. 1997), these initial formation theories needed to be revised as no such bodies exist in the SS. Subsequent discoveries of eccentric, inclined, and other exoplanets non-resembling to the SS bodies (e.g. Cochran et al. 1997; Butler et al. 1997, 1999; Fischer et al. 1999), made it clear that planet formation and evolution is a complex mechanism.

Planets are formed as a natural result of the star formation process. Stars form by the gravitational collapse of a giant molecular cloud. A protostar is formed in the inner regions embedded in a surrounding envelope of gas and dust (e.g. Shu et al. 1987; Hogerheijde 1998). Along the rotational axis of the system, material is swept out, either through jets or bipolar outflows. With the outflow angle growing larger, the star becomes visible since it helps to clear the young star from the opaque cloud wherein it is forming. In the equatorial regions, through accretion, a rotating protoplanetary disk forms, consisting mainly of dust and gas. Planet formation is thought to happen in these protoplanetary disks, also called accretion disks. For a review of star formation, see for example Luhman (2012) and references therein.

For terrestrial rocky planet formation, there is currently one theory (grain coagulation). For giant planets however, there are two scenarios for planet formation, core-accretion (bottom-up) and gravitational instability (top-down). The main scenario is thought to be the core-accretion model. However, the formation of some giant exoplanets, especially the ones with long periods, may be better explained by the gravitational instability model. Here, I will explain the theory of grain coagulation and both models of giant planet formation in some detail. A helpful overview on planet formation can be found in Matsuo et al. (2007) and references therein.

1.2.1 Terrestrial planet formation

Formation theories for rocky planets state that planets are formed by the binary accretion of small dust particles and later planetesimals (as first stated by Safronov & Zvjagina 1969). The protoplanetary disk around a star contains mostly gas, but also small dust particles (size $\sim \mu$m). By collisions and aggregation, the dust grows to become centimeter-sized grains.

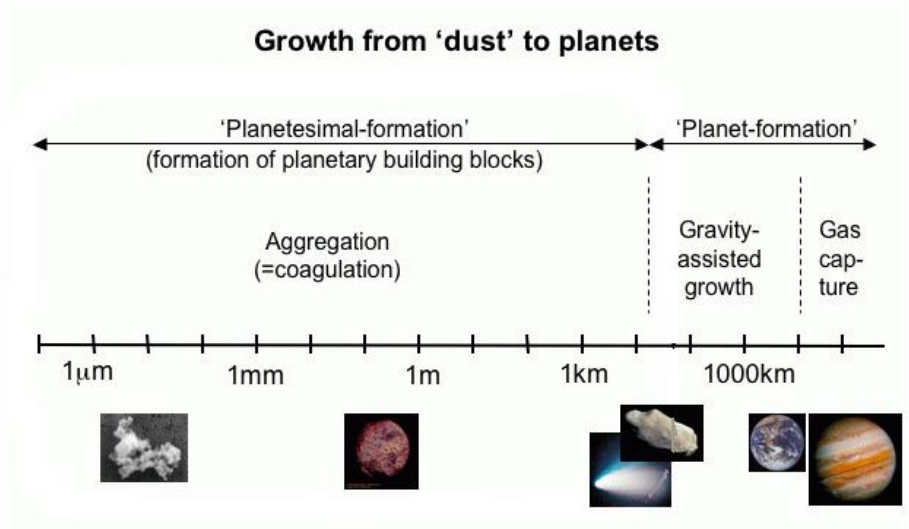

Figure 1.4: Illustration of planet formation, following the core-accretion model (courtesy C. Dullemond).

These dust grains eventually become planetesimals. It is to this day not well understood how exactly these planetesimals form. Different mechanisms have been proposed, like gravitational instability, particle sticking, turbulent concentration, etc (e.g. Goldreich & Ward 1973; Weidenschilling 1997; Kretke & Lin 2007). All mechanisms however suffer from the 'meter-size barrier'. This problem handles the further growth of meter-sized particles. Particles of that size have a low probability of sticking together after a collision, due to their relative velocities (Supulver et al. 1997). Furthermore, meter-sized particles will be easily influenced by the surrounding disk gas and gain high velocities towards the star (Weidenschilling 1977). Due to a radial pressure gradient, the gas in the disk will move slightly slower than the dust which thus feels a continuous head wind of gas. This makes the particle loose angular momentum causing it to spiral inwards (also called the gas drag or Poynting-Robertson drag Robertson 1937). This will cause the particles to fall into the star before having the time to grow larger (Brauer et al. 2008).

Despite this long-standing problem with the formation of planetesimals, it is assumed that enough planetesimals with sizes beyond this meter-barrier are formed at some point. Mutual collisions of these planetesimals will then lead to further growth or fragmentation (Chambers 2011). The result of such collisions depend on the impact velocity and the strength and size of the planetesimals. When the planetesimals reach sizes of several kilometers, they are large enough to have a gravitational effect on surrounding clumps, increasing their chances on a collision. From that point on, the growth speeds up, resulting in a process called runaway growth (Wetherill & Stewart 1989). When the fast growing planetesimal has cleared its orbit of other large planetesimals, the growth slows down (Ida & Makino 1993) and a new regime of oligarchic growth begins (Kokubo & Ida 1998). Each large body will grow now in its own

orbital zone of influence. A planetary system with protoplanets has formed.

This process can end when the planet ends up in a stable orbit with no more material around it. This means a terrestrial planet has been formed (Chambers 2006). For a complete recent overview of terrestrial planet formation, see for example Chambers (2011) or Morbidelli et al. (2012). An illustration can be seen in Fig. 1.4.

1.2.2 Giant planet formation by core-accretion

The most popular theory for giant planet formation is the core-accretion theory (e.g. Pollack et al. 1996). It starts with the formation of a rocky or icy core, just like terrestrial planets form. When planetesimals have grown sufficiently large, the rocky/icy core will slowly start to accrete gas due to the surface's escape velocity being greater than the gas' thermal speed (D'Angelo et al. 2011).

When the pressure in the envelope can no longer balance the gravitational force of the core, the envelope contracts and the gas can be accreted more rapidly. This process is called runaway gas accretion (Pollack et al. 1996) and a giant planet has been formed. More information on the core-accretion theory can be found for example in Rice & Armitage (2003); Alibert et al. (2004); Dullemond & Dominik (2008) and references therein.

This model for planet formation is a slow process that happens at timescales of about $10^6 - 10^8$ years. The core growth is fast as is the runaway gas accretion phase. However, the slow gas accretion regime in the middle takes about 10 Myr (Pollack et al. 1996). Unfortunately Haisch et al. (2001) found that in general disk lifetimes are shorter than this value. According to this theory and its timescales, giant planets can thus not be formed this way. Maybe, this timescale issue is not an issue at all. Disks may live longer than previously stated (Bary et al. 2003) or the model's timescale is wrong. The gas accretion process can also be sped up by including other mechanims such as disk evolution, random motion or migration (e.g. Rice & Armitage 2003; Alibert et al. 2004).

Migration

Core-accretion is the preferred scenario for the giant planets in the Solar System. However, the existence of hot Jupiters could not be explained with this theory alone since close-in giant planets cannot be formed in-situ owing to the lack of material at close distances to the star. Another observational surprise was the discovery of several planetary systems in low-order mean motion resonance (e.g. Goździewski & Maciejewski 2001; Marcy et al. 2001). As an addition to the core-accretion model, the process of migration was thus needed which could

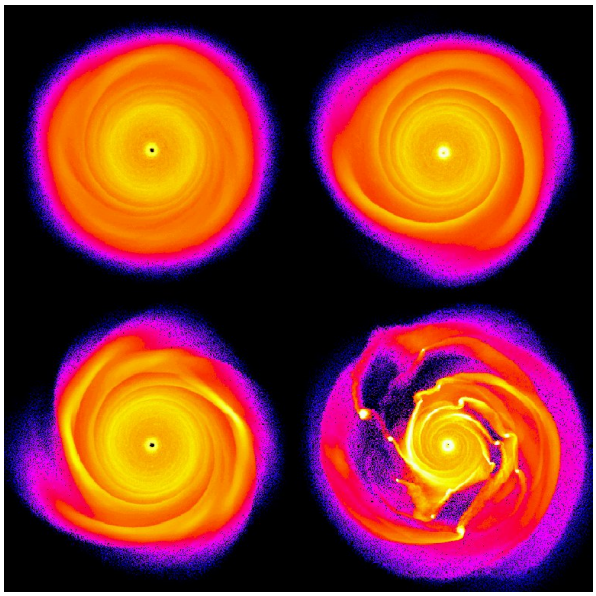

Figure 1.5: Snapshots of simulations showing face-on protoplanetary disks at different times during the process of forming planets through gravitational instability (Mayer et al. 2002). Upper panels are for a less massive disk than the lower panels. Left panels are after 160 years of evolution, right panels after 350 years.

explain these close-in giant planets and the resonant systems. Moreover it would solve the timescale issue of in-situ planet formation.

Planetesimals and planets interact with the surrounding gas disk. These planet-disk interactions can result in the inward (in isotermal disks) or outward (in radiative disk) migration of the bodies (e.g. Lin et al. 1996; Alibert et al. 2004, 2005; Mordasini et al. 2009). This migration can then create gaps in the disk (depending on the mass of the body and its orbital inclination), clearing it from left-over materials or smaller-sized bodies.

The theory of the migration processes is still under development as several discoveries of exoplanet still cannot be explained by current models. For example, there are the hot Jupiters where the orbital plane and the stellar rotation axis are misaligned (e.g. WASP-17b - Triaud et al. 2010). Possible mechanisms to explain this misalignment could be Kozai cycles or planet-planet scattering (e.g. Fabrycky & Tremaine 2007; Beaugé & Nesvorný 2012).

1.2.3 Giant planet formation by gravitational instability

Another theory for the formation of giant planets is the theory of gravitational instability (Boss 1997; Mayer et al. 2002). In this model a planet is formed due to a direct gravitational instability in the protoplanetary disk, in the same way as stars form from interstellar clouds. The disk is then called self-gravitating. Density fluctuations originate from these instabilities

until spiral arms are formed in which planets arise (see Figure 1.5 - Mayer et al. 2002).

It is not well known if the right conditions exist for the disk instability model to work. Theoretical works have shown that while a protoplanetary disk can become gravitationally unstable, the gas cannot cool fast enough for the disk to fragment into planets, at least not in the inner regions of the disk (Rafikov 2005; Matzner & Levin 2005). However, the main advantage of the instability model is the timescale that is needed to form the planets. This scenario is fast and happens on short timescales of about 1000 years, well within the lifetime of a protoplanetary disk (Haisch et al. 2001).

This model seems to work well for distant planets as disk instability is expected to occur only in the outer regions of a disk. It could be the preferred model to explain among other things the existence of massive long-period planets, as discovered by direct imaging, like HR8799b, c and d (Marois et al. 2008). However, this does not exclude that short period planets may also be formed by gravitational instability. Baruteau et al. (2011) suggest that planets formed by gravitational instability may migrate very rapidly inwards.

Several studies worked on numerically modeling the different scenarios of giant planet formation (e.g. Marley et al. 2007; Mordasini et al. 2012b; Mordasini 2013). Some works distinct core-accretion and gravitational instability as cold-start and hot-start mechanisms (Marley et al. 2007). However, Mordasini et al. (2012b) discusses the possibility of hot-core-accretion scenarios. No satisfying solution explaining all detected exoplanets has been found so far.

1.3 Stellar parameters

As mentioned in Section 1.1, the derivation of the essential planetary parameters like their mass and radius depends directly on the stellar mass and radius. For a transiting planet, analysis of the light curve only determines the planetary radius relative to the stellar radius (R_p/R_*). The planetary mass depends on the stellar mass ($M_p \propto M_*$), as derived from the radial velocity curve. Deriving the stellar radius and mass in turn depends on the star's atmospheric parameters (effective temperature T_{eff}, surface gravity logg, and metallicity [Fe/H]). The more precise the stellar parameters, the more precise the planetary parameters will be. Figure 1.6 illustrates the importance of precise planetary parameters to characterize the composition of the exoplanets.

Another reason for precise stellar parameters are the several star-planet interactions and correlations that give us insight into the processes of planet formation and evolution. Without precise parameters, no significant statistics can be done on the samples to look for these correlations. For the same reason, it is also favorable that all parameters are derived as homogeneously as possible.

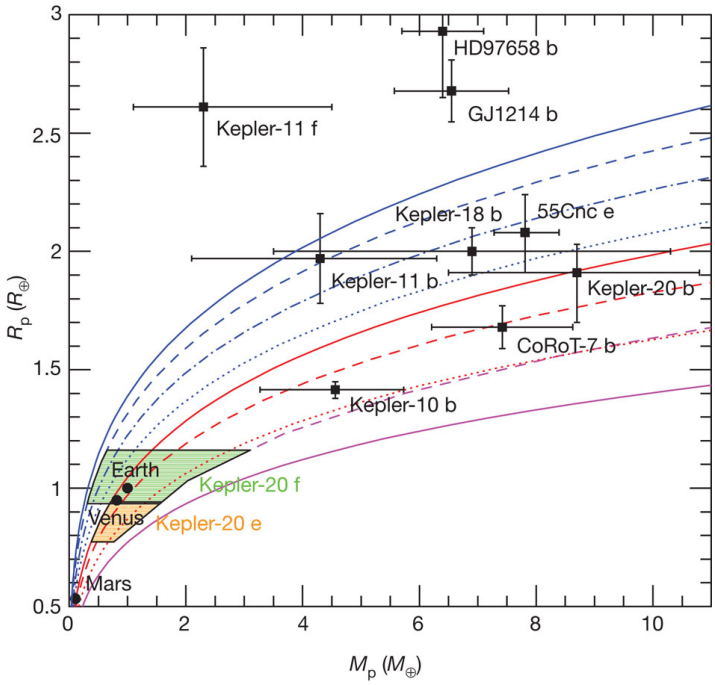

Figure 1.6: Planetary radius versus planetary mass, taken from Fressin et al. (2012). The solid lines represent homogeneous compositions for planets: water ice, $MgSiO_3$ perovskite, and iron (top to bottom), while non-solid lines give mass-radius relations for differentiated planets.

Since the work during my PhD was mainly focused on the relation between stellar parameters and the frequency of giant planets, I will explain hereafter in detail some theory on stellar atmospheres (following Gray 2008), the methods used to derive stellar parameters and their correlation with planet frequency.

1.3.1 Stellar atmospheres

Light emitted by a star can be measured with a spectrograph, creating a spectrum of the star. The inner regions of a star, consisting of very dense, hot material, will produce a continuum spectrum. As these photons pass through the stellar atmosphere, some are absorbed by atoms (or molecules) that exist in the cooler outer layers of the atmosphere (the photospere). This lack of photons due to specific atoms, will create absorption lines in the spectrum. Stellar temperature, pressure (or surface gravity), and chemical composition of the stellar atmosphere have an impact on the strength of specific absorption lines. By carefully studying a stellar spectrum, one can thus determine the basic atmospheric parameters of a star, such as the effective temperature T_{eff}, the surface gravity $\log g$, the metallicity [Fe/H] and the microturbulence ξ.

Photons can only be absorbed by an atom if it has the right amount of energy to allow a change in the atom's energy state. Atoms have a set of discrete energy levels, referring to the orbit where the electrons circle around the atom's nucleus (small orbits have low energies, wide orbits high energy). A photon will thus be absorbed if its energy exactly matches the difference between the current energy value of the atom and the value of a higher level. A fully ionized atom has no electrons left and as such won't produce any absorption lines in the spectrum. The photosphere of FGK stars consists of many atoms that are not fully ionized, making these stars perfect to analyze spectroscopically.

A stellar atmosphere is not in thermodynamic equilibrium (with a constant temperature, pressure gradient and chemical potential), but the variations in the parameters are so small, that one usually, and for simplicity, assumes thermodynamic equilibrium in local regions (local thermodynamic equilibrium - LTE). This is valid since collisions dominate the energy transitions in atoms rather than radiation for stellar atmospheres. In the case of LTE, the following equations apply:

Maxwellian distribution: With v the velocity of the particle, m the mass, k the Boltzmann constant, and T the temperature, all particles have a velocity distribution

$$f(v)dv = 4\pi \left(\frac{m}{2\pi kT}\right)^{(3/2)} e^{\left(-mv^2/2kT\right)} v^2 dv$$

Boltzmann equation: The populations of an atom in specific energy levels follow the Boltzmann law, where n_i is the number of atoms in energy level i, g_i the degeneracy of level i, and E_i the excitation potential of level i (u and l denote upper and lower levels of energy):

$$\frac{n_u}{n_l} = \frac{g_u}{g_l} e^{-(E_u - E_l)/kT}$$

Saha equation: The population ratio of atoms in successive ionization stages is described by Saha, with n_+ the number of atoms in an ionized state, n_l the number of neutral atoms, m_e the electron mass, h the Planck constant, and χ_l the ionization potential:

$$\frac{n_+}{n_l} = \frac{2}{n_e} \frac{g_+}{g_l} \left(\frac{2\pi m_e kT}{h^2}\right)^{(3/2)} e^{-\chi_l/kT}$$

As seen from Fig. 1.7, the number of absorbed photons by an atom, depends on the absorption coefficient κ and the number of atoms along the line of sight with the correct energy level to absorb the photon (as derived from the Boltzmann and Saha equations). The more atoms

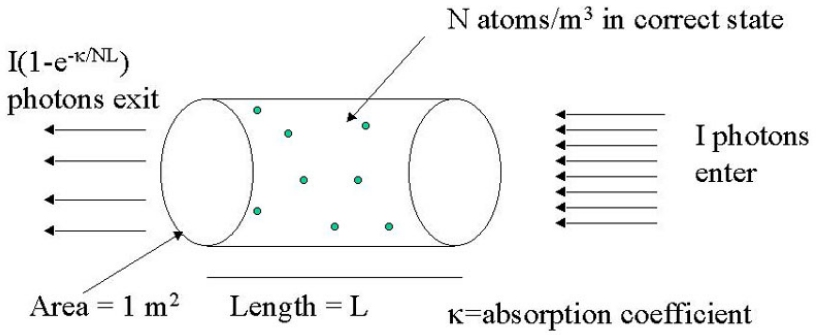

Figure 1.7: Illustration of the photon absorption by atoms (taken from the lecture notes by Prof. Marcia Rieke[4]).

present in the right excitation state, the more photons will be absorbed and the stronger the absorption line will be. The strength of a spectral absorption line (i.e. the total absorption of a line) is defined by its equivalent width, EW:

$$\mathrm{EW} = \int_0^\infty \frac{F_c - F_\nu}{F_c} d\nu,$$

where F_c is the continuum flux and F_ν the flux in the spectral line. EW is thus the width of a rectangle with the height of the continuum level and the same area of the line.

From the Boltzmann and Saha equations, it is already clear that the temperature of the star plays an important role in the atom populations and thus also in the absorption line strengths. Other stellar parameters like the surface gravity, metal abundance, and microturbulence also influence the EW of the spectral lines. The dependences I will describe here are only valid for weak lines (with EW$\leq$ 200mÅ). Stronger lines may additionally be influenced by NLTE effects.

According to Gray (2008), the fractional change in strength of a weak absorption line depends both on the temperature itself and on the excitation potential. The effective temperature of a star can thus be determined by applying excitation equilibrium: abundances calculated for several lines of the same species, all with different excitation potentials, must be the same for a given temperature. By using a set of lines with a large range of excitation potentials, one can determine the effective temperature.

Spectral lines are affected by pressure (from the gas and from the electrons). The strength of neutral metal lines, for which most of that species is in a higher ionization stage (as is the case

[4]see `http://ircamera.as.arizona.edu/astr_250/`

for solar-type stars), is not affected by pressure, while absorption lines of ionized species are affected by changes in the pressure. For FGK stars, both gas pressure and electron pressure are related with the surface gravity ($P_g \propto g^{(2/3)}$ and $P_e \propto g^{(1/3)}$). Surface gravity can thus be determined by using a set of neutral and ionized lines of the same species that need to give the same abundances (i.e. ionization equilibrium).

Abundance of a species (number of atoms) is directly related to the strength of the spectral line. However, the relation is not linear over all. For weak metal lines, the relation is linear though between the EW and the abundance of an absorption species.

Finally, there is a dependence with the microturbulent velocity. Microturbulence delays the saturation of a spectral line by stretching the absorption over a larger spectral band (the absorption coefficient κ is influenced by this microturbulent velocity). Observed EWs of saturated lines can thus be greater for stars with greater microturbulent velocities. By assuming no dependence of the species abundances on the reduced EWs, one can determine the microturbulence.

1.3.2 Atmospheric parameters

These days, astronomers have access to several instruments that perform high-resolution spectrography, among which UVES (VLT, ESO Chile), HARPS (La Silla, ESO Chile), and NARVAL (Pic du Midi, France). From high-resolution spectra, several atmospheric stellar parameters can be derived with high precision and accuracy: the effective temperature T_{eff}, the gravity $\log g$, the metallicity [Fe/H] and the microturbulence ξ (as discussed in the previous section). Two methods are commonly used for this purpose, spectral synthesis and spectral line analysis.

There are many codes available using the spectral synthesis methods. One of them is Spectroscopy Made Easy (SME - Valenti & Piskunov 1996). This method compares the observed spectrum with a grid of synthetic spectra, using a χ^2 minimization of the differences between the spectra. Another, more recent method, is the MATrix Inversion for Spectral SythEsis (MATISSE - Recio-Blanco et al. 2006), based on the projection of the observed spectra on the synthetic ones.

For this work, however, I have used the spectral line analysis method. It makes use of the equivalent width (EW) of iron absorption lines (Fe I and Fe II). These EWs can be measured by hand with IRAF [5] using the task `SPLOT` (for an example, see Fig. 1.8). However, automatic routines exist that reproduce the manual measurements with success. The routine I used is ARES (Automatic Routine for line Equivalent widths in stellar Spectra - Sousa et al. 2007).

[5]IRAF is distributed by National Optical Astronomy Observatories, operated by the Association of Universities for Research in Astronomy, Inc., under contract with the National Science Foundation, USA.

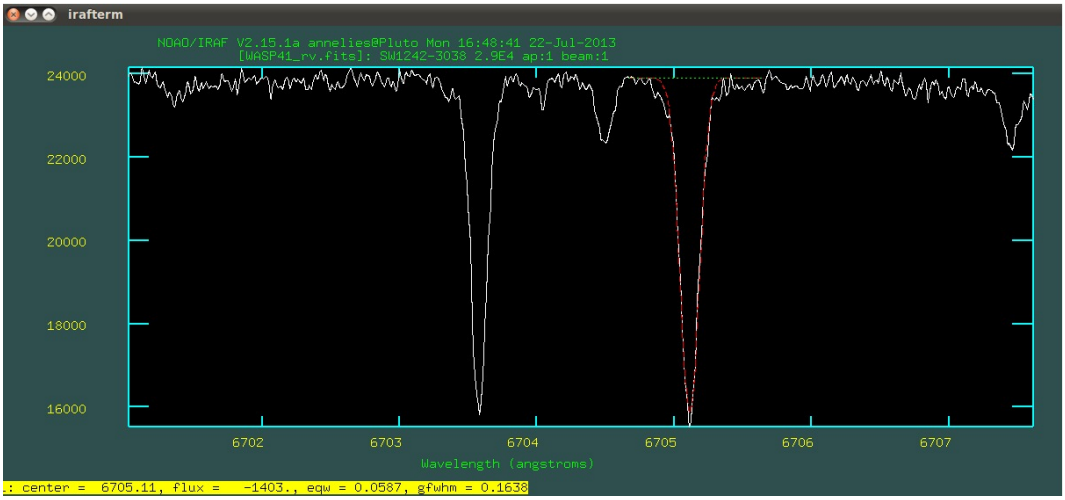

Figure 1.8: Example of a Fe I line (at 6705.11Å) in a stellar spectrum and the calculation of the equivalent width (red dotted line) with IRAF.

In order to use ARES, the spectra need to be corrected for radial velocity, to put them in their rest frame. This can be done with the IRAF task `DOPCOR`. To increase the signal-to-noise ratio (S/N) of the spectrum, one can add several individual spectra of the same star, observed with the same instrument, using `SCOMBINE` in IRAF. ARES also needs an atomic linelist. The standard linelist that is used for this purpose is the one from Sousa et al. (2008). Using a large sample of 451 stars, observed with the HARPS spectrograph, unstable lines that suffer from blending or other systematic effects were removed, ending up with a stable linelist of 263 Fe I and 36 weaker Fe II lines, with a large range of excitation potentials.

For cool stars ($T_{eff} < 5000$ K), however, the results from using this linelist have shown to be unsatisfactory. The derived temperatures were too high, when compared with other methods, like the InfraRed flux Method (Casagrande et al. 2006). Therefore a new linelist was built, specifically for these cooler stars (Tsantaki et al. 2013), based on the linelist of Sousa et al. (2008). This new linelist consists of 120 Fe I and 17 weaker Fe II lines and provides better temperatures while maintaining comparable other atmospheric parameters. If a star turns out to be cooler than 5200 K, according to the results based on the Sousa et al. (2008) linelist, the analysis is repetaed with the smaller linelist from Tsantaki et al. (2013).

ARES calculates the EWs by fitting a small, local part of the spectrum with multiple Gaussians. The spectrum is normalized locally before this fit. Therefor, ARES needs a set of calibration parameters. Most of these parameters are fixed, following the suggestions in Sousa et al. (2008): *smoothder = 4, space = 3, lineresol = 0.07, miniline = 2.* The *smoothder* parameter controls the noise in the computed derivatives of the local spectrum. These derivatives are used to determine the location and amount of lines that need to be fitted. *Space* controls the wavelength region where the local continuum is fit. Therefore, *space = 3* means

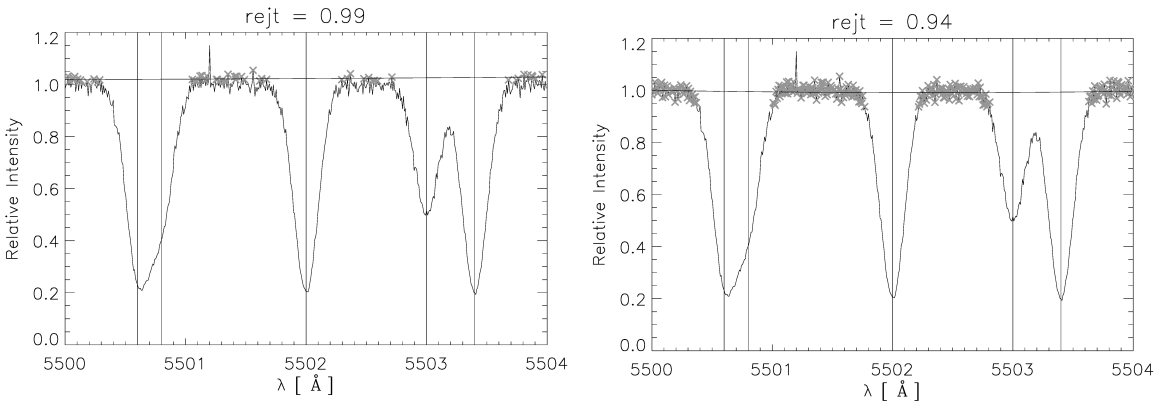

Figure 1.9: Importance of *rejt* parameter in ARES (taken from Sousa et al. 2007). A synthetic spectrum region with S/N $\sim$ 50. The filled line represents the fit to the local continuum through a 2nd-order polynomial based on the points that are marked as gray crosses in the spectrum.

that a local fit will be made over 6Å. The *lineresol* parameter handles the resolution of the lines. It defines the minimum separation (in Å) allowed for consecutive lines. Finally, *miniline* puts a lower limit on the value of EW (in mÅ) that will be returned.

The most important calibration parameter for ARES is the *rejt* parameter. This parameter determines the calibration of the continuum position. The value is between 0 and 1, where 1 indicates a noiseless spectrum (see Figure 1.9 for an example with a synthetic spectrum). This parameter thus strongly depends on the S/N of the spectra and different values are needed for different spectra. Some spectrographs attach an indication of the S/N to the header of the spectrum. However, since I mostly use stacked spectra and spectra from different spetrographs, there is a need for a uniform S/N value. A uniform S/N value can be derived for the spectra with the IRAF routine `BPLOT`. Herefor, I use three spectral regions: [5744Å, 5747Å], [6047Å, 6053Å] and [6068Å, 6076Å]. The *rejt* parameter was set by eye for ten spectra with different S/N. Afterwards, a simple interpolation of these values was done to get appropriate *rejt* parameters for all spectra. The dependence of the *rejt* parameter on the resulting S/N can be found in Mortier et al. (2013b) which is shown in Chapter 4.

Based on these EWs, iron excitation and ionization equilibrium is imposed, assuming local thermodynamic equilibrium (LTE). This is done with the 2002 version of the code MOOG[6] (Sneden 1973). This code needs a grid of model atmospheres, for which I chose to adopt the Kurucz Atlas 9 plane-parallel model atmospheres (Kurucz 1993). To derive the four atmospheric parameters (T_{eff}, [Fe/H], logg, and ξ_t), a minimization code is used, based on the Downhill Simplex Method (Press et al. 1992), over this four-dimensional parameter space. The program starts with an initial guess of the parameters, for which usually the solar

[6] `http://www.as.utexas.edu/~chris/moog.html`

parameters are taken. It keeps iterating untill several conditions are fulfilled.

For the Fe I lines, there should be no dependence between the individual abundances per line and the excitation potential χ_l of that line (determining the temperature). Similarly, no dependence should be present between the individual line abundances and the reduced EW $\log(W_\lambda/\lambda)$ (determining the microturbulence). Furthermore, the mean abundances from the Fe I and Fe II lines should be the same (determining the surface gravity) as the abundance of the input model atmosphere (determining the metallicity). More details on the method can be found in Santos et al. (2004).

The above-mentioned method is only one of the methods to use spectral line analysis to derive stellar parameters. Other model atmospheres, like the MARCS models (Gustafsson et al. 2008), or other abundance derivation codes, like WIDTH (written by Kurucz and described in Castelli 2005), can be used. Including non-LTE effects or different linelists can also affect the derived parameters. It has been shown that the results of using the method described here deliver precise parameters that compare well with other methods (e.g. Sousa et al. 2008, 2011; Tsantaki et al. 2013; Santos et al. 2013).

Over the years, a significant effort was done to use this uniform spectroscopic method to homogeneously derive stellar parameters for planet hosts. During the time of my PhD and with my help, this resulted recently in the largest homogeneously analysed planet-host sample existing: SWEETCat (Santos et al. 2013)[7]. Currently, I am maintaining this catalogue, updating it whenever new planets are discovered.

Chemical abundances

The metallicity of a star, [M/H], entails all metals present in the star (basically all elements other than hydrogen and helium). However, more often than not, iron abundance is used as a proxy for metallicity, [Fe/H]. Other metals are usually less abundant, but possibly significant. Chemical abundances of other elements (like Mg, Ca, Ni, Li) can also be determined using high-resolution spectra. Similarly to the atmospheric parameters, this can also be done through spectrum synthesis or spectral line analysis. The derivation of these abundances though depends on the atmospheric parameters which must be derived first. More details of some of these methods can be found in Adibekyan et al. (2012b) and Delgado Mena et al. (2013).

[7] `https://www.astro.up.pt/resources/sweet-cat`

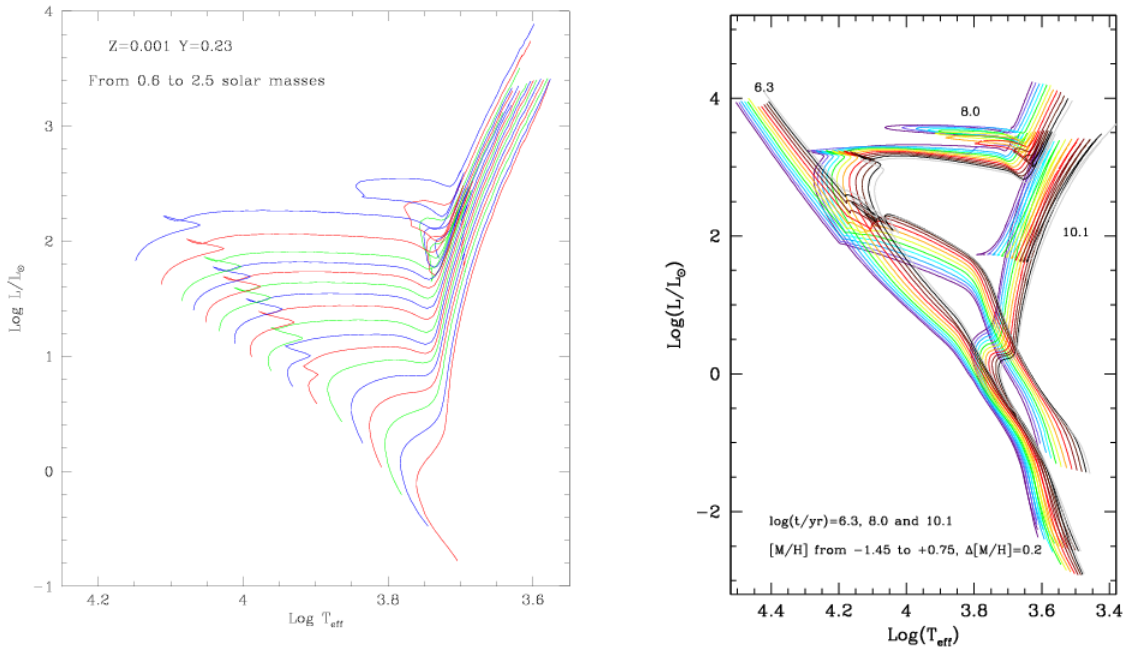

Figure 1.10: Left panel: mass tracks for main sequence FGK stars in a HR diagram (taken from Bertelli et al. 2008). Right panel: 3 sets of isochrones at fixed ages of logt = 6.3, 8.0, and 10.1 for different metallicities (taken from Bressan et al. 2012)

1.3.3 Stellar masses and radii

Precise stellar masses and radii are crucial in planetary science, and other fields in astronomy. Several methods exist to derive them. Here, I will only explain the two methods that I have used during my PhD, one using stellar evolution models and one using calibration formulae.

Stellar evolution models

With the apparent magnitude and the parallax of a star, the stellar luminosity can be calculated. Adding the effective temperature of the star, it can be placed in a Hertzsprung-Russell diagram. Using this position combined with evolutionary mass tracks, isochrones, and the metallicity of the star, the mass and age of the star can be determined. Figure 1.10 presents an example of mass tracks (left panel) and isochrones (right panel).

For this work, stellar evolutionary models from the Padova group were used, through their webpage `http://stev.oapd.inaf.it/cgi-bin/cmd` (da Silva et al. 2006). This web interface needs four parameters. For the temperature and metallicity, the values from the MOOG analysis can be used (see 1.3.2). For the V magnitude and parallax, the Hipparcos values are

preferred (van Leeuwen 2007), or other values as listed in the Simbad Database[8]. If no errors are provided for the magnitude or parallax, typical values of 0.05 and 1.0 respectively, are used.

Once the mass is known, stellar radii are then easily calculated with Newton's formula ($2 \log R = \log M - \log g + 4.44$, with R and M in solar values) or a luminosity formula ($L = R^2 \cdot T^4$, with L and R in solar values). In the case of an unprecise parallax (when the error is larger than 10% of the value) or if the parallax is not known, an iterative method can be used to get stellar masses, as explained below, if the surface gravity logg of the star is known.

1. Make a first estimate for the mass, using for example calibration formulae or literature values.
2. Using this mass, the temperature, the logg and the V magnitude, a parallax can be calculated. This calculation is based on relations for luminosity, mass and bolometric magnitude. For the latter, the bolometric correction from Flower (1996) is used.
3. The resulting parallax can now be used as an input on the Padova website to get a new estimate for the mass.
4. Compare the prior and posterior values for the mass.
5. Repeat steps 2-4 till the masses converge.

Calibration formulae

For FGK dwarfs, one can also use the calibration formulae given by Torres et al. (2010) to derive masses and radii, using Monte Carlo simulations. Those calibrations depend on the effective temperature, surface gravity and metallicity of the star. I have made a small second order correction on the mass formula since the calibration has a small offset around a solar mass, using a large sample of stars with masses calculated from the Padova stellar evolution models:

$$M_{cor} = 0.791 \cdot M_T^2 - 0.575 \cdot M_T + 0.701,$$

where M_{cor} and M_T denote the corrected stellar masses and the mass from the Torres et al. (2010) calibration, respectively.

From the spectroscopic analyis the effective temperature, surface gravity, and metallicity of star were derived, including their error bars. Considering Gaussian errors, a distribution of

[8]The Simbad Database is operated at CDS, Strasbourg, France: `http://simbad.u-strasbg.fr/`

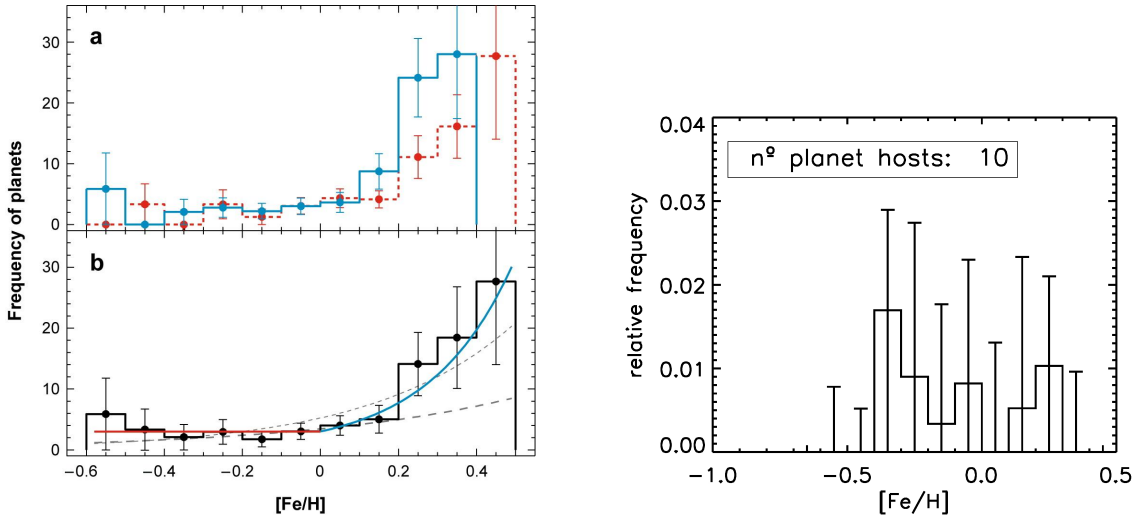

Figure 1.11: Left panel: Figure taken from Udry & Santos (2007). (a) Percentage of planet hosts found amid the stars in the CORALIE (blue) and Lick-Keck (dashed red) samples as a function of stellar metallicity. (b) Average distribution of the two samples. Right panel: Neptune frequency as a function of metallicity (taken from Sousa et al. 2011)

10000 values is created for these three parameters. After using the calibration formulae, the final value for the mass and radius and their errors are calculated through the mean and standard deviation of the 10000 resulting values.

1.3.4 Correlation with planet frequency

Since planet formation happens as a result of star formation, it only makes sense that correlations should exist between stellar and planetary parameters (for a general overview see e.g. Udry & Santos 2007). The most discussed relation, and the one this thesis revolves around, is the frequency of planets around stars of different metallicities and mass.

Stellar metallicity

More metal-rich stars have a higher probability of harboring a giant planet than their lower metallicity counterparts (Santos et al. 2001, 2004; Fischer & Valenti 2005; Udry & Santos 2007). The occurrence rate even increases dramatically with increasing metallicity. Current numbers suggest that at least 25% of the stars with twice the metal content of our Sun ($[Fe/H] \geq 0.3$) are orbited by a giant planet, and this number decreases to below 5% for solar-metallicity objects (Sousa et al. 2011).

This has been well established now, but was already suspected very early after the discovery

of the first exoplanets (Gonzalez 1997; Fuhrmann et al. 1997). Thanks to the discovery of more and more exoplanets, statistical studies could be done to verify these suspicions (e.g. Santos et al. 2001, 2004; Fischer & Valenti 2005; Johnson et al. 2010; Sousa et al. 2011). Comparing the stellar metallicities for planet hosts and comparison samples of field dwarfs confirmed the suspected correlation as shown in the left panel of Figure 1.11 (Udry & Santos 2007). In the top panel, the percentage of planet hosts is shown for the CORALIE (Santos et al. 2004) and the Lick-Keck sample (Fischer & Valenti 2005). The difference between the two distributions is probably explained by differences in the samples and in the metallicity analysis method. The bottom panel shows the average distribution of the two samples. A power-law, represented by the blue curve, was fitted by Fischer & Valenti (2005), only for stars with positive metallicities. This fit provides the relation: frequency $= 3.01 \cdot 10^{2.04[Fe/H]}$.

The observed metallicity correlation does not imply that giant planets cannot be formed around more metal-poor stars, but it does imply that the probability of formation around these stars is lower (Rice & Armitage 2003; Ida & Lin 2004). Indeed, as seen in the left panel of Figure 1.11, there is some hint that for lower metallicity, the frequency of planets may be constant (Santos et al. 2004). For the negative metallicities, a constant is fitted, represented by the red curve. Fitting one single power-law to the whole range of metallicities turned out to be very difficult. This suggests that there may be two regimes of planet formation (Santos et al. 2004). This is however still under debate (see Chapter 3).

For low-mass planets this correlation does not seem to exist. For Neptune-mass planets, it appears that the metallicity distribution is flat (Mayor et al. 2011; Sousa et al. 2011; Buchhave et al. 2012, see also the right panel of Figure 1.11). Although the statistics are based on a low number of planets, the existence of this non-correlation is most likely real since some Neptunes were detected through follow-up observations of known giant planet hosts. This would essentially bias the results towards higher metallicities.

These observed correlations that the frequency of giant planets is an increasing function of metallicity and the Neptune-mass planet frequency is not metallicity-dependent favors the core-accretion model (Ida & Lin 2004; Udry & Santos 2007; Mordasini et al. 2009). In the case of giant planets, higher metallicity means a higher grain content of the disk which would make it easier to build the cores that will later accrete gas. Figure 1.12 represents the results of planet synthesis models where it can be seen that Neptune-mass planets are common around all stars, while higher mass planets prefer metal-rich stars and lower mass planets prefer metal-poor stars. According to the instability model, the presence of planets would not be dependent on stellar metallicity (Boss 2002)[9]. It is worth to note here that the possible existence of a constant fit for giant planet frequency at low metallicities, means that

[9]However, see also Cai et al. (2006) who predict an anti-correlation between giant planet frequency and metallicity.

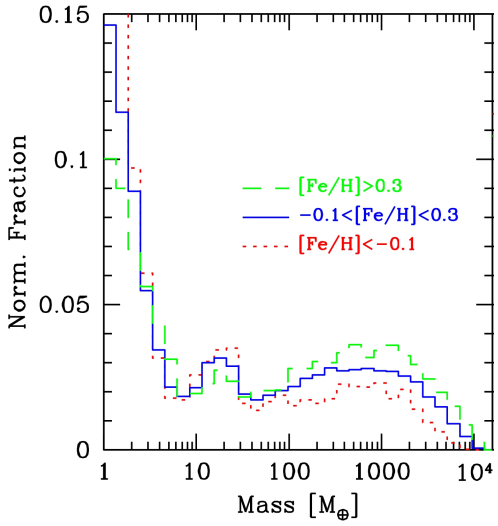

Figure 1.12: Planet frequency as a function of planetary mass for different metallicity regimes (taken from Mordasini et al. 2012a).

gravitational instability is the preferred formation mechanisms for these iron-poor stars.

Stellar mass

Planet frequency is also believed to depend on the protoplanetary disk properties. These properties depend in their turn on the stellar mass (see e.g. Szűcs et al. 2010; Williams & Cieza 2011, and references therein). Since stellar masses are overall easier to derive than disk properties, scientists have tried to relate planet frequency with stellar mass. In contrast with the quick discovery of the metallicity correlation, a possible correlation with stellar mass was only found much later. Statistical studies suggested a slight tendency for higher mass stars (up to $\sim 1.5 M_{\odot}$) to have a higher frequency of planets (Laws et al. 2003).

For FGK dwarfs, the mass range is fairly narrow. Planetary searches around M dwarfs revealed less giant planets than what would be expected from the results of the FGK dwarfs. Despite long and elaborate searches for planets around M dwarfs, only a few Jupiters were found, in contrast with the several detected Neptunes (Butler et al. 2006; Bonfils et al. 2007). At the high-mass regime, the opposite phenomenon has been witnessed as plenty of Jovians were detected around massive stars (e.g. Bowler et al. 2010). Planet frequency is thus most likely correlated with metallicity and stellar mass. Disentangling the effects coming from both parameters is not always so straightforward. Careful analyses must therefore be done on planetary samples.

Furthermore, Lovis & Mayor (2007) found a relation between planetary mass and stellar mass. Figure 1.13 represents the average planetary mass for 3 stellar mass bins. A clear increasing

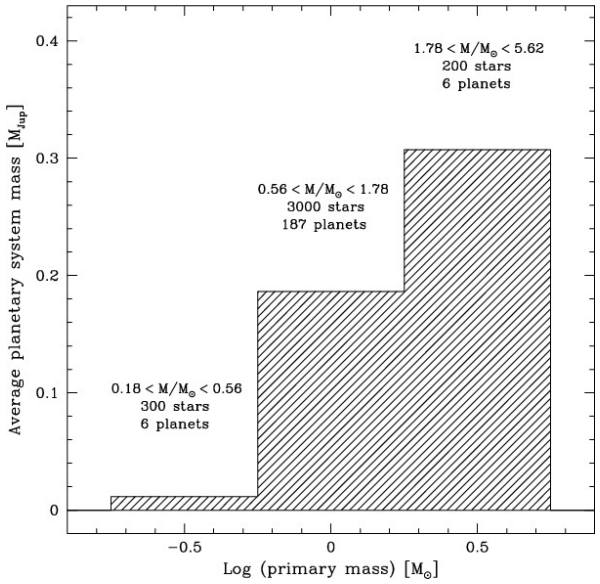

Figure 1.13: Average planetary mass as a function of stellar mass (taken from Lovis & Mayor 2007).

trend can be seen. This result is also expected from the core-accretion model (e.g. Ida & Lin 2005), since more massive stars would have more massive disks providing more material to form heavier planets. However, population synthesis simulations do expect the effect to be lower than can be seen in Figure 1.13 (Alibert et al. 2011). It is not clear how stellar mass would influence the planet frequency if planets are formed through gravitational instability, but Boss (2006) does not expect a correlation.

A word of caution should be placed here. Stellar metallicities can be determined with high precision and accuracy, using high-resolution spectra. Stellar masses however are not that precisely determined through spectroscopy. In Section 1.3.3, we explained that stellar masses are usually determined through stellar evolution models or calibration formulae. Both these models and the calibrations suffer from uncertainties. Besides, these methods all depend on previously determined parameters which also have uncertainties. Using asteroseismology provides much more precise measurements for the stellar mass (e.g. Bruntt et al. 2010; Huber et al. 2013). Upcoming missions such as Gaia will provide high-quality asteroseismic data that can be used for this purpose.

1.4 Contents and approach

This thesis presents mainly the results of a study of the correlation between giant planet frequency and metallicity for different types of stars. Furthermore, the need and importance of precise stellar parameters is emphasised and explored. The work is presented in the form of refereed and accepted publications, as they are published by the journal, from the last three years. The structure of this thesis is as follows:

Chapter 2: Giant planet frequency around metal-poor stars is explored. Herefor, I used two stellar samples of metal-poor FGK dwarfs, that are used for planet searches. The stars were observed with HARPS (3.6m, La Silla, Chile) and HIRES (Keck, Hawaii, USA). Detection limits that are present in these samples are calculated, using a periodogram analysis. Finally, giant planet frequencies are calculated for these metal-poor stars.

Chapter 3: It has been clear for a long time that giant planet frequency and metallicity are exponentially correlated. At least, this is the case for metal-rich stars. The metallicity dependence for metal-poor stars (exponential or constant) and the possible involvement of stellar mass are explored here. I use a Bayesian analysis to distinguish between the different functional models to describe giant planet frequency.

Chapter 4: The same increasing metallicity trend that is present in dwarf stars with planets, can not always be seen in subgiant and giant stars. In this work, I test different linelists for the derivation of stellar atmospheric parameters for (sub)giant stars. With these uniform parameters, specifically the metallicity, I investigate if the same metallicity trend can also be seen for (sub)giants.

Chapter 5: Precise stellar parameters are crucial for the precise determination of planetary parameters. Spectroscopic surface gravities, however, are not precisely determined. Using a sample of transit hosts, these surface gravities are derived again based on the stellar density, taken from the light curve. I explore the effect of the surface gravity on the stellar mass and radius determinations, and thus the planetary parameters.

Chapter 6 will handle the overall conclusions of these works and discuss some future work that can, and hopefully will, be done. Appendix A describes in more detail some of the methods I used for this work. This thesis is finally concluded with a list of publications, relevant to this work, of which I am a (co-)author, in Appendix B.

Chapter 2

The frequency of giant planets around metal-poor stars

Foreword

As first part of my research, I focused on metal-poor stars, specifically FGK dwarfs. It was already clear that the presence of giant planets correlates with metallicity. Dedicated planet searches around metal-rich stars were therefore undertaken (e.g. Fischer et al. 2005) to increase the chances of finding exoplanets. However, searches around metal-poor stars were still happening also. For this work, I combined two radial velocity planet search samples of metal-poor stars (Sozzetti et al. 2009; Santos et al. 2011).

A detailed study of the inherent detection limits in these data was undertaken, based on the GLS periodogram (see Appendix A). With these limits, I calculated planet frequencies for giant planets and hot jupiters in particular using a binomial distribution function (see Appendix A). This work has been peer-reviewed and published in Astronomy & Astrophysics.

A&A 543, A45 (2012)
DOI: 10.1051/0004-6361/201118651

Astronomy & Astrophysics

The frequency of giant planets around metal-poor stars⋆,⋆⋆,⋆⋆⋆

A. Mortier[1], N. C. Santos[1,2], A. Sozzetti[3], M. Mayor[4], D. Latham[5], X. Bonfils[6], and S. Udry[4]

[1] Centro de Astrofísica, Universidade do Porto, Rua das Estrelas, 4150-762 Porto, Portugal
e-mail: amortier@astro.up.pt
[2] Departamento de Física e Astronomia, Faculdade de Ciências, Universidade do Porto, Portugal
[3] INAF – Osservatorio Astronomico di Torino, strada dell'Osservatorio 20, 10025 Pino Torinese, Italy
[4] Observatoire de Genve, Université de Genève, 51 Ch. des Maillettes, 1290 Sauverny, Switzerland
[5] Harvard-Smithsonian Center for Astrophysics, 60 Garden Street, Cambridge, MA 02138, USA
[6] UJF-Grenoble 1/CNRS-INSU, Institut de Planétologie et d'Astrophysique de Grenoble (IPAG) UMR 5274, 38041 Grenoble, France

Received 15 December 2011 / Accepted 11 May 2012

ABSTRACT

Context. The discovery of about 700 extrasolar planets, so far, has lead to the first statistics concerning extrasolar planets. The presence of giant planets seems to depend on stellar metallicity and mass. For example, they are more frequent around metal-rich stars, with an exponential increase in planet occurrence rates with metallicity.
Aims. We analyzed two samples of metal-poor stars ($-2.0 \leq$ [Fe/H] ≤ 0.0) to see if giant planets are indeed rare around these objects. Radial velocity datasets were obtained with two different spectrographs (HARPS and HIRES). Detection limits for these data, expressed in minimum planetary mass and period, are calculated. These produce trustworthy numbers for the planet frequency.
Methods. A general Lomb-Scargle (GLS) periodogram analysis was used together with a bootstrapping method to produce the detection limits. Planet frequencies were calculated based on a binomial distribution function within metallicity bins.
Results. Almost all hot Jupiters and most giant planets should have been found in these data. Hot Jupiters around metal-poor stars have a frequency lower than 1.0% at one sigma. Giant planets with periods up to 1800 days, however, have a higher frequency of $f_{\rm p} = 2.63^{+2.5}_{-0.8}$%. Taking into account the different metallicities of the stars, we show that giant planets appear to be very frequent ($f_{\rm p} = 4.48^{+4.04}_{-1.38}$%) around stars with [Fe/H] > -0.7, while they are rare around stars with [Fe/H] ≤ -0.7 ($\leq$2.36% at one sigma).
Conclusions. Giant planet frequency is indeed a strong function of metallicity, even in the low-metallicity tail. However, the frequencies are most likely higher than previously thought.

Key words. techniques: radial velocities – planetary systems – planets and satellites: formation – stars: abundances – stars: statistics

1. Introduction

Since the discovery of the first extrasolar planet in 1995 (51 Peg b, Mayor & Queloz 1995), the search for extrasolar planetary systems accelerated. Today, around 750 planets are announced. Most of them were detected using the radial velocity technique. Although 750 is a relatively high number, the theory of planet formation and evolution is still under debate (Pollack et al. 1996; Mayer et al. 2002; Mordasini et al. 2009). The situation is particularly difficult for giant planet formation. Currently, there are two proposed models: core-accretion (e.g. Pollack et al. 1996; Rice & Armitage 2003; Alibert et al. 2004), where gas from the protoplanetary disk is accreted around a previously formed rocky/icy core, and the disk instability model (e.g. Boss 1997; Mayer et al. 2002), where a planet is formed because of a direct gravitational instability in the protoplanetary disk, in the same way as stars form from interstellar clouds. A helpful overview of both models is given by Matsuo et al. (2007).

One of the main advantages of the instability model is the timescale that is needed to form the planets. Early results suggested that the slow accretion phase (about 10 Myr) in the core-accretion model may take longer than the lifetime of a T Tauri disk (Pollack et al. 1996). In that sense, giant planets could not form within the core-accretion model. However, more recent results suggest that this may not be a real problem. In fact, it has been shown that the process can, for example, be accelerated by including disk-induced orbital migration (Alibert et al. 2004; Mordasini et al. 2009).

Theories of migration became more important with the discovery of 51 Peg b and other *hot Jupiters*. These close-in giant planets are highly unlikely to have formed in situ. Interestingly, however, disk-induced migration does not necessarily provide the correct explanation for all these hot Jupiters. Other ideas have been put forward (e.g. Triaud et al. 2010; Morton & Johnson 2011; Socrates et al. 2012), which include more "violent" migration mechanisms. Discoveries of giant planets on wide orbits of tens to hundreds AU (Marois et al. 2008; Lagrange et al. 2010) also raise questions. Overall there is still space to support that the disk-instability model may be at work, at least

⋆ The data presented herein are based on observations collected at the La Silla Parana Observatory, ESO (Chile) with the HARPS spectrograph at the 3.6-m telescope (ESO runs ID 72.C-0488, 082.C-0212, and 085.C-0063) and at the W. M. Keck Observatory that is operated as a scientific partnership among the California Institute of Technology, the University of California and the National Aeronautics and Space Administration. This Observatory was made possible by the generous financial support of the W. M. Keck Foundation.
⋆⋆ Full Table 1 is only available at the CDS via anonymous ftp to cdsarc.u-strasbg.fr (130.79.128.5) or via http://cdsarc.u-strasbg.fr/viz-bin/qcat?J/A+A/543/A45
⋆⋆⋆ Appendix A is available in electronic form at http://www.aanda.org

Table 1. Relevant values for the targets in the two samples.

Star	n	Mean rms [m s^{-1}]	Timespan [days]	$T_{\rm eff}$ [K]	[Fe/H]	M_* [$M_\odot$]	Reference
HD 123517	9	3.02	1596	6082 ± 29	0.09 ± 0.02	1.21 ± 0.08	(1)
HD 124785	17	2.01	1518	5867 ± 21	−0.56 ± 0.01	0.87 ± 0.02	(1)
HD 126681	13	2.23	1964	5570 ± 34	−1.15 ± 0.03	0.71 ± 0.02	(1)
G15-7	6	9.27	890	5280	−0.88	0.74	(2)
G151-10	7	10.91	891	5287	−0.70	0.76	(2)
G157-93	3	4.43	115	5409	−0.78	0.78	(2)
...	...	...	...	...	...	...	...

Notes. The complete table is provided in electronic form at the CDS.

References. (1) Sousa et al. (2011a); (2) Sozzetti et al. (2009).

to explain part of the detected planets (Vorobyov & Basu 2010; Boss 2011).

Additional clues about this problem come from the analysis of planet-host stars. The presence of a planet seems to depend on several stellar properties, such as mass and metallicity (Udry & Santos 2007). Concerning metallicity, it has been well-established that more metal-rich stars have a higher probability of harboring a giant planet than their lower metallicity counterparts (Gonzalez 1997; Santos et al. 2001, 2004; Fischer & Valenti 2005; Udry & Santos 2007; Sozzetti et al. 2009; Sousa et al. 2011b). The occurrence rate even increases dramatically with increasing metallicity. Current numbers, based on the CORALIE and HARPS samples, suggest that around 25% of the stars with twice the metal content of our Sun are orbited by a giant planet. This number decreases to ∼5% for solar-metallicity objects (Sousa et al. 2011b; Mayor et al. 2011). A similar trend was also obtained by previous results (e.g. Santos et al. 2004; Fischer & Valenti 2005; Johnson et al. 2010). Curiously, no such trend is observed for the lower mass planets (Udry et al. 2006; Sousa et al. 2008; Mayor et al. 2011). The Neptune-mass planets found so far seem to have a rather flat metallicity distribution (Sousa et al. 2008, 2011b; Mayor et al. 2011).

This observed metallicity correlation favors the core-accretion model for the formation of giant planets (Ida & Lin 2004; Udry & Santos 2007; Mordasini et al. 2012) because the higher the grain content of the disk, the easier it is to build the cores that will later accrete gas. According to the disk-instability model, the presence of planets would not be strongly dependent on stellar metallicity (Boss 2002).

Understanding the frequency of different types of planets around stars of different mass and metallicity is thus providing clues about the processes of planet formation and evolution. This has inspired the construction of specific samples to search for planets around different types of stars (e.g. Santos et al. 2007; Sato et al. 2008; Sozzetti et al. 2009). Statistics of these samples will help in understanding the formation processes and constrain the models.

We present an analysis of two metal-poor samples that were designed for planet-finding purposes. In Sect. 2, an overview is given of the samples and their data. Section 3.1 reports on the detection limits of these samples. Planet frequencies are calculated in Sect. 4. Finally, conclusions are made in Sect. 5, together with a discussion.

2. Data

Radial velocity measurements from two different samples of metal-poor, solar-type stars were used in this paper.

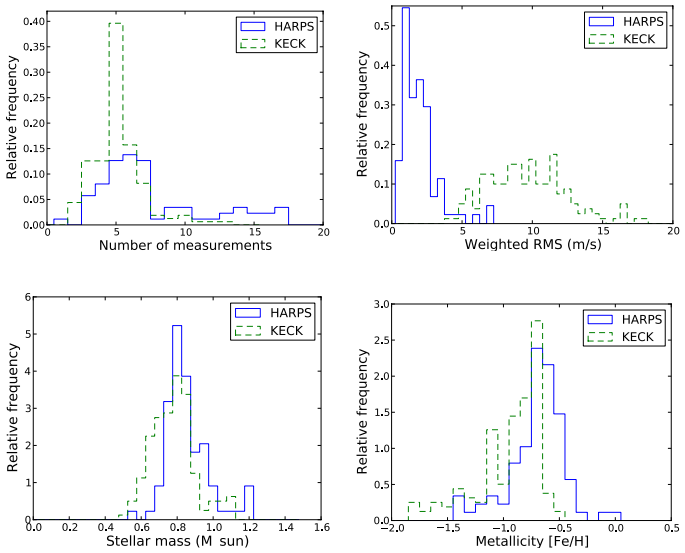

Fig. 1. Relative histogram of the number of measurements (*top left panel*), rms noise (*top right panel*), stellar mass (*bottom left panel*) and metallicity (*bottom right panel*) in the two datasets. The blue line represents the HARPS sample, the green line the KECK-HIRES sample. Both graphs in the top panel are cut at 20 for better visibility. The *top left panel* has 19 stars from the HARPS sample higher then 20. The *top right panel* has 1 star from the KECK sample higher then 20.

2.1. The HARPS sample

Santos et al. (2011) reported on the first sample. They observed 104 metal-poor or mild metal-poor solar-type stars with the HARPS spectrograph (Mayor et al. 2003). The objects were observed from October 2003 till July 2010. Based on the catalog of Nordström et al. (2004), all late-F, G and K stars south of +10° declination with a V magnitude brighter than 12 were chosen. After discarding spectroscopic binaries, giant stars and active stars, Santos and coworkers only recovered the 104 stars with an estimated photometric [Fe/H] between −0.5 and −1.5. After the observations, 16 stars were also discarded because they were unsuitable targets for planet-finding purposes (binarity, activity, high rotation). Most of the stars in the final sample of 88 stars have five or more measurements with an rms of ∼1−2.5 m s^{-1} as shown in Fig. 1 and Table 1. In the bottom panels of Fig. 1, the mass and metallicity distribution is shown. Values were taken from Sousa et al. (2011a). The (spectroscopic) metallicities differ slightly from the photometric estimate that was initially used, including a few outliers. All values are listed in Table 1.

Table 2. Names and number of measurements of stars that are present in the two samples.

Name HARPS	n_H	Name KECK	n_K
BDp062932	4	G66-22	4
BDp083095	3	G16-13	5
HD 104800	6	G11-36	4
HD 111515	5	G14-5	7
HD 126681	13	HD 126681	6
HD 131653	4	G151-10	7
HD 134440	10	HD 134440	6
HD 148211	31	HD 148211	3
HD 148816	6	HD 148816	10
HD 193901	3	HD 193901	5
HD 196892	3	HD 196892	5
HD 215257	37	G27-44	8
HD 22879	36	G80-15	5
HD 88725	22	G44-6	5

Three planetary mass companions were found in this sample. They are orbiting HD 181720, HD 190984 (Santos et al. 2010), and HD 171028 (Santos et al. 2007). All three are giant planets in long-period orbits. A fourth planet candidate, orbiting HD 107094, was announced in Santos et al. (2011). With a 4.5 $M_{\rm Jup}$ minimum mass and a 1870 day period, it would again be a giant planet in a long-period orbit. However, this planet could not be fully confirmed yet.

2.2. The KECK-HIRES sample

Sozzetti et al. (2009) reported on the second sample. They observed 160 metal-poor solar-type stars with the HIRES spectrograph on the Keck 1 telescope at Mauna Kea in Hawaii (Vogt et al. 1994). The objects were all observed at least twice over a timespan of three years (2003−2006). This sample of stars was drawn from the Carney-Latham and Ryan samples (e.g. Carney et al. 1994; Ryan 1989). Additional criteria were applied, and in the end, Sozzetti and collaborators chose the 160 stars with a V magnitude brighter than 12, an effective temperature $T_{\rm eff}$ lower than 6000 K and a metallicity [Fe/H] between −0.4 and −1.8. All stars are situated north of −25° declination. Most stars in this sample have 4 to 10 measurements with a rms of ∼9 m s^{-1} as seen in Fig. 1 and Table 1. Photon noise is the main contributor to these higher rms values. The mass and metallicity values, seen in this figure, are taken from Sozzetti et al. (2009). All values are listed in Table 1. Typical uncertainties on $T_{\rm eff}$, [Fe/H], and M_* are 100 K, 0.1 dex, and 0.1 $M_\odot$ respectively.

No planetary signals were found in this sample.

2.3. The combined sample

Fourteen (14) stars have measurements in both samples. This amounts to a complete sample of 234 metal-poor solar-type stars. The two samples use different naming for the stars (see Table 2). In this paper, the naming from the HARPS sample will be used for these 14 stars.

Combining the measurements of these stars provides more data to look for possible planetary signals. The data of two different telescopes were combined by subtracting the mean of the data from each set in the overlapping time-interval. A general Lomb-Scargle (GLS) periodogram analysis (see Sect. 3.1) was then performed on the 14 stars. No significant peaks were found in these periodograms.

3. Detection limits

3.1. Methodology

In the literature, different authors used two main approaches to find detection limits in RV data. One is based on χ^2- and F-tests (e.g. Lagrange et al. 2009; Sozzetti et al. 2009), another is based on a periodogram analysis (e.g. Cumming et al. 1999; Cumming 2004; Endl et al. 2001; Narayan et al. 2005). In this paper, the second approach was chosen because we consider that we have enough measurements for a reliable periodogram analysis (see below for a comparison of the methods).

A frequency analysis of unevenly sampled data (like RV data) can be performed by using the GLS periodogram (Scargle 1982; Zechmeister & Kürster 2009). The GLS is equivalent to a least-squares fitting of a full sine-wave, including weights and an offset, representing a circular orbit. In the resulting periodogram, the power $p(\omega)$ is calculated as a function of frequency. This power measures how much the fit to the measurements improves by using a sinusoid instead of a constant. This analysis can also be performed by replacing the "sine-wave" with a Keplerian function. An example of a GLS periodogram for a Keplerian fit is shown in Fig. 2 (top panel). This plot refers to a GLS of the RV data of HD 134440, a star that has 16 measurements with an average rms of 4.9 m s^{-1} and a timecoverage of 1885 days. We used both the circular and Keplerian approach.

The significance of a peak in the GLS periodogram can be determined analytically. However, not all values, like the number of independent frequencies, are properly determined in this way (Zechmeister & Kürster 2009). Alternatively, the significance can be accessed if we use a bootstrapping method (e.g. Endl et al. 2001; Dumusque et al. 2011). Multiple time series of radial velocities are made by shuffling (with repetition) the real radial velocities while preserving the original times. On each virtual time series, a GLS is performed to determine the highest peak (frequency independent) in the periodogram. This can be used to determine the percentage of bootstrapped periodograms with maximum peaks above the one observed in the GLS of the actual data. This procedure allows us then to derive the false alarm probability (FAP) level (see top panel Fig. 2). For this work, we have chosen to adopt 1000 bootstrapping series to estimate the significance of the peaks.

Detection limits in RV data are derived by inserting a fake planetary signal in the data (circular or Keplerian). The procedure goes as follows. Virtual time series are made by adding these signals to the original data, which are treated as random noise. For a circular orbit, a fake signal

$$y(t) = K \sin\left[\frac{2\pi}{P}t + \varphi\right] + c \qquad (1)$$

is added to the original data. Virtual series were made for periods P from 0.5 to 3000 days, semi-amplitudes K from 0 to 10 km s^{-1} and ten phases φ, evenly separated by $\pi/10$. On each series, a GLS periodogram is performed. For each period, a signal is considered detected if the periodogram gives a peak at that period with a FAP of 1% for all 10 phases. The minimum semi-amplitude K for which a signal is detected expresses the lower limit for detectable planets in these data.

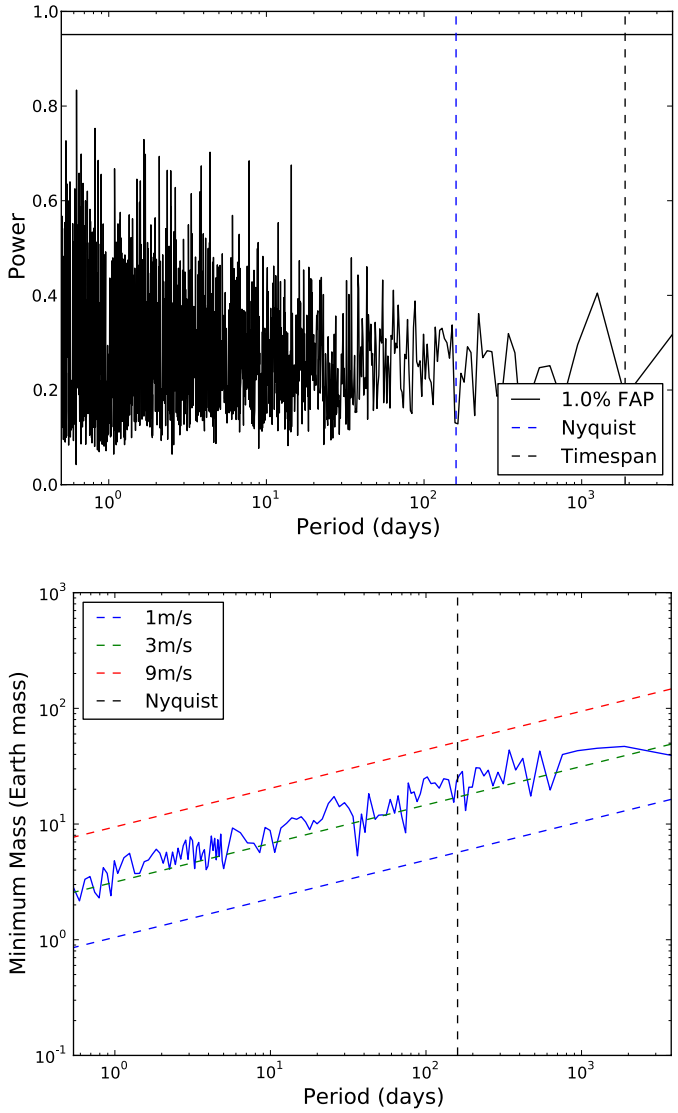

Fig. 2. Example of the GLS periodogram (*top panel*) and the detection limits (*bottom panel*) for the star HD 134440 with measurements from HARPS and KECK-HIRES. For both plots, a Keplerian fit was made. In the top panel, the power is plotted against the period. The horizontal solid line marks the power level for an FAP of 1%. The bottom panel plots the minimum planetary mass against the period. The solid line represents the detection limits for these data. The dashed lines indicate a circular planetary signal with an RV semi-amplitude of 1, 3 and 9 m s^{-1} (lower to higher line).

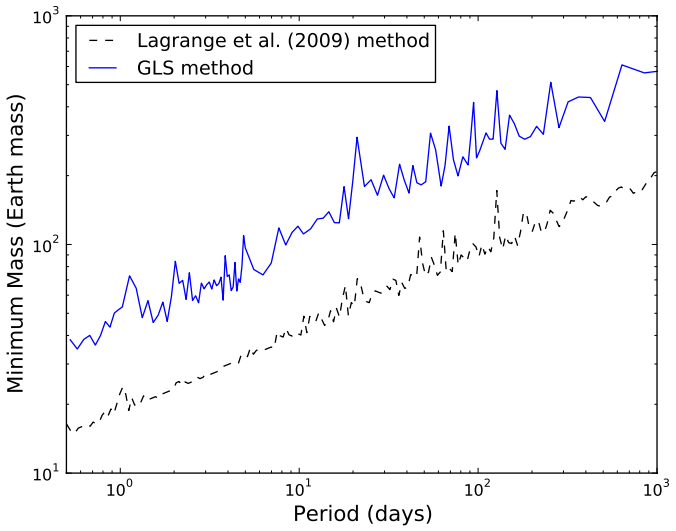

Fig. 3. Planetary mass is plotted against period for G19-27 (Keck sample). The blue (upper solid) line shows the detection limits for circular planetary signals in the data with a FAP of 1%. The black (lower dashed) line shows the detection limits based on the method described in Lagrange et al. (2009).

The same approach can be taken for eccentric Keplerian signals. The fake signal, added to the original data, can in this case be described as follows:

$$y(t) = a\cos\nu(t) + b\sin\nu(t) + c, \tag{2}$$

with $a = K\cos\varpi$, $b = -K\sin\varpi$ and $c = Ke\cos\varpi+\gamma$. Here, K is the RV amplitude, e the eccentricity, ϖ the longitude of periastron, γ the constant system RV and $\nu(t)$ the true anomaly. This true anomaly is a function of t, e, P and T_0, the time of periastron passage. Again, virtual series were made for periods P from 0.5 to 3000 days and semi-amplitudes K from 0 to 10 km s^{-1} were tried. For each period and semi-amplitude, 1000 virtual signals were created, with 10 different eccentricities e (between 0 and 1), 10 different longitudes of periastron ϖ (between 0 and 2π) and 10 different times of periastron T_0 (between 0 and P), all evenly separated. In this case, a planet at a specific period P is considered detected if the periodogram gives a peak with a FAP of 1% for all 1000 signals.

The minimum semi-amplitudes can then be transformed into planetary masses (expressed in Earth mass) with the following formula:

$$M_{\rm p}\sin i = 7.4\times10^{-24}K\sqrt{1-e^2}\left(\frac{PM_*^2}{2\pi G}\right)^{1/3}, \tag{3}$$

where the semi-amplitude K is expressed in m/s, the period P in days, the stellar mass M_* in kg and the gravitational constant G in m^3 kg^{-1} s^{-2}. An example of these detection limits for HD 134440 is shown in Fig. 2 (bottom panel). A Keplerian signal was inserted to obtain these limits.

As a comparison, for some stars, the detection limits were also calculated following the method described in Lagrange et al. (2009). Virtual RV sets are created with the expected RVs for a circular orbit, added with a random noise between ±RV error, where the RV error is the mean error of the real data. For every given period considered (between 0.5 and 1000 days), 200 virtual data sets were taken by varying the phase of the signal. This was then performed for different semi-amplitudes till the signal was detected. A signal was considered detected if the standard deviation of the real RV measurements was less than the average value of the virtual standard deviations. This resulted in detection limits with overall the same shape, but a factor of 2.5 lower, as can be seen in Fig. 3. This shift can be explained by the fact that the periodogram analysis used in this work is more conservative in its definition of detectability, because it needs a peak above the 1% FAP level for all phases. Because the overall shape is the same, the conservative periodogram analysis is favored for the purposes of this work.

Note that in all these analyses, a circular (resp. Keplerian) fit to RV data needs at least four (resp. seven) measurements. To be more conservative, the choice was made for at least six (resp. ten) measurements for the analysis.

3.2. Stars with at least six measurements

Detection limits based on a circular fit were made only for stars with at least six measurements. This resulted in 64, 50, and 114 stars (72.7, 31.25, and 48.7%) for the HARPS, KECK-HIRES, and the combined sample, respectively.

The long-period signals (longer than the timespan of the measurements) produce a high-amplitude power in the GLS periodograms. To analyze the data for the presence of "shorter" period peaks, it is consequently necessary to remove these. A linear function was fitted to the RV data of each star, using a least-squares fit. If the correlation coefficient r^2 was greater than 0.7, the linear fit was considered relevant and subtracted from the original data. This was the case for HD 107094, HD 11397, HD 215257, HD 123517, HD 88725, HD 144589, and HD 113679 in the HARPS sample, G135-46, G63-5, G197-45, HD 134439, G237-84, HD 192718, HD 215257, HD 7424, and G63-44 in the KECK-HIRES sample and all these objects together with HD 193901 in the combined sample. The planetary signals from the three confirmed planets in the HARPS sample (with the parameters taken from Santos et al. 2011) were also subtracted, because we did not aim to confirm their existence but rather to search for additional signals.

Figure 4 displays the detection limits for circular planetary signals in the three samples. Minimum planetary mass is plotted against period. The limits shown in the figure correspond to the values for which a signal can be detected in 80% and 95% (blue and green curve, respectively) of the stars in the sample. For clarity, we also include two dashed lines at Jupiter mass and at 50 $M_{\oplus}$, a value close to the generally accepted lower limit for giant planets. From these plots, it is clear that at a 80% level no hot Jupiters (here defined as having an orbital period <10 days) could have been missed in the HARPS sample, though none was detected. In the KECK and the combined sample, most hot Jupiters should have been found.

3.3. Stars with at least ten measurements

For stars with at least ten measurements, the detection limits were also calculated for Keplerian signals. This was mainly useful for the HARPS sample, where more stars have dozens of measurements. In the HARPS, KECK-HIRES, and combined sample, respectively, there are 37, 7 and 47 stars (42, 4.4 and 20.1%) with at least ten measurements.

Figure 5 displays the Keplerian detection limits for the HARPS sample. The same trends and planetary signals as for the circular fit were subtracted before the analysis. The limits are for a 80% and 95% sample completeness (blue and green curve, respectively). The limits for the KECK sample are not shown because there are too few stars in the sample with at least ten measurements. Again, it is clear that no hot Jupiters were missed in the HARPS sample. The same is true for the combined sample. Note also that our data in the HARPS sample are sensitive to the detection of planets with masses above that of Jupiter for the whole covered period range.

4. Planet frequency

With these limits and the number of planets found in the samples, a statistical analysis can be made of the giant planet frequency as a function of stellar metallicity. There are again several approaches to perform this analysis, among which the two main ones are a binning approach and a parametric approach (see below). The former makes use of a binomial distribution.

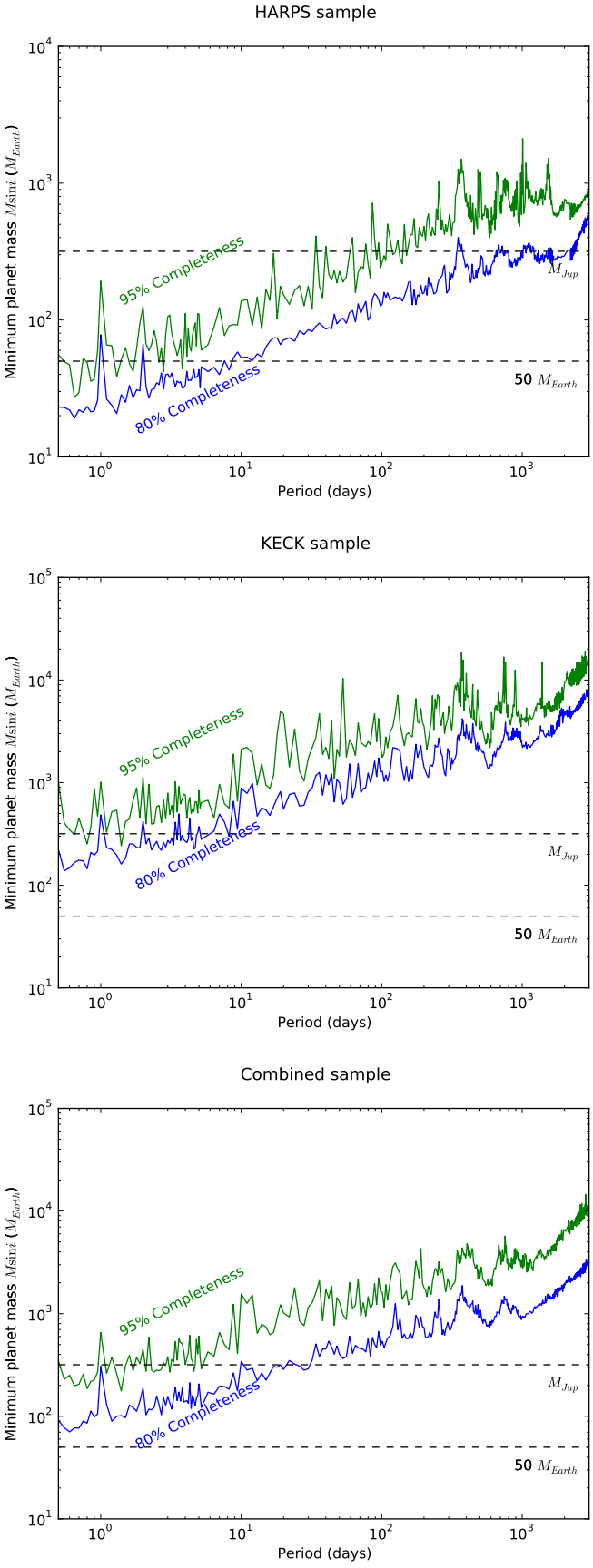

Fig. 4. Planetary mass is plotted against period. The blue line shows the detection limits for circular planetary signals in the data with a FAP of 1%. In the *top panel*, the data from the HARPS sample are shown. In the *middle panel* the data from the KECK-HIRES sample are shown and in the *bottom panel*, the combined sample is shown.

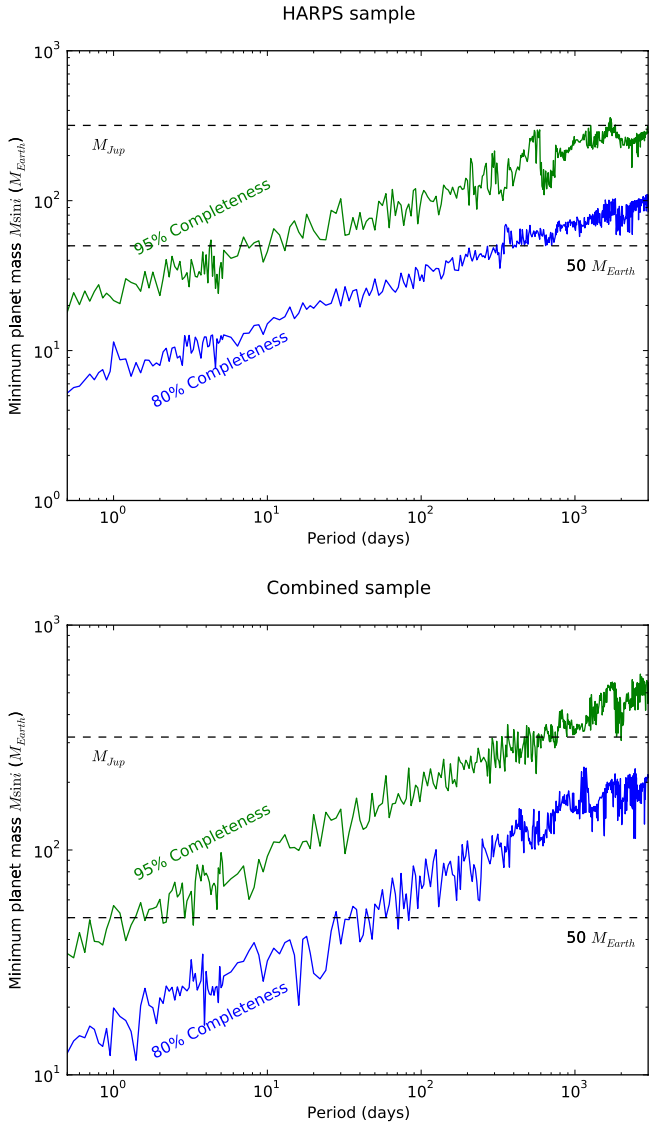

Fig. 5. Planetary mass is plotted against period. The blue line shows the detection limits for Keplerian (non-circular) planetary signals in the data with a FAP of 1%. In the *top panel*, the data from the HARPS sample are shown and in the *bottom panel*, the combined sample is shown.

The probability of finding n detections in a sample of size N can be calculated as a function of the true planet frequency f_p:

$$P\left(f_\mathrm{p}; n, N\right) = \frac{N!}{n!(N-n)!} f_\mathrm{p}^n \left(1 - f_\mathrm{p}\right)^{N-n}. \quad (4)$$

This method is described in the appendix of Burgasser et al. (2003). For this asymmetric distribution, the errorbars can be computed by measuring the range in f_p that covers 68% of the integrated probability function. This is equivalent to the 1-sigma errorbars for a Gaussian distribution.

As seen above, no hot Jupiters were found in our samples, while the detection limits indicate that they most likely should have been detected. Zero (0) detections in a sample of 114 stars (stars in the combined sample with at least six measurements) leads to a frequency $f_\mathrm{p} \leq 1.00\%$ (calculated from $f_\mathrm{p} = 0.37^{+0.6}_{-0.4}$). The frequency rises to $f_\mathrm{p} \leq 2.36\%$ if only the 47 stars with at least ten measurements are taken into account.

For giant planets in general (i.e. planets with a mass higher than 50 M_Earth), there are three detections in a sample of

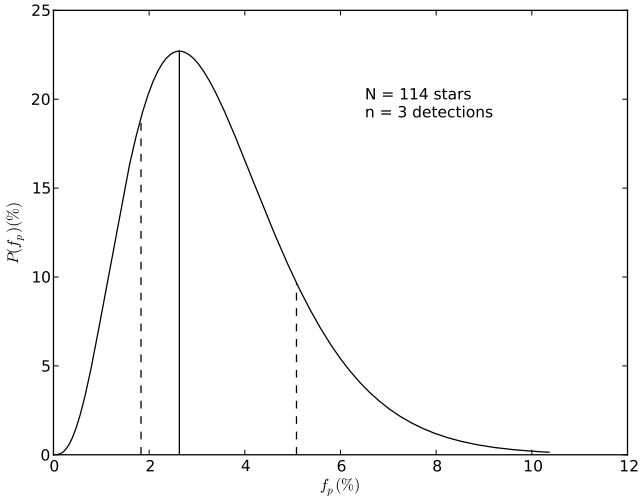

Fig. 6. Probability as a function of true planet frequency for a given amount of detections n and sample size N. The solid vertical line denotes the observed planet frequency, while the dashed lines show the limits of the centered 68% area, thus expressing the 1-sigma errorbars.

114 stars, which gives a frequency $f_\mathrm{p} = 2.63^{+2.5}_{-0.8}\%$ (see Fig. 6). In this sample of stars, 90% have timespans longer than 900 days. This makes these frequencies sensitive to planets with periods up to 1800 days. If the sample is limited to only the 47 stars with at least ten measurements, the frequency becomes $f_\mathrm{p} = 6.38^{5.6}_{-2.0}\%$. For this smaller sample, this frequency is sensitive to planets with periods up to 2600 days.

Our sample has a metallicity distribution that peaks around −0.7 dex. If we divide it into two parts (above and below this limit), we find that on the high-metallicity side there are 67 (resp. 35) stars with at least six (resp. ten) measurements. This is also the side of the distribution of the detected giant planets. This thus leads to percentages of $f_\mathrm{p} = 4.48^{+4.04}_{-1.38}\%$ (resp. $f_\mathrm{p} = 8.57^{+7.21}_{-2.69}\%$). Around the stars in our sample with metallicities lower than −0.7 (47 stars with at least six measurements), no planets were detected. This again gives a frequency of $f_\mathrm{p} \leq 2.36\%$. To check if the values are dependent on the choice of the bins, we repeated the calculation changing the position of the bins by 0.1 dex (the typical 3-sigma error of the individual metallicity estimates), thus changing the high (low) metallicity side of the distribution to cover the range of [Fe/H] > −0.8 dex (≤−0.8 dex, respectively). In these bins, the planet frequencies for stars with at least six measurements become $f_\mathrm{p} = 3.70^{+3.39}_{-1.13}\%$ resp. $f_\mathrm{p} \leq 3.32\%$. Both results are comparable within the errorbars.

Alternatively, a parametric approach, similar to the one used by Johnson et al. (2010), was also considered. Here, the data are fitted with a functional form, dependent on stellar metallicity. As a functional form, we chose

$$f_\mathrm{p} = C \times 10^{\beta[\mathrm{Fe/H}]}, \quad (5)$$

which is typically used for solar neighbourhood samples. The best parameters (β, C) are then determined by using a numerical fitting procedure, based on Bayesian inference. Details of this procedure can be found in Johnson et al. (2010). As a prior, the choice was made for uniformly distributed parameters over $[0.0, 3.0]$ and $[0.01, 0.30]$ for β and C, respectively. The best parameters were found to be $\beta = 1.3$ and $C = 0.17$. The mean metallicity for stars with six measurements and a metallicity higher than −0.7 dex, is −0.55 dex. For the derived β and C,

the corresponding expected frequency would be 3.29%, compatible with the results of the binning procedure. Owing to the limited size of the sample and because we are exploring a metallicity regime not previously explored with high-precision radial velocities, it is unclear which appropriate functional form should be used.

5. Conclusions and discussion

Radial velocities of two samples of metal-poor solar-type stars, taken with two different instruments (HARPS and KECK-HIRES), were used to detect extrasolar planets. Only three giant long-period planets were found out of the 234 stars, together with one giant candidate. Fourteen stars were present in both samples, but the expanded datasets and extended baseline of the observations did not reveal any additional signals.

After subtracting linear trends or planetary signals, detection limits in the samples were calculated. The method was based on a GLS periodogram analysis and bootstrapping. Limits were calculated for circular and Keplerian signals. These lower limits, as shown in Figs. 4 and 5, are expressed in minimum planetary mass and period. For the stars in the KECK sample, detection limits were already derived by Sozzetti et al. (2009). They used a method based on χ^2- and F-tests. The detection limits derived in this work perfectly agree with their results.

A statistical analysis was performed to estimate the planet frequency around metal-poor main-sequence stars. Taking into account only the stars with at least six measurements, we showed that the frequency of hot Jupiters around metal-poor stars is lower than 1.00%. This is consistent with previous studies (Udry & Santos 2007).

Giant planets, however, seem to be more frequent around these stars. The detection limits show that most of the giant planets should have been detected in this sample. A frequency of 2.63% for giant planets around metal-poor stars was calculated for stars with at least six measurements, with a sensitivity to periods up to 1800 days. If indeed a giant planet was missed in the sample, the frequency would be even higher. According to several studies (e.g. Santos et al. 2004; Fischer & Valenti 2005), 3% is the frequency of giant planets around stars of solar metallicity. Given the same number, derived in this work, for metal-poor stars, this can mean two things: either the planet frequency becomes constant for stars with [Fe/H] ≤ 0.0 (for a discussion, see also e.g. Santos et al. 2004; Udry & Santos 2007; Johnson et al. 2010) or previous frequency-models should be higher.

The metallicities of the stars with discovered giant planets all lie above −0.7 dex. Within this metallicity bin, the planet frequency increases to $4.48^{+4.04}_{-1.38}$%. For a metallicity of −0.55 dex and a stellar mass of 0.8 $M_\odot$ (mean value for this sample), previous studies report values of $f_\mathrm{p} = 1.22^{+0.7}_{-0.5}$% (Johnson et al. 2010) and $f_\mathrm{p} = 0.14$% (Sousa et al. 2011b). However, in both cases, a powerlaw was fitted over the whole metallicity range (up to 0.6 and 0.5 dex, respectively). In the low-metallicity end, their fit is clearly lower than their observed fraction (~4.6% and 3.77%, respectively). The value reported here is thus higher than previous fits, but consistent within one sigma with the observed fraction in these previous studies.

For stars with metallicities lower than −0.7, the frequency is lower than 2.36%. In this context, it is worth mentioning that so far, only one (giant) planet has been detected around a main-sequence star with metallicity lower than −0.6 dex (Cochran et al. 2007). There are some other candidates where planets orbit stars with metallicities lower than −0.6 dex (Niedzielski et al. 2009; Setiawan et al. 2003, 2010). These stars are all giants, however. Furthermore, there is a candidate planet detected by imaging that orbits a young main-sequence star with a metallicity of −0.64 dex (Chauvin et al. 2005). These planets are therefore not relevant for the purpose of this work.

All the above results are strong evidence that giant planet frequency is a non-constant function of stellar metallicity. This was already established for the high-metallicity tail, but this work shows that it is also true for lower metallicities. Moreover, the frequencies are probably higher than previously thought. A powerlaw may not be the best function to describe the planet frequency over the whole metallicity range. As mentioned before, this correlation between giant planet frequency and stellar metallicity favors the core-accretion model as the main mechanism for giant planet formation.

With the statistics presented in this work, a metallicity limit can be established below which no giant planets can be found anymore. According to these statistics, this metallicity limit would be about −0.5−−0.6 dex. This value agrees with the recent results of the theoretical study of Mordasini et al. (2012). These authors looked at correlations between stellar and planetary properties, based on a synthetic planet population, built by the core accretion model. They found that giant planets are not formed below −0.5 dex.

However, more data are still needed to produce better statistics. Future missions, such as *Gaia*, will produce better precision in the data. For example, in its all-sky global astrometric survey, *Gaia* will probe thousands of nearby metal-poor stars for gas giant planets within 3−4 AU (e.g. Sozzetti 2010), thus crucially helping to shed light on the planet-metallicity connection.

Acknowledgements. We thank the ananymous referee for his/her useful comments. This work was supported by the European Research Council/European Community under the FP7 through Starting Grant agreement number 239953. N.C.S. also acknowledges the support from Fundação para a Ciência e a Tecnologia (FCT) through program Ciência 2007 funded by FCT/MCTES (Portugal) and POPH/FSE (EC), and in the form of grants reference PTDC/CTE-AST/098528/2008 and PTDC/CTE-AST/09860/2008.

References

Alibert, Y., Mordasini, C., & Benz, W. 2004, A&A, 417, L25
Boss, A. P. 1997, Science, 276, 1836
Boss, A. P. 2002, ApJ, 567, L149
Boss, A. P. 2011, ApJ, 731, 74
Burgasser, A. J., Kirkpatrick, J. D., Reid, I. N., et al. 2003, ApJ, 586, 512
Carney, B. W., Latham, D. W., Laird, J. B., & Aguilar, L. A. 1994, AJ, 107, 2240
Chauvin, G., Lagrange, A.-M., Zuckerman, B., et al. 2005, A&A, 438, L29
Cochran, W. D., Endl, M., Wittenmyer, R. A., & Bean, J. L. 2007, ApJ, 665, 1407
Cumming, A. 2004, MNRAS, 354, 1165
Cumming, A., Marcy, G. W., & Butler, R. P. 1999, ApJ, 526, 890
Dumusque, X., Udry, S., Lovis, C., Santos, N. C., & Monteiro, M. J. P. F. G. 2011, A&A, 525, A140
Endl, M., Kürster, M., Els, S., Hatzes, A. P., & Cochran, W. D. 2001, A&A, 374, 675
Fischer, D. A., & Valenti, J. 2005, ApJ, 622, 1102
Gonzalez, G. 1997, MNRAS, 285, 403
Ida, S., & Lin, D. N. C. 2004, ApJ, 616, 567
Johnson, J. A., Aller, K. M., Howard, A. W., & Crepp, J. R. 2010, PASP, 122, 905
Lagrange, A.-M., Desort, M., Galland, F., Udry, S., & Mayor, M. 2009, A&A, 495, 335
Lagrange, A.-M., Bonnefoy, M., Chauvin, G., et al. 2010, Science, 329, 57
Marois, C., Macintosh, B., Barman, T., et al. 2008, Science, 322, 1348
Matsuo, T., Shibai, H., Ootsubo, T., & Tamura, M. 2007, ApJ, 662, 1282
Mayer, L., Quinn, T., Wadsley, J., & Stadel, J. 2002, Science, 298, 1756
Mayor, M., & Queloz, D. 1995, Nature, 378, 355
Mayor, M., Pepe, F., Queloz, D., et al. 2003, The Messenger, 114, 20

Mayor, M., Marmier, M., Lovis, C., et al. 2011, A&A, submitted [arXiv:1109.2497]
Mordasini, C., Alibert, Y., Benz, W., & Naef, D. 2009, A&A, 501, 1161
Mordasini, C., Alibert, Y., Benz, W., Klahr, H., & Henning, T. 2012, A&A, 541, A97
Morton, T. D., & Johnson, J. A. 2011, ApJ, 729, 138
Narayan, R., Cumming, A., & Lin, D. N. C. 2005, ApJ, 620, 1002
Niedzielski, A., Nowak, G., Adamów, M., & Wolszczan, A. 2009, ApJ, 707, 768
Nordström, B., Mayor, M., Andersen, J., et al. 2004, A&A, 418, 989
Pollack, J. B., Hubickyj, O., Bodenheimer, P., et al. 1996, Icarus, 124, 62
Rice, W. K. M., & Armitage, P. J. 2003, ApJ, 598, L55
Ryan, S. G. 1989, AJ, 98, 1693
Santos, N. C., Israelian, G., & Mayor, M. 2001, A&A, 373, 1019
Santos, N. C., Israelian, G., & Mayor, M. 2004, A&A, 415, 1153
Santos, N. C., Mayor, M., Benz, W., et al. 2010, A&A, 512, A47
Santos, N. C., Mayor, M., Bouchy, F., et al. 2007, A&A, 474, 647
Santos, N. C., Mayor, M., Bonfils, X., et al. 2011, A&A, 526, A112
Sato, B., Izumiura, H., Toyota, E., et al. 2008, in Extreme Solar Systems, ed. D. Fischer, F. A. Rasio, S. E. Thorsett, & A. Wolszczan, ASP Conf. Ser., 398, 67
Scargle, J. D. 1982, ApJ, 263, 835
Setiawan, J., Hatzes, A. P., von der Lühe, O., et al. 2003, A&A, 398, L19
Setiawan, J., Klement, R. J., Henning, T., et al. 2010, Science, 330, 1642
Socrates, A., Katz, B., Dong, S., & Tremaine, S. 2012, ApJ, 750, 106
Sousa, S. G., Santos, N. C., Mayor, M., et al. 2008, A&A, 487, 373
Sousa, S. G., Santos, N. C., Israelian, G., et al. 2011a, A&A, 526, A99
Sousa, S. G., Santos, N. C., Israelian, G., Mayor, M., & Udry, S. 2011b, A&A, 533, A141
Sozzetti, A. 2010, in EAS Pub. Ser. 42, ed. K. Gożdziewski, A. Niedzielski, & J. Schneider, 55
Sozzetti, A., Torres, G., Latham, D. W., et al. 2009, ApJ, 697, 544
Triaud, A. H. M. J., Collier Cameron, A., Queloz, D., et al. 2010, A&A, 524, A25
Udry, S., & Santos, N. C. 2007, ARA&A, 45, 397
Udry, S., Mayor, M., Benz, W., et al. 2006, A&A, 447, 361
Vogt, S. S., Allen, S. L., Bigelow, B. C., et al. 1994, in SPIE Conf. Ser. 2198, ed. D. L. Crawford, & E. R. Craine, 362
Vorobyov, E. I., & Basu, S. 2010, ApJ, 714, L133
Zechmeister, M., & Kürster, M. 2009, A&A, 496, 577

Pages 9 to 13 are available in the electronic edition of the journal at http://www.aanda.org

Appendix A: Figures of the GLS periodograms

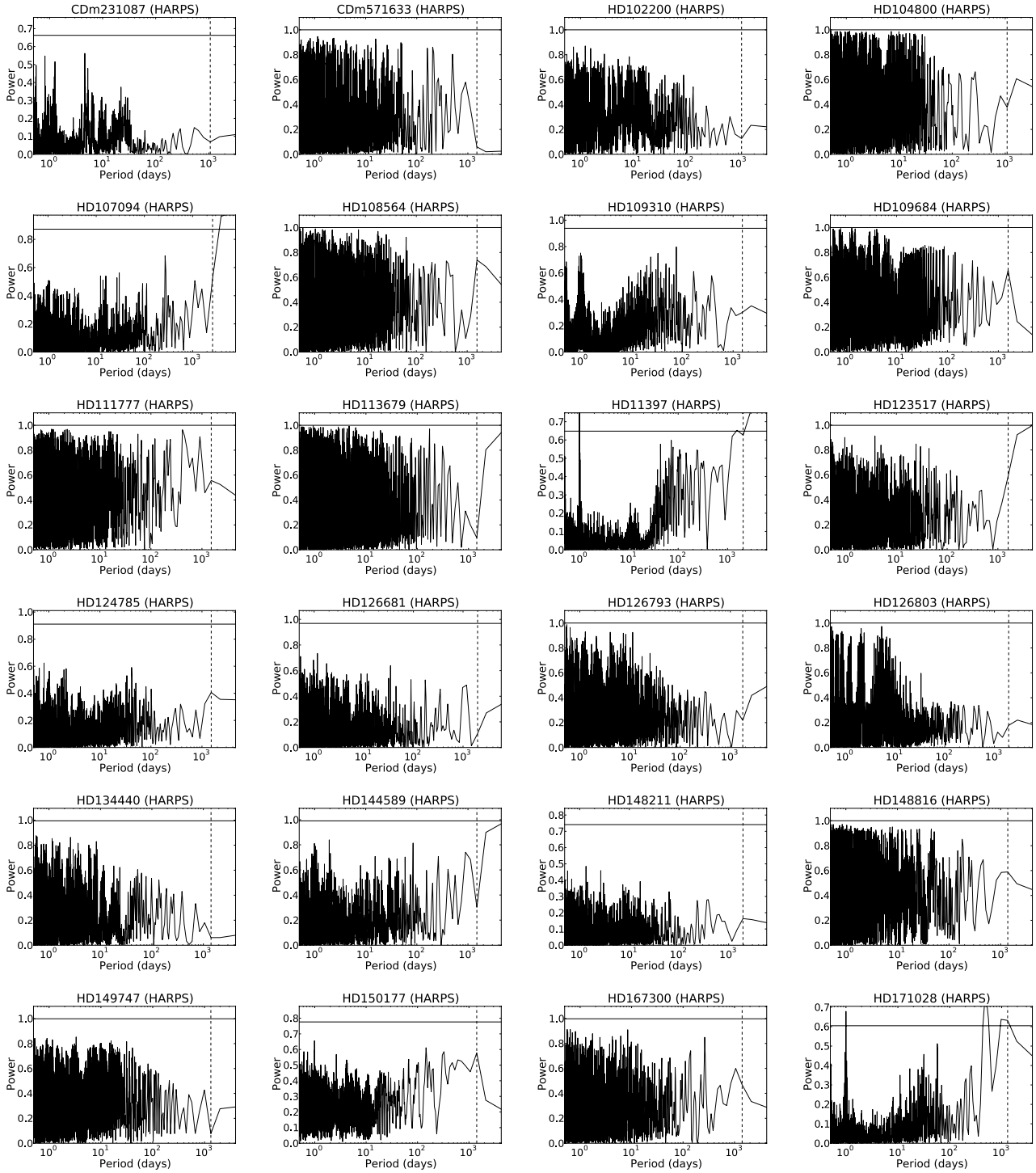

Fig. A.1. Figures of the GLS periodograms for stars with at least six measurements. The horizontal black line notes the power of the 0.1% FAP and the vertical dotted line, the timespan of the measurements.

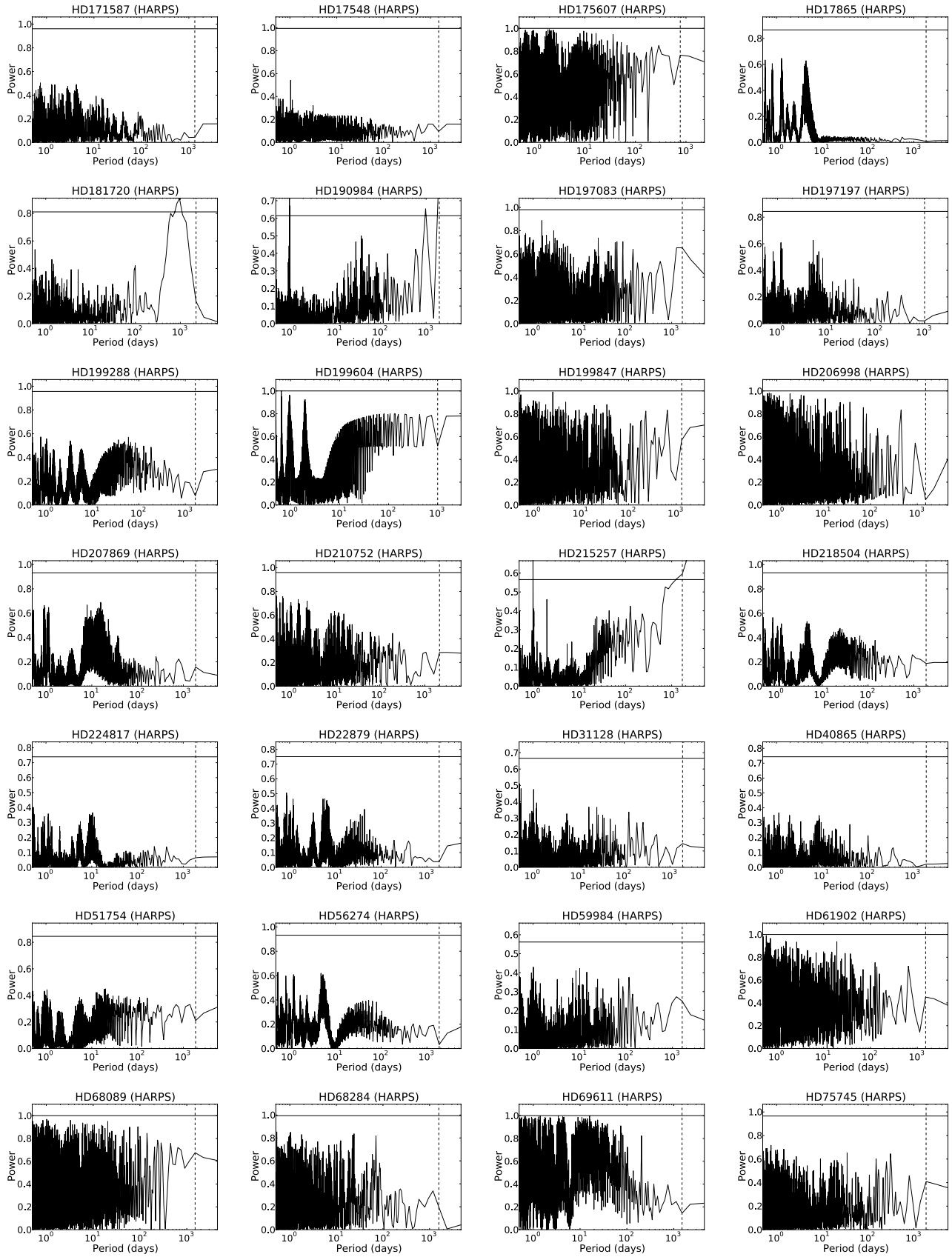

Fig. A.1. continued.

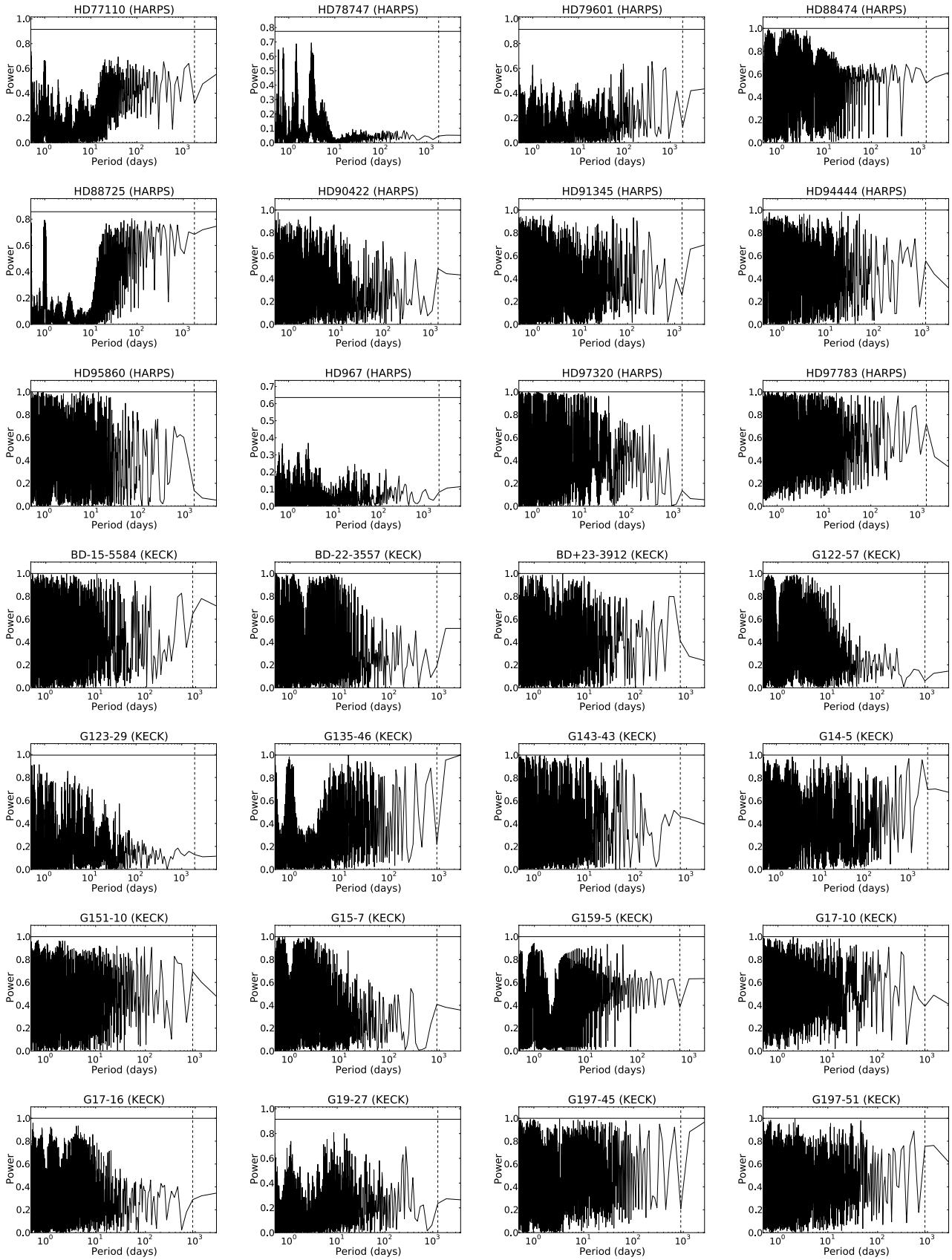

Fig. A.1. continued.

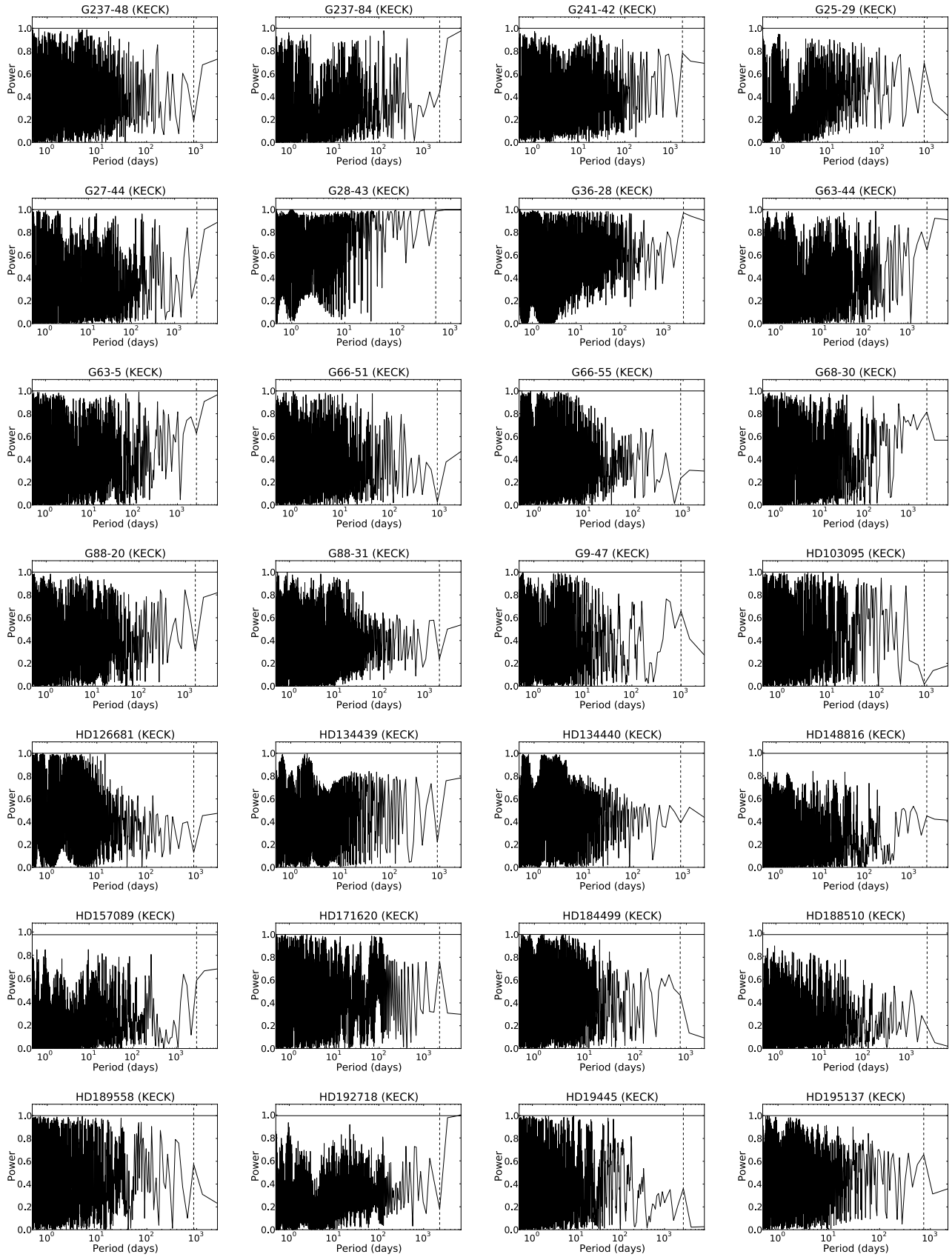

Fig. A.1. continued.

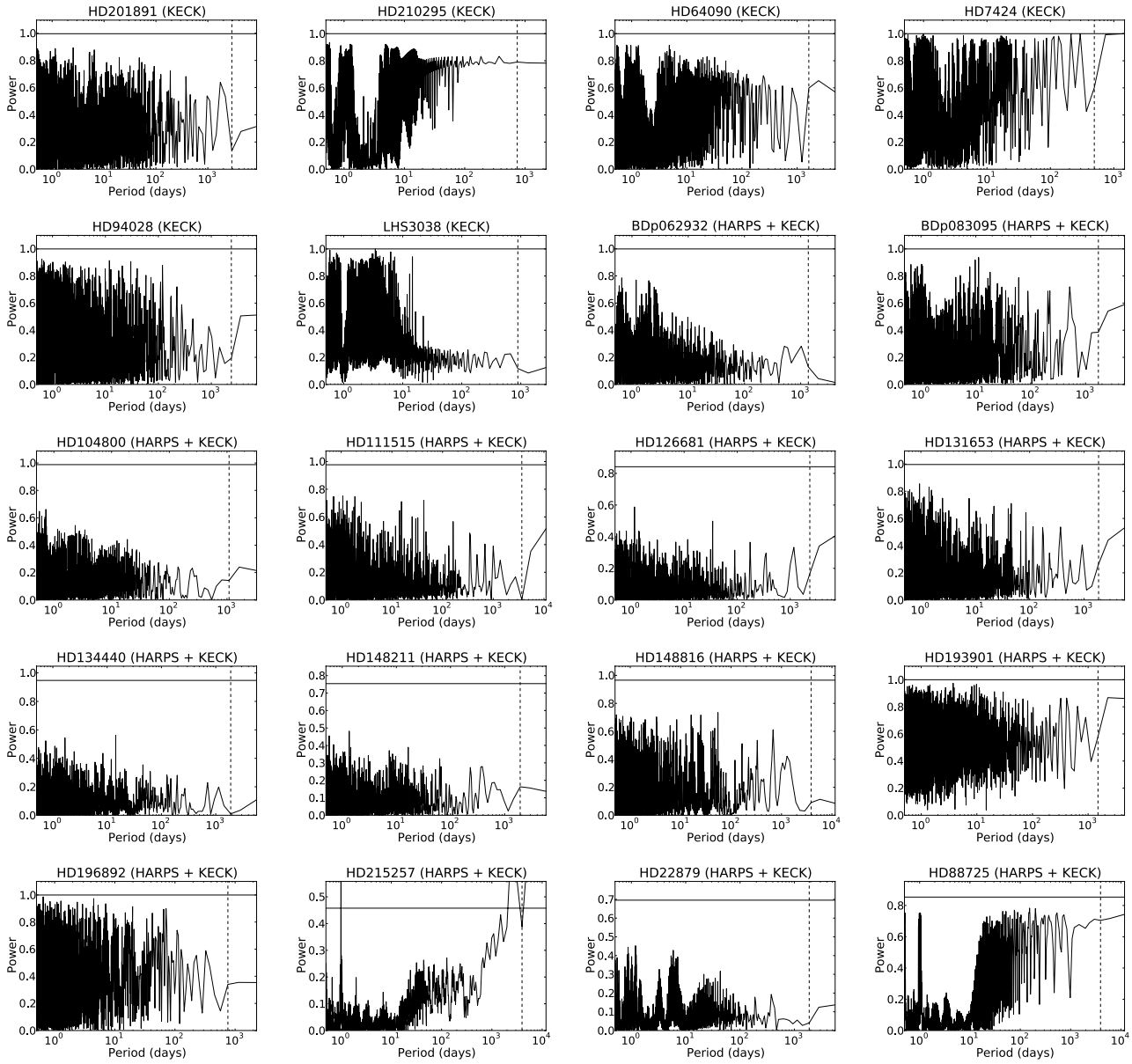

Fig. A.1. continued.

Chapter 3

On the functional form of the metallicity-giant planet correlation

Foreword

The exponential dependence of the presence of a giant planet on metallicity was clear for metal-rich stars. In the literature it was debated, however, whether this trend still holds for metal-poor stars or if the frequency is rather a constant in that regime (Santos et al. 2004; Johnson et al. 2010). My previous work showed that, although giant planets are indeed rare around metal-poor stars, they may be more frequent than previously thought. Additionally, I suggested that there may be a lower limit in metallicity below which no more giant planets can be formed.

I used the large volume-limited CORALIE and HARPS planet search samples of FGK dwarfs to investigate this issue further. Seven different functional forms were tested, including a constant or an exponential dependence for metal-poor stars, the possible absence of giant planets below a certain metallicity and the possible dependence of stellar mass. With a Bayesian formalism (see Appendix A), I was able to distinguish betwwen the different functional forms. This work has been peer-review and published by Astronomy & Astrophysics.

A&A 551, A112 (2013)
DOI: 10.1051/0004-6361/201220707

Astronomy & Astrophysics

On the functional form of the metallicity-giant planet correlation⋆

A. Mortier[1,2], N. C. Santos[1,2], S. Sousa[1,3], G. Israelian[3,4], M. Mayor[5], and S. Udry[5]

[1] Centro de Astrofísica, Universidade do Porto, Rua das Estrelas, 4150-762 Porto, Portugal
e-mail: amortier@astro.up.pt
[2] Departamento de Física e Astronomia, Faculdade de Ciências, Universidade do Porto, Portugal
[3] Instituto de Astrofísica de Canarias, 38200 La Laguna, Tenerife, Spain
[4] Departamento de Astrofísica, Universidad de La Laguna, 38206 La Laguna, Tenerife, Spain
[5] Observatoire de Genève, Université de Genève, 51 Ch. des Maillettes, 1290 Sauverny, Switzerland

Received 8 November 2012 / Accepted 28 January 2013

ABSTRACT

Context. It is generally accepted that the presence of a giant planet is strongly dependent on the stellar metallicity. A stellar mass dependence has also been investigated, but this dependence does not seem as strong as the metallicity dependence. Even for metallicity, however, the exact form of the correlation has not been established.
Aims. In this paper, we test several scenarios for describing the frequency of giant planets as a function of its host parameters. We perform this test on two volume-limited samples (from CORALIE and HARPS).
Methods. By using a Bayesian analysis, we quantitatively compared the different scenarios.
Results. We confirm that giant planet frequency is indeed a function of metallicity. However, there is no statistical difference between a constant or an exponential function for stars with subsolar metallicities contrary to what has been previously stated in the literature. The dependence on stellar mass could neither be confirmed nor be discarded.

Key words. methods: statistical – planet-star interactions – stars: abundances

1. Introduction

Since the discovery of the first extrasolar planet around a solar-like star in 1995 (51 Peg b, Mayor & Queloz 1995), the search for extrasolar planetary systems has accelerated. As of today, more than 800 planets have been announced. Most of them were detected using the radial velocity technique. Although 800 is a relatively high number, the theory of planet formation and evolution is still being debated (Pollack et al. 1996; Mayer et al. 2002; Mordasini et al. 2009). The situation is particularly difficult for giant planet formation. Currently, there are two proposed models: core accretion (e.g. Pollack et al. 1996; Rice & Armitage 2003; Alibert et al. 2004), where gas from the protoplanetary disk is accreted around a previously formed rocky/icy core; and the disk instability model (e.g. Boss 1997; Mayer et al. 2002), where a planet is formed because of a direct gravitational instability in the protoplanetary disk, in the same way as stars form from interstellar clouds. A helpful overview of both models is given by Matsuo et al. (2007).

This problem may be solved with the help of planet-host stars. Observational and theoretical evidence shows that the presence of a planet seems to depend on several stellar properties, such as mass and metallicity (Udry & Santos 2007). Concerning metallicity, it has been well-established that more metal-rich stars have a higher probability of harboring a giant planet than their lower metallicity counterparts (Gonzalez 1997; Santos et al. 2001, 2004; Fischer & Valenti 2005; Udry & Santos 2007; Sousa et al. 2011b; Mortier et al. 2012). The occurrence rate even increases dramatically with increasing metallicity. Current numbers, based on the CORALIE and HARPS samples, suggest that around 25% of the stars with twice the metal content of our Sun are orbited by a giant planet. This number decreases to ∼5% for solar-metallicity objects (Sousa et al. 2011b; Mayor et al. 2011). A similar trend has also been found by previous results (e.g. Santos et al. 2004; Fischer & Valenti 2005; Johnson et al. 2010). Curiously, no such trend is observed for the lower mass planets (Udry et al. 2006; Sousa et al. 2008; Mayor et al. 2011). The Neptune-mass planets found so far seem to have a rather flat metallicity distribution (Sousa et al. 2008, 2011b; Mayor et al. 2011).

While this exponential trend is very clear for solar and super-solar metallicities, the situation for lower (subsolar) metallicities is still uncertain. Santos et al. (2004) and Udry & Santos (2007) suggest that a constant frequency may be a better fit for sub-solar metallicities than a continuous exponential. They used the sample from Fischer & Valenti (2005) as well as the CORALIE sample. Their suggestion has been discarded by Johnson et al. (2010), based on a Bayesian analysis on a large SPOCS sample. Recently, it has also been suggested that there may be a lower limit below which no giant planets can be formed anymore (Mortier et al. 2012). The issue of giant planet frequency dependence on stellar properties is still not resolved.

The observed metallicity correlation in the metal-rich region favors the core-accretion model for the formation of giant planets (Ida & Lin 2004; Udry & Santos 2007; Mordasini et al. 2012) because the higher the grain content of the disk, the easier it is to build the cores that will later accrete gas. According to the disk-instability model, however, the presence of giant planets would not be strongly dependent on stellar metallicity (Boss 2002). It is thus important that we fully understand what happens around stars with different metallicities and masses since it

⋆ Full Tables 1 and 2 are only available in electronic form at the CDS via anonymous ftp to cdsarc.u-strasbg.fr (130.79.128.5) or via http://cdsarc.u-strasbg.fr/viz-bin/qcat?J/A+A/551/A112

Table 1. Stellar parameters for the stars in the CORALIE sample.

Star	[Fe/H]	M_* ($M_\odot$)	$T_{\rm eff}$ (K)	Planet?
HD 967	−0.68	0.8	5557.82	
HD 1108	0.04	0.94	5656.61	
HD 1237	0.07	0.92	5506.26	yes
HD 1320	−0.27	0.89	5688.25	
HD 1388	−0.01	1.05	5967.46	
HD 1461	0.19	1.04	5780.9	yes
...	...	...	...	...

Notes. The complete table is provided in electronic form at the CDS.

can provide clues to the processes of planet formation and evolution. Different formation mechanisms may play a role around stars with different metallicities.

In the light of this ongoing debate, we analyze two volume-limited samples in this paper to find out how the situation looks in this low-metallicity end. In Sect. 2, an overview is given of the samples and their data. Section 3 reports on the analysis of these samples. Finally, conclusions are made in Sect. 4, together with a discussion.

2. The samples

To test the giant planet frequency dependence on the stellar properties, we used two volume-limited samples. In each sample, there are several planet hosts. Since this paper is about giant-planet frequency, we considered planet hosts as only those stars with at least one planet with a mass between 0.1 and 25 Jupiter mass. These planets have periods between 5 and 5000 days. Mayor et al. (2011) calculated the detection limits on these samples. They show that the maximum orbital period out to which a 0.1 Jupiter-mass planet could be detected lies around 1000−2000 days.

2.1. Coralie sample

The CORALIE sample is a large one of 1216 stars. It was constructed from the larger CORALIE sample that consisted of about 1650 stars (Udry et al. 2000). A color cut-off was then made. Stars with a $B - V > 1.2$ were discarded from the sample. This leaves us with a sample of about ∼1250 stars, as used in several previous works (e.g. Santos et al. 2004; Sousa et al. 2011b).

Since high-resolution spectra were not available for all of these stars, metallicities were derived using the cross correlation function (CCF) calibration. From the Hipparcos catalog (van Leeuwen 2007), the color $B - V$ was used to derive temperatures with the calibration formula, reported in Sousa et al. (2008). Stellar masses were estimated following the same procedure as in Sousa et al. (2011a) where stellar evolutionary models from the Padova group were applied using their web interface. This could not be done for 37 stars, leaving us with a final sample of 1216 stars. The parameters can be found in Table 1. In the bottom panel of Fig. 1, the data is presented in a metallicity-mass diagram. Metallicity and mass for the stars in this sample have typical error bars of 0.07 dex and 0.1 $M_\odot$, respectively.

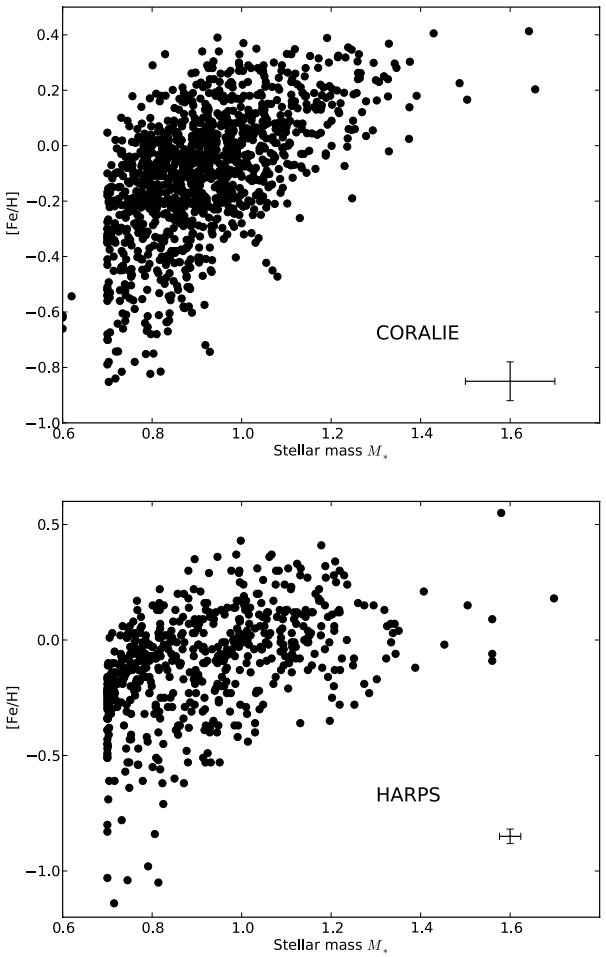

Fig. 1. Mass−metallicity coverage of the CORALIE (*top panel*) and the HARPS (*bottom panel*) sample.

2.2. Harps sample

Our second sample was constructed as part of a HARPS GTO program that aims to detect and obtain accurate orbital elements of Jupiter-mass planets in a well-defined volume of the solar neighborhood (out to 57.5 pc from the Sun – Lo Curto et al. 2010). It can be seen as an extension to the CORALIE sample.

High-resolution spectra were taken with the HARPS spectrograph (Mayor et al. 2003). In total, 582 stars had good enough spectra to spectroscopically derive accurate stellar parameters. The metallicities for these stars were all derived with the method described in Santos et al. (2004). The equivalent widths were automatically measured with the ARES code (Automatic Routine for line Equivalent widths in stellar Spectra – Sousa et al. 2007). Sousa et al. (2011b) compared metallicities, derived with this method and the CCF correlation, for a subsample of the CORALIE sample. The values are consistent with a mean difference of 0.01 dex and a dispersion of 0.07 dex. Stellar masses were estimated following the same procedure as in Sousa et al. (2011a), where stellar evolutionary models from the Padova group were applied using their web interface. All parameters have been previously reported in Sousa et al. (2011b) and can also be found in Table 2. In the top panel of Fig. 1, the data is presented in a metallicity-mass diagram. Metallicity and mass for the stars in this sample have typical error bars of 0.03 dex and 0.025 $M_\odot$, respectively.

Table 2. Stellar parameters for the stars in the HARPS sample.

Star	[Fe/H]	M_* ($M_\odot$)	Planet?
HD 5388	−0.28	1.22	
HD 6718	−0.07	0.95	yes
HD 8038	0.15	1.01	
HD 8535	0.04	1.15	yes
HD 8930	−0.23	0.9	
HD 8985	−0.01	1.2	
...	...	...	...

Notes. The complete table is provided in electronic form at the CDS.

3. Bayesian analysis

The analysis performed in this paper is based on the methods described in Kass & Raftery (1995) and Johnson et al. (2010). It uses a Bayesian inference to find the best relationship between stellar mass and metallicity and the presence of a giant planet.

3.1. Technique

Giant-planet frequency can be expressed in terms of metallicity and/or stellar mass with a particular functional form $f(M_*, [\mathrm{Fe/H}])$, having a set of free parameters X. According to the theorem of Bayes (Bayes & Price 1763), we have

$$P(X|d)P(d) = P(d|X)P(X) \tag{1}$$

where d represents the data. In our case, d can only have two results: a star does have a detectable planet or it does not. For a specific functional form f, the best set of parameters to fit the data will be found if $P(X|d)$ is maximized. This means that, given the data, the probability that the parameters X fit the data, is at its maximum.

The probability of the data itself, $P(d)$, is constant. For the parameter probability, $P(X)$, we have chosen to adopt a uniform distribution, allowing us to keep an open mind towards the results. Since these two terms are constant, this means that $P(X|d)$ will be maximized if $P(d|X)$ is maximized.

Now, assume you have N stars in your sample of which H stars are planet hosts. Then you can write $P(d|X)$ as the product of all the separate probabilities per star:

$$\begin{aligned} P(d|X) &= \prod_i^N P(d_i|X) \\ &= \prod_i^H f(M_*, [\mathrm{Fe/H}]) \prod_i^{N-H} [1 - f(M_*, [\mathrm{Fe/H}])]\,. \end{aligned} \tag{2}$$

If a star has a detectable planet, its probabilty thus equals f. In the absence of a giant planet around the star, the probabilty is then obviously $1 - f$.

Since the stellar mass M_* and metallicity [Fe/H] are measured values with errorbars, it is more correct to use a probability distribution function (pdf) $p(M_i, F_i)$ instead of their actual values. Per star, the giant planet frequency is then actually calculated by

$$f(M_i, F_i) = \int\int p(M_i, F_i) f(M, F) \mathrm{d}M \mathrm{d}F. \tag{3}$$

The pdf p can be approximated by a product of Gaussians with means (M_i, F_i) and standard deviations $(\sigma_{M_i}, \sigma_{F_i})$.

Different functional forms can be evaluated by using the Bayesfactor, as described in Kass & Raftery (1995). When testing two functional forms f and g, the Bayesfactor is expressed as

$$B_{fg} = \frac{P(\mathrm{d}|f)}{P(\mathrm{d}|g)} = \frac{\int P(\mathrm{d}|X_f)P(X_f)\mathrm{d}X_f}{\int P(\mathrm{d}|X_g)P(X_g)\mathrm{d}X_g} \tag{4}$$

with X_f, X_g the set of parameters for f and g, respectively. The integration limits are the limits of the explored parameter space. According to Kass & Raftery (1995), a Bayesfactor of about 100 is needed to statistically rule out a specific functional form.

3.2. Functional forms

Previous studies (e.g. Fischer & Valenti 2005; Lovis & Mayor 2007; Udry & Santos 2007; Johnson et al. 2010; Sousa et al. 2011b) have shown that giant planet frequency is most likely exponentially dependent on metallicity [Fe/H] and polynomially dependent on stellar mass M_*. By including those two dependencies, we adopted the following general functional form:

$$f(M_*, [\mathrm{Fe/H}]) = c\left(\frac{M_*}{M_\odot}\right)^a 10^{b[\mathrm{Fe/H}]}. \tag{5}$$

As stated before, there are still questions regarding the correct form in the low-metallicity tail. While it must be noted that there are still many other functional forms that may fit the data, we tested seven different functional forms in our analysis:

1. The traditional metallicity and mass dependence (Eq. (5)),
2. only a metallicity dependence ($a = 0$),
3. only a mass dependence: $f \cdot M_*^g + h$,
4. Eq. (5) with a fixed to 1,
5. a combination of several functional forms, like

$$f(M_*, [\mathrm{Fe/H}]) = \begin{cases} cM_*^a 10^{b[\mathrm{Fe/H}]} & \text{if } [\mathrm{Fe/H}] \geq d \\ c10^{bd} & \text{if } e \leq [\mathrm{Fe/H}] < d \\ 0 & \text{if } [\mathrm{Fe/H}] < e \end{cases}, \tag{6}$$

6. Eq. (6) with $e = -\infty$,
7. Eq. (6) with $d = e$.

Form number 4 takes both metallicity and stellar mass into account, but fixes the mass dependence to a linear dependence. The last three forms will vary the behavior of the function for the lower metallicities. It is considered that for decreasing metallicity, the function flattens out, resulting in a constant rather than an exponential (parameter d). Another consideration is a sudden lack of giant planets. Mortier et al. (2012) suggested that there may be a lower limit in metallicity below which no giant planets can be formed. This lower limit is represented by parameter e. Option 5 takes both the constant and the stop into account, while options 6 and 7 take only the constant, resp. stop into account.

In our parameter space, we assumed a uniform distribution over several intervals as seen in Table 3. These assumptions are based on what has been written in the literature in previous studies (e.g. Lovis & Mayor 2007; Udry & Santos 2007; Johnson et al. 2010), and the derived parameters do not depend on the a priori chosen intervals.

3.3. Results

Finding the best solution of one functional form, means maximizing the probability that the parameters X fit the data.

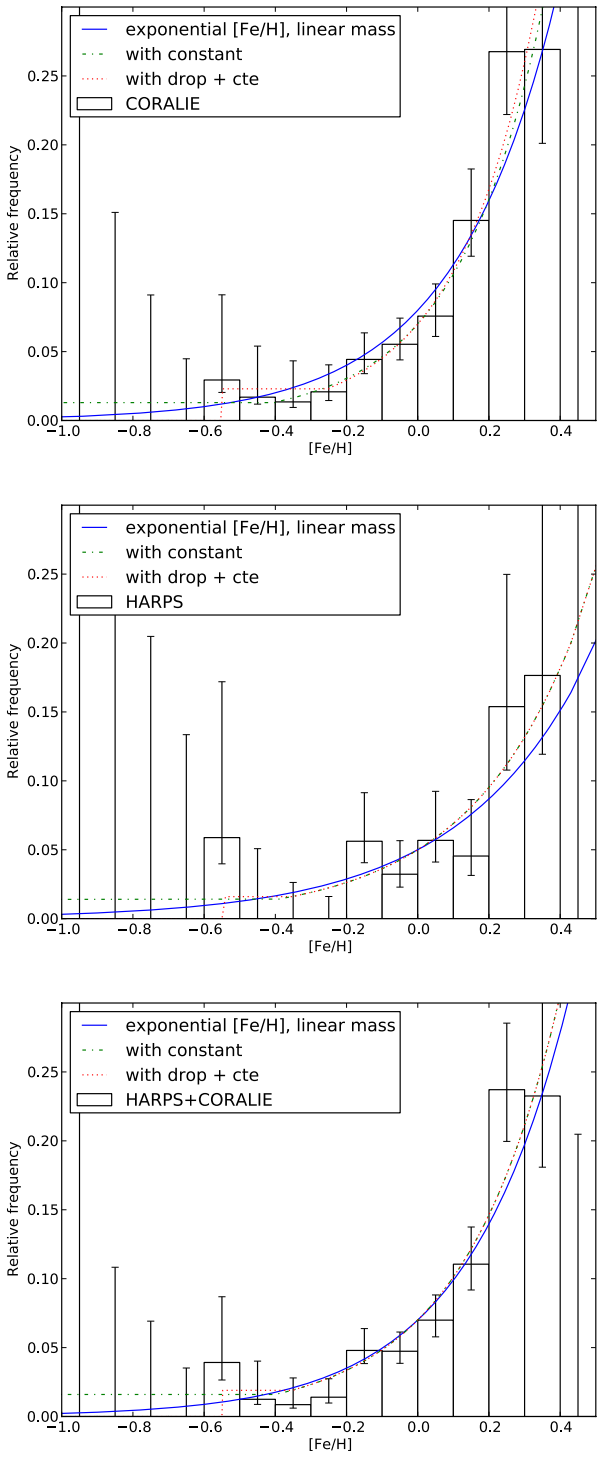

Fig. 2. Frequency of giant planets as a function of metallicity and mass of the HARPS (*top panel*), the CORALIE (*middle panel*) and the combined (*bottom panel*) sample. Three different functional forms are shown: a complete exponential with linear mass (blue curve), an exponential and a constant (green curve), and an exponential, a constant plus a drop (red curve). The stellar mass is fixed to $M_* = 1.0\ M_\odot$.

Since there are many local maxima throughout our parameter space, we chose to adopt the conservative (but time-consuming) method of stepping through a dense grid. The step sizes we used are given in Table 3. To transform the products of Eq. (2) into sums, we also worked in logarithmic space (see e.g. Johnson et al. 2010).

Table 3. Chosen interval for the parameters in the functions.

Parameter	Interval	Step
a	$[0.0, 2.0]$	0.1
b	$[0.0, 3.0]$	0.1
c	$[0.01, 0.15]$	0.01
d	$[-0.5, 0]$	0.05
e	$[-0.75, -0.55]$	0.05
f	$[0.05, 0.55]$	0.05
g	$[0.0, 2.4]$	0.1
h	$[-0.50, -0.05]$	0.05

Table 4. Results of the Bayesian analysis for the three samples.

HARPS		CORALIE		HARPS+CORALIE	
Funct.	B_{fg}	Funct.	B_{fg}	Funct.	B_{fg}
4 ↘		4 ↘		7 ↘	
	1.02		1.03		1.06
7 ↗↘		7 ↗↘		4 ↗↘	
	1.09		1.17		1.20
1 ↗↘		2 ↗↘		2 ↗↘	
	1.00		1.01		1.01
2 ↗↘		1 ↗↘		1 ↗↘	
	1.44		1.25		1.19
5 ↗↘		5 ↗↘		5 ↗↘	
	1.34		2.07		2.71
6 ↗↘		6 ↗↘		6 ↗↘	
	73.13		$1.32 \cdot 10^6$		$> 10^{10}$
3 ↗		3 ↗		3 ↗	

Notes. For each sample, the functions are ordered from the best to the worst in the left columns. The Bayesfactors that compare two functions are given in the right columns.

Comparing the seven different functional forms, leads to interesting results. In Table 4, the order of functional forms is given for both samples, as well as the combined sample (HARPS + CORALIE). The top functional form is the best, the bottom one the worst. On the right of these functions, the Bayesfactors are represented that compare these two functions. As can be seen, the only functional form that can statistically be ruled out is form number 3, where there is only a mass dependence. The other six forms cannot be distinguished statistically. By multiplying the Bayesfactors, we calculate that the "best" form and the "worst" form of these six function relate with a Bayesfactor of 2.15, 3.15, and 4.12 for the HARPS, the CORALIE, and the combined sample, respectively. According to Kass & Raftery (1995), these numbers are too low to conclude anything from it.

In Fig. 2, the best solutions for three functional forms are shown for both our samples. The functional forms that are shown are the traditional exponential with a linear mass dependence (form nr 4), the exponential with a constant (form nr 6) and the exponential with a constant and a drop (form nr 5). Even from the figures, it is clear that it is hard to distinguish between the different forms in the metal-poor regime.

The conducted planet search surveys (Mayor et al. 2011) were not complete for all period ranges. This is particularly true for longer periods (>1000−2000 days), where the results are incomplete. About a quarter of our sample have these long-period planets. By excluding them, however, we obtain comparable results from the analysis. Our conclusions are thus not sensitive to the inclusions of these planets.

4. Conclusions and discussion

We performed a statistical Bayesian analysis to look for the best function to describe giant planet frequency in terms of stellar properties, specifically stellar mass and metallicity. We performed this test with seven different functional forms, based on three volume-limited samples. One sample was observed with CORALIE, the other one with HARPS. The test was also performed for the combined sample.

The test concluded that giant planet frequency is definitely not a function of stellar mass alone. There was no statistically significant result for the other functions. The Bayesfactors, used to compare between the functions, are all between 1.0 and 4.12. According to Kass & Raftery (1995), this means that the difference is not worth more than a bare mention, so it is still unclear what happens exactly in the metal-poor regime.

While the dependence on metallicity is clear, an additional dependence on stellar mass could neither be confirmed nor discarded. The difference between the functional forms was mostly focused on the metal-poor regime. We tested whether the giant planet frequency in that regime is flat rather than exponential. No statistical difference was found between the two options. These results contrast strongly with the results of Johnson et al. (2010). For our analysis, we used the formalism as described by Kass & Raftery (1995) where Bayesfactors are calculated as can be seen in our Eq. (4) and their Eqs. (1)−(2). Even though Johnson et al. (2010) cite the same work, it seems that they use a different formulation for comparing models (Eq. (7) in their work). These different formulas may explain the different results.

It has to be noted, however, that their sample has a much wider mass range, including both A and M stars. This makes their analysis more sensitive to a possible mass dependence. The metallicity range of their sample, however, is comparable to ours.

The very clear trend that giant planet frequency is an increasing function of metallicity in the metal-rich regime can be explained with the theory of core-accretion. The lack of such a trend can be explained more easily with the theory of gravitational instability. In recent works (e.g. Meru & Bate 2010; Rogers & Wadsley 2012), simulations have shown that planet formation induced by gravitational instability is more likely to occur around metal-poor stars than around metal-rich ones.

Disk instability is expected to occur only in the outer regions, explaining among other things the existence of massive long-period planets like HR8799b, c and d (Marois et al. 2008). However, this does not exclude that short period planets may also be formed by gravitational instability. Baruteau et al. (2011) suggest that planets formed by gravitational instability may migrate very rapidly inwards. Several giant planets around metal-poor stars have periods between 50 and 1000 days (not very short, not very long). They may also be the result of a gravitationally unstable disk.

These theoretical works suggest that a different trend in giant planet frequency may be expected. If gravitational instability dominates in the metal-poor regime and core-accretion in the metal-rich regime, we would expect to see a constant followed by an exponential. It has to be noted that the samples that we are testing are simply too small to be able to distinguish between a constant or an exponential in the low-metallicity end. We need a much bigger unbiased, volume-limited sample to be able to form any distinctive conclusions. A sample of about 5000 stars will enable us to better distinguish between the different models. With all the current efforts to discover planets in large samples of solar-type stars like *Gaia*, *Kepler*, etc., it is likely that this problem will be solved in the near future.

Acknowledgements. This work was supported by the European Research Council/European Community under the FP7 through Starting Grant agreement number 239953. N.C.S. also acknowledges the support from Fundação para a Ciência e a Tecnologia (FCT) through program Ciência 2007 funded by FCT/MCTES (Portugal) and POPH/FSE (EC), and in the form of grants reference PTDC/CTE-AST/098528/2008 and PTDC/CTE-AST/09860/2008.

References

Alibert, Y., Mordasini, C., & Benz, W. 2004, A&A, 417, L25
Baruteau, C., Meru, F., & Paardekooper, S.-J. 2011, MNRAS, 416, 1971
Bayes, M., & Price, M. 1763, Phil. Trans., 53, 370
Boss, A. P. 1997, Science, 276, 1836
Boss, A. P. 2002, ApJ, 567, L149
Fischer, D. A., & Valenti, J. 2005, ApJ, 622, 1102
Gonzalez, G. 1997, MNRAS, 285, 403
Ida, S., & Lin, D. N. C. 2004, ApJ, 616, 567
Johnson, J. A., Aller, K. M., Howard, A. W., & Crepp, J. R. 2010, PASP, 122, 905
Kass, R. E., & Raftery, A. E. 1995, JASA, 90, 773
Lo Curto, G., Mayor, M., Benz, W., et al. 2010, A&A, 512, A48
Lovis, C., & Mayor, M. 2007, A&A, 472, 657
Marois, C., Macintosh, B., Barman, T., et al. 2008, Science, 322, 1348
Matsuo, T., Shibai, H., Ootsubo, T., & Tamura, M. 2007, ApJ, 662, 1282
Mayer, L., Quinn, T., Wadsley, J., & Stadel, J. 2002, Science, 298, 1756
Mayor, M., & Queloz, D. 1995, Nature, 378, 355
Mayor, M., Pepe, F., Queloz, D., et al. 2003, The Messenger, 114, 20
Mayor, M., Marmier, M., Lovis, C., et al. 2011, A&A, submitted [arXiv:1109.2497]
Meru, F., & Bate, M. R. 2010, MNRAS, 406, 2279
Mordasini, C., Alibert, Y., Benz, W., & Naef, D. 2009, A&A, 501, 1161
Mordasini, C., Alibert, Y., Benz, W., Klahr, H., & Henning, T. 2012, A&A, 541, A97
Mortier, A., Santos, N. C., Sozzetti, A., et al. 2012, A&A, 543, A45
Pollack, J. B., Hubickyj, O., Bodenheimer, P., et al. 1996, Icarus, 124, 62
Rice, W. K. M., & Armitage, P. J. 2003, ApJ, 598, L55
Rogers, P. D., & Wadsley, J. 2012, MNRAS, 423, 1896
Santos, N. C., Israelian, G., & Mayor, M. 2001, A&A, 373, 1019
Santos, N. C., Israelian, G., & Mayor, M. 2004, A&A, 415, 1153
Sousa, S. G., Santos, N. C., Israelian, G., Mayor, M., & Monteiro, M. J. P. F. G. 2007, A&A, 469, 783
Sousa, S. G., Santos, N. C., Mayor, M., et al. 2008, A&A, 487, 373
Sousa, S. G., Santos, N. C., Israelian, G., et al. 2011a, A&A, 526, A99
Sousa, S. G., Santos, N. C., Israelian, G., Mayor, M., & Udry, S. 2011b, A&A, 533, A141
Udry, S., & Santos, N. C. 2007, ARA&A, 45, 397
Udry, S., Mayor, M., Naef, D., et al. 2000, A&A, 356, 590
Udry, S., Mayor, M., Benz, W., et al. 2006, A&A, 447, 361
van Leeuwen, F. 2007, A&A, 474, 653

Chapter 4

On the metallicity - giant planet connection of evolved planet hosts

Foreword

While the metallicity dependence for giant planet frequency is pretty clear for dwarf stars, the situation is not as straightforward for subgiant and giant stars. In the literature, there is a debate whether the same correlation still holds for these evolved stars (e.g. Hekker & Meléndez 2007; Takeda et al. 2008; Ghezzi et al. 2010a). Access to precise stellar metallicities is key in understanding this (non-)correlation.

As part of my thesis I learned how to derive stellar parameters from high-resolution spectra (for details of the method, see section 1.3). The method makes use of a large stable line list of iron lines (Fe I and Fe II). A colleague of mine created a sublist of this larger list that that could specifically be used for cool stars with temperatures $T_{eff} < 5000\,\mathrm{K}$ (Tsantaki et al. 2013). In the literature, a small list of stable lines for the analysis of giant stars was also developed (Hekker & Meléndez 2007).

For this work, I compared stellar parameters for a sample of evolved planet hosts derived with these 3 line lists. I compared these parameters also with literature data. Finally, with these precise metallicities, I looked into giant planet frequency around (sub)giants. This work was peer-reviewed and published in Astronomy & Astrophysics.

A&A 557, A70 (2013)
DOI: 10.1051/0004-6361/201321641

Astronomy & Astrophysics

New and updated stellar parameters for 71 evolved planet hosts

On the metallicity–giant planet connection⋆,⋆⋆,⋆⋆⋆

A. Mortier[1,2], N. C. Santos[1,2], S. G. Sousa[1,3], V. Zh. Adibekyan[1], E. Delgado Mena[1], M. Tsantaki[1,2], G. Israelian[3,4], and M. Mayor[5]

[1] Centro de Astrofísica, Universidade do Porto, Rua das Estrelas, 4150-762 Porto, Portugal
e-mail: amortier@astro.up.pt
[2] Departamento de Física e Astronomia, Faculdade de Ciências, Universidade do Porto, 4099-002 Porto, Portugal
[3] Instituto de Astrofísica de Canarias, 38200 La Laguna, Tenerife, Spain
[4] Departemento de Astrofísica, Universidad de La Laguna, 38206 La Laguna, Tenerife, Spain
[5] Observatoire de Genève, Université de Genève, 51 Ch. des Maillettes, 1290 Sauverny, Switzerland

Received 4 April 2013 / Accepted 12 July 2013

ABSTRACT

Context. It is still being debated whether the well-known metallicity–giant planet correlation for dwarf stars is also valid for giant stars. For this reason, having precise metallicities is very important. Precise stellar parameters are also crucial to planetary research for several other reasons. Different methods can provide different results that lead to discrepancies in the analysis of planet hosts.
Aims. To study the impact of different analyses on the metallicity scale for evolved stars, we compare different iron line lists to use in the atmospheric parameter derivation of evolved stars. Therefore, we use a sample of 71 evolved stars with planets. With these new homogeneous parameters, we revisit the metallicity–giant planet connection for evolved stars.
Methods. A spectroscopic analysis based on Kurucz models in local thermodynamic equilibrium (LTE) was performed through the MOOG code to derive the atmospheric parameters. Two different iron line list sets were used, one built for cool FGK stars in general, and the other for giant FGK stars. Masses were calculated through isochrone fitting, using the Padova models. Kolmogorov-Smirnov tests (K-S tests) were then performed on the metallicity distributions of various different samples of evolved stars and red giants.
Results. All parameters compare well using a line list set, designed specifically for cool and solar-like stars to provide more accurate temperatures. All parameters derived with this line list set are preferred and are thus adopted for future analysis. We find that evolved planet hosts are more metal-poor than dwarf stars with giant planets. However, a bias in giant stellar samples that are searched for planets is present. Because of a colour cut-off, metal-rich low-gravity stars are left out of the samples, making it hard to compare dwarf stars with giant stars. Furthermore, no metallicity enhancement is found for red giants with planets ($\log g < 3.0$ dex) with respect to red giants without planets.

Key words. stars: abundances – stars: fundamental parameters – techniques: spectroscopic – methods: observational – methods: statistical

1. Introduction

Since the discovery of the first extrasolar planet around a solar-like star in 1995 (51 Peg b, Mayor & Queloz 1995), the search for extrasolar planetary systems has accelerated. Today, more than 900 planets have been announced[1]. Most of them were detected using the very successful radial velocity technique or the photometric transit technique. This high number of known planetary systems enables us to perform a significant statistical analysis which can bring clarity to the theory of planet formation and evolution. Currently, there are still two main theories being debated in the literature, core-accretion (Pollack et al. 1996; Mordasini et al. 2009) and gravitational instability (Mayer et al. 2002; Boss 2011).

Observational and theoretical evidence shows that the presence of a planet seems to depend on several stellar properties, such as mass and metallicity (Udry & Santos 2007). It has been well-established that dwarf stars with igher metallicity have a higher probability of harbouring a giant planet than their lower metallicity counterparts (Gonzalez 1997; Santos et al. 2001, 2004; Fischer & Valenti 2005; Sousa et al. 2011; Mortier et al. 2012). This result is expected from the core-accretion models of planetary formation. Curiously, no such trend is observed for the lower mass planets. The Neptune-mass planets found so far

⋆ The data presented here are based on observations collected at the La Silla Paranal Observatory, ESO (Chile) with the FEROS spectrograph at the 2.2 m telescope (ESO runs ID 70.C-0084, 088.C-0892, 089.C-0444, and 090.C-0146) and the HARPS spectrograph at the 3.6 m telescope (ESO run ID 72.C-0488); at the Paranal Observatory, ESO (Chile) with the UVES spectrograph at the VLT Kueyen telescope (ESO runs ID 074.C-0134, 079.C-0131, 380.C-0083, and 083.C-0174); at the Spanish Observatorio del Roque de los Muchachos of the Instituto de Astrofisica de Canarias with the FIES spectrograph at the Nordic Optical Telescope, operated on the island of La Palma jointly by Denmark, Finland, Iceland, Norway, and Sweden (program ID 44-210); and at the Observatoire de Haute-Provence (OHP, CNRS/OAMP), France with the SOPHIE spectrographs at the 1.93 m telescope (program ID 11B.DISC.SOUS).

⋆⋆ Tables 1, 5, 6 and Appendix A are available in electronic form at http://www.aanda.org

⋆⋆⋆ Tables 5, 6, and A.1 are also available at the CDS via anonymous ftp to cdsarc.u-strasbg.fr (130.79.128.5) or via http://cdsarc.u-strasbg.fr/viz-bin/qcat?J/A+A/557/A70

[1] See http://www.exoplanet.eu for an updated table.

Table 2. Spectrograph details: resolving power and spectral ranges.

Instrument	Resolving power $\lambda/\Delta\lambda$	Spectral range Å	Stars
UVES	110 000	3000–6800	19
FEROS	48 000	3600–9200	38
HARPS	100 000	3800–7000	4
CORALIE	50 000	3800–6800	1
SOPHIE	75 000	3820–6920	2
SARG	57 000–86 000	5100–10 100	5
FIES	67 000	3700–7300	1
UES	55 000	4000–10 000	1

seem to have a rather flat metallicity distribution (Udry & Santos 2007; Sousa et al. 2008, 2011; Mayor et al. 2011; Buchhave et al. 2012). It has also been suggested that intermediate-mass giant stars with planets have a different trend in metallicity (Pasquini et al. 2007; Ghezzi et al. 2010a; Hekker & Meléndez 2007).

There is also growing evidence that stellar mass may play a role in the formation of giant planets. Giant planet frequency around low-mass M dwarfs is much lower than the one found for FGK dwarfs (Bonfils et al. 2005; Endl et al. 2006; Neves et al. 2013). For higher mass stars, on the other hand, the frequency of giant planets seems to be higher (Lovis & Mayor 2007; Johnson et al. 2007).

To address these issues in a consistent way, it is important that a correct determination of stellar parameters is performed. In addition, a uniform derivation of the stellar parameters is a must for a thorough statistical analysis.

The determination of stellar parameters for evolved stars, and especially the cool giant stars, has been debated in the literature for several years (e.g. Hekker & Meléndez 2007; Cohen et al. 2008; Santos et al. 2009, 2010; Ghezzi et al. 2010a). Several authors raise doubts about the metallicity scale in these evolved stars. This has lead to significant discrepancies in the different studies of giant and sub-giant samples. In this work, we compare two iron line lists to derive stellar parameters for giant stars with planets. We show that using different line lists will lead to different results. The impact on the metallicity–giant planet connection is then presented and discussed.

In Sect. 2, we present the sample that has been used. Section 3 describes the spectroscopic analysis that was used, together with the different line lists. Results are given in Sect. 4. The effect on planet frequency as a function of metallicity is discussed in Sect. 6. We give a discusion in Sect. 7 and we conclude in Sect. 8.

2. The sample

For this analysis, we used a sample of 71 stars. All these stars are of spectral type F, G, or K and are known to be orbited by a planet (according to the online catalogue[2]). They were selected on the basis of their surface gravity, derived with the line list of Sousa et al. (2008), see next section: $\log g < 4.0$. Twenty of these stars were previously analysed with the same method presented in this work and their parameters were published by members of our team. The references can be found in Table 1. For the 51 remaining stars, we gathered optical spectra through observations made by our team, and with the use of the ESO archive.

In total, eight different spectrographs were used (see Table 2): UVES (VLT Kueyen telescope, Paranal, Chile); FEROS (2.2 m ESO/MPI telescope, La Silla, Chile); HARPS (3.6 m ESO telescope, La Silla, Chile); CORALIE (1.2 m Swiss telescope, La Silla, Chile); SOPHIE (1.93 m telescope, OHP, France); SARG (TNG Telescope, La Palma, Spain); FIES (Nordic Optical Telescope, La Palma, Spain); and UES (William Herschel Telescope, La Palma, Spain). The spectra were reduced using the available pipelines and IRAF[3]. The spectra were corrected for radial velocity with the IRAF task `DOPCOR`. Individual exposures of multiple observed stars with the same instrument, were added using the task `SCOMBINE` in IRAF. The data log can be found in Table 1.

The usage of different spectrographs and different pipelines can introduce systematic offsets in the analysis of the data. However, Santos et al. (2004) show that the spectroscopic analysis used in this work is not significantly affected by the use of different spectrographs. They observed several stars with different spectrographs and the resulting atmospheric parameters were all similar and within the 1-σ errorbars.

3. Spectroscopic analysis

3.1. Technique

From the spectra, we derived atmospheric stellar parameters: the effective temperature $T_{\rm eff}$, the surface gravity $\log g$, the metallicity [Fe/H] and the microturbulence ξ. The procedure we followed is described in Santos et al. (2004), and is based on the equivalent widths of Fe I and Fe II lines, and iron excitation and ionization equilibrium, assumed in local thermodynamic equilibrium (LTE). Therefore, the 2002 version of MOOG[4] (Sneden 1973) and a grid of ATLAS plane-parallel model atmospheres (Kurucz 1993) are used. This, mostly automatic, analysis was also used for the 20 stars whose parameters were previously published (see Table 1).

To measure the equivalent widths (EWs) of the iron lines, the code ARES is used (Automatic Routine for line Equivalent widths in stellar Spectra – Sousa et al. 2007). The input parameters for ARES, are the same as in Sousa et al. (2008, hereafter SO08), except for the *rejt* parameter, which determines the calibration of the continuum position. Since this parameter strongly depends on the signal-to-noise ratio (S/N) of the spectra, different values are needed. A uniform S/N value is derived for the spectra with the IRAF routine `BPLOT`. Therefore, three spectral regions are used: [5744 Å, 5747 Å], [6047 Å, 6053 Å], and [6068 Å, 6076 Å].

Then, the *rejt* parameter was set by eye for ten spectra with different S/N (representable for the whole sample). Afterwards, all the *rejt* parameters were derived by a simple interpolation of these values. This method ensures a uniform usage of the *rejt* parameter, since we otherwise do not have access to a uniform source for the S/N as they do in SO08. Table 3 lists the dependence of the *rejt* parameter to the S/N.

We performed the spectroscopic analysis in LTE. Stellar parameters, especially metallicity, can differ if non-LTE effects are considered. Results obtained with classical models depend on the choice of the line list and, in particular, on the ionization balance of Fe I/Fe II (Bergemann et al. 2012). In a recent study, Lind et al. (2012) quantified the corrections between an LTE and a non-LTE analysis. They show that the largest impact is seen for

[2] http://www.exoplanet.eu

[3] IRAF is distributed by National Optical Astronomy Observatories, operated by the Association of Universities for Research in Astronomy, Inc., under contract with the National Science Foundation, USA.

[4] http://www.as.utexas.edu/~chris/moog.html

Table 3. Dependence of the *rejt* parameter on the S/N.

S/N condition	*rejt*	S/N condition	*rejt*
$S/N \leq 20$	0.989	$80 < S/N \leq 120$	0.994
$20 < S/N \leq 30$	0.990	$120 < S/N \leq 160$	0.995
$30 < S/N \leq 40$	0.991	$160 < S/N \leq 200$	0.996
$40 < S/N \leq 60$	0.992	$S/N > 200$	0.997
$60 < S/N \leq 80$	0.993		

very metal-poor and hot giant stars. Since our sample consists of cool giant stars with metallicities higher than −1.0 dex, our assumption of LTE is justified.

3.2. Different line lists

The iron lines that are used to derive atmospheric parameters should be chosen carefully so that the equivalent widths can be measured accurately. Ideal lines are single and not blended or saturated. Different line lists exist in the literature, some very general, some for specific types of stars. To find a reliable line list for evolved stars, in this work we used two different Fe line list sets to measure the equivalent widths and then derived the atmospheric parameters.

First, all stars were analysed with the large line list taken from SO08, as our team usually does. For some stars that were analysed before 2008, the smaller line list from Santos et al. (2004) was used. In SO08, the authors show that the stellar parameters, obtained with both lists, compare very well. Since more lines allow for smaller errorbars, the large SO08 line list is preferred. For cool stars (below 5200 K), however, the results from using these line lists were unsatisfactory. The derived temperatures were too high, when compared with other methods like the InfraRed flux Method (Sousa et al. 2008). Therefore, a new line list was built, specifically for these cooler stars (Tsantaki et al. 2013, hereafter TS13), based on the SO08 line list. Only weak and isolated lines were left, since blending effects play a huge role in cool stars. The authors show that their new temperatures are in very good agreement with the results from the InfraRed flux Method. The other atmospheric parameters are comparable with the results from using the SO08 line list. Since most giant stars in our sample (61 out of 71) have temperatures lower than 5200 K, we used this line list for these 61 stars. For the remaining 10 stars, we still used the SO08 line list. Hereafter we will refer to this line list set as TS13–SO08.

Second, we also derived the parameters by making use of the small line list (20 Fe I and 6 Fe II lines) from Hekker & Meléndez (2007, hereafter HM07). This line list was made specifically for giant stars where all lines were carefully selected to avoid blends by atomic and CN lines. The reference solar iron abundance used to make this list is $A(\mathrm{Fe})_\odot = 7.49$. For the line lists of SO08 and TS13, the reference value of $A(\mathrm{Fe})_\odot = 7.47$ was used.

3.3. Reference star Arcturus

To test our line lists, we derived parameters for the *K* giant Arcturus. This star is an excellent reference star for giant studies since it is very bright and easy to observe with different telescopes. Furthermore, it has been studied multiple times, so there is a lot of data for comparison. For our analysis, we used a spectrum from the archive from the NARVAL spectrograph (with a resolution of 70 000) at the 2 m Bernard Lyot Telescope in Toulouse, France.

Table 4 lists our results derived using the three different line lists mentioned above. These all compare remarkebly well. In Fig. 1, this reference star is overplotted. We also list the values from a recent study by Ramírez & Allende Prieto (2011). Furthermore, we take the mean and standard deviation of all values listed in the PASTEL catalogue (Soubiran et al. 2010). All values compare within the errorbars. We are thus confident that our line lists are suited for analysing cool giant stars.

The agreement in temperature between the line lists of SO08 and TS13 is remarkable, since the SO08 line list normally results in overestimated temperatures. This star is so bright that the spectrum is of very good quality, with both high resolution and high S/N. The SO08 line list is thus probably less affected by blended lines resulting in compatible results with the TS13 line list.

3.4. Stellar masses

Stellar masses were estimated as in previous works (e.g. Santos et al. 2004; Sousa et al. 2011). Stellar evolutionary models from the Padova group were used, through their webpage[5] (da Silva et al. 2006). This web interface needs four parameters. For the temperature and metallicity, the values from our analysis were used. For the *V* magnitude and parallax, the HIPPARCOS values were used (van Leeuwen 2007) whenever possible. If no errors were provided in the database, the typical values 0.05 and 1.0 mas, respectively, were used.

If no *V* magnitude was present in the HIPPARCOS database, we used the value presented by Simbad. If the HIPPARCOS database did not provide a parallax or if the parallax error was larger than 10% of the value, an iterative method was used to get the masses. This method was previously introduced in Santos et al. (2010) and makes use of the bolometric correction from Flower (1996) and the Padova web interface.

4. Stellar parameters

Table 5 lists all stellar parameters derived with the TS13 line list for stars cooler than 5200 K, and SO08 for stars with a temperature above this value (the TS13–SO08 line list set). For the cooler stars, we list the SO08 results in Appendix A (Table A.1). In Table 6, we list the parameters derived with the HM07 line list.

With the TS13 line list, no solution could be found for HD13189. This star was observed with the SARG spectrograph at the TNG telescope in 2002. The spectrum was very noisy and the spectral lines were hard to measure. We calculated all EWs by hand, using the TS13 line list, but could not converge to a viable solution with MOOG. The results from the SO08 line list are thus used for this star. For HIP75458, the EWs were also measured by hand, using the TS13 line list.

Using the smaller HM07 line list did not always allow for good microturbulence determinations because of the small EW interval of the measured Fe I lines. This is a disadvantage of using small line lists. For 17 stars, the microturbulence was thus derived with the formula

$$\xi_\mathrm{t} = 3.7\text{–}5.1 \times 10^{-4}\, T_\mathrm{eff}.$$

This formula was empirically derived by HM07 based on their results, using their small line list. These 17 stars are marked with an asterisk in Table 6. We ran a test for 10 stars, where

[5] http://stev.oapd.inaf.it/cgi-bin/param

Table 4. Atmospheric parameters for the reference giant star Arcturus.

	$T_{\rm eff}$ (K)	$\log g_{\rm spec}$ (cm s^{-2})	[Fe/H] (dex)	ξ (km s^{-1})
This work – SO08	4392 ± 56	1.92 ± 0.13	–0.57 ± 0.03	1.90 ± 0.05
This work – TS13	4368 ± 63	1.86 ± 0.19	–0.59 ± 0.04	1.86 ± 0.07
This work – HM07	4411 ± 104	2.30 ± 0.21	–0.56 ± 0.07	2.08 ± 0.15
MARCS models – TS13	4408 ± 70	1.89 ± 0.19	–0.55 ± 0.04	1.89 ± 0.06
Ramírez & Allende Prieto (2011)	4286 ± 30	1.66 ± 0.05	-0.52 ± 0.04	1.74
PASTEL mean	4317 ± 63	1.68 ± 0.32	–0.54 ± 0.11	

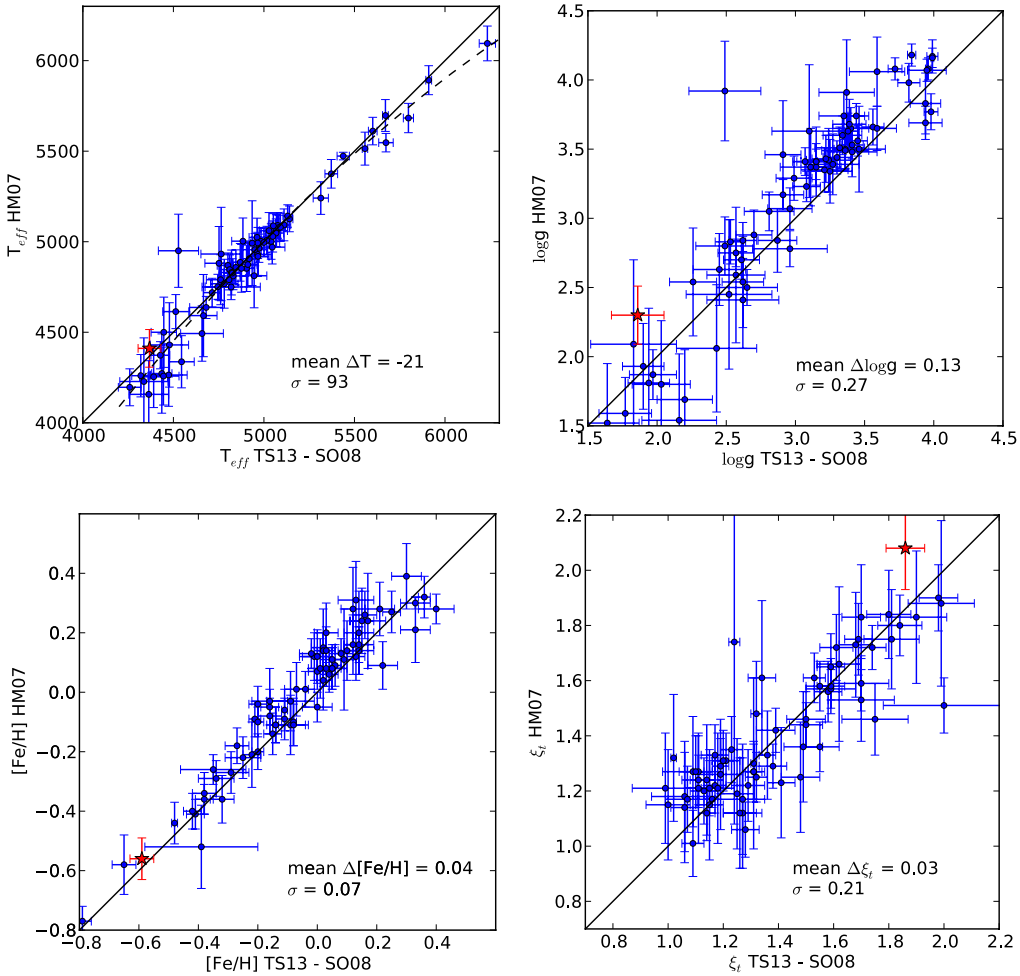

Fig. 1. Comparisons of the spectroscopic results from the TS13–SO08 line list versus the HM07 line list for effective temperature, surface gravity, metallicity, and microturbulence. The measurements for the reference star Arcturus are overplotted with a star symbol. The dashed line in the top-left panel represents a second degree polynomial fit.

we derived the atmospheric parameters both with the standard method and with this formula for the microturbulence derivation. We find that all parameters compare well, within errorbars. Especially for metallicity, the most important parameter in this work, the agreement is striking. The standard deviation for the differences for these stars are 54 K, 0.19 dex, 0.04 dex, and 0.20 km s^{-1} for effective temperature, surface gravity, metallicity and microturbulence, respectively, while the mean error of these parameters are 94 K, 0.16 dex, 0.08 dex, and 0.15 km s^{-1}. This test shows that the use of the above-mentioned formula does not compromise the uniformity of the analysis.

When we used the HM07 line list for giant stars, there were also four stars where we calculated the EWs by hand: HD104985, HD13189, HD177830, and HIP 75458. The stars were all observed with the SARG spectrograph at the TNG telescope. The spectra were not good enough to calculate the EWs automatically with ARES.

In Fig. 1, we compare the atmospheric parameters derived with the different line lists. All differences presented in this work are calculated as y-axis–x-axis, as they are presented in Fig. 1. The comparisons with the cool SO08 results are presented in Appendix A.

4.1. Effective temperature

The TS13–SO08 line list set and the HM07 line list provide comparable temperatures. A mean difference of −21 K is found between the results of HM07 and TS13–SO08. The temperatures

differ more for the coolest stars. If we only consider the temperatures higher than 4700 K, there is a mean difference of only −4 K. The values from the TS13–SO08 line list set are preferred thanks to the good comparison with the HM07 line list, designed for giant stars, and the smaller errorbars (because the line lists of TS13–SO08 have more lines than the HM07 line list). We fitted a second degree polynomial to the data,

$$T_{\rm eff,HM07} = -0.00014 \cdot T^2_{\rm eff,TS13} + 2.39 \cdot T_{\rm eff,TS13} - 3556,$$

so one can correct for the slight offset amongst the coolest stars, if judged necessary. Our temperatures are not corrected with this polynomial.

4.2. Surface gravity and microturbulence

The determined surface gravities with the two line list sets are comparable with a mean difference of 0.13 dex for HM07 versus TS13–SO08 (see top right panel in Fig. 1). Gravities determined with the HM07 line list are slightly higher than the other $\log g$ values, but every value lies within the errorbars.

Microturbulences also compare very well with each other (bottom right panel in Fig. 1) with a mean difference of 0.03 km s^{-1}. These results compare remarkably well. Thanks to these very good comparisons, the values from the TS13–SO08 line list set were again preferred as a reference.

4.3. Metallicity

Hekker & Meléndez (2007) found comparable metallicity results in their sample with literature data. They also compared their results with the homogeneous analysis of Luck & Heiter (2007) for giant stars in the local region; HM07 find slightly lower metallicities than Luck & Heiter (2007) with a mean difference of −0.05 dex. They claim the differences are due to the use of different model atmospheres (Kurucz versus MARCS). We have derived parameters for our reference star Arcturus by using the spherical MARCS models and the TS13 line list. We find that the metallicities derived with the Kurucz models are marginally lower than the one derived with the MARCS model (see Table 4).

We find slightly higher metallicities by using the HM07 line list with respect to using the TS13–SO08 line list set with a mean differences of 0.04 dex. The results of the TS13–SO08 line list set are thus even more different from the results of Luck & Heiter (2007). This offset in metallicities cannot be explained by different model atmospheres since both this work as HM07 use the Kurucz models. Furthermore, Fig. 1 shows that this offset is constant and does not vary with metallicity. It has to be noted that the offset is smaller than the spread. So, although the values from the HM07 line list are slightly higher, all values are comparable within errorbars. To guarantee uniformity, we adopt the metallicities derived with the TS13–SO08 line list set.

4.4. Stellar masses

Stellar masses were calculated for the parameters derived with the TS13–SO08 line list set and for the parameters derived with the HM07 line list. The results are listed in Tables 5 and 6. A comparison between the values can be seen in Fig. 2. The values agree within errorbars. They show a mean difference of −0.07 $M_\odot$ between the values of HM07 and TS13–SO08. We prefer to use the values derived with the TS13–SO08 line list set for further analysis, as we do for the atmospheric parameters.

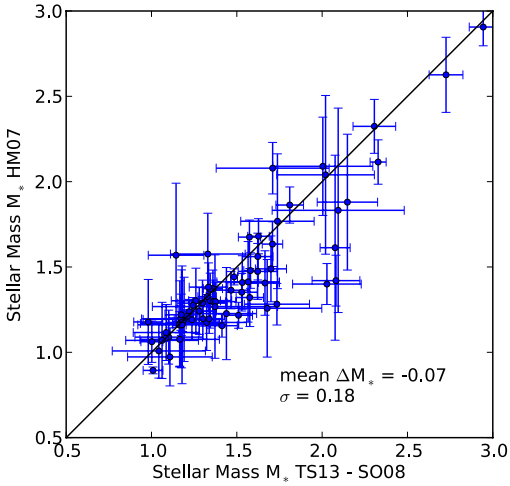

Fig. 2. Comparison of stellar masses derived with the line lists of TS13 and HM07.

5. Comparison with the literature

We used six different works (Hekker & Meléndez 2007; da Silva et al. 2006, 2011; Valenti & Fischer 2005; Gonzalez et al. 2010; Takeda et al. 2008) to compile a list of literature data for 31 stars in our sample (see Table 7). These works all use spectroscopic methods to obtain the stellar parameters. We compared our stellar parameters (derived with the TS13 line list for the stars cooler than 5200 K and the SO08 line list for the stars hotter than this value) with these literature values.

The result is plotted in Fig. 3 where different symbols denote different references. The mean differences (defined as literature – this work) for temperature, surface gravity, and metallicity are −24 K, 0.00 dex, and 0.01 dex. Given the spread in the data, we can say that the differences are essentially zero. This reinforces our choice for adopting the results derived from the TS13–SO08 line list set.

Of particular relevance for the analysis in this paper is the comparison with the data from da Silva et al. (2006) and Takeda et al. (2008) (see Sect. 6.3). For their values only, the mean differences with our values are –50 K, –0.11 dex, and 0.01 dex for temperature, surface gravity, and metallicity, respectively.

6. Planet frequency

All evolved stars in this sample are orbited by at least one giant planet (with a mass between 0.1 and 25 $M_{\rm Jup}$). For main-sequence FGK dwarfs, it has been shown that stars hosting a giant planet are more metal-rich than average field dwarfs (e.g. Santos et al. 2001, 2004; Fischer & Valenti 2005). There have been studies to check whether this metallicity enhancement can also be found in planet-hosting giants (Hekker & Meléndez 2007; Pasquini et al. 2007; Takeda et al. 2008; Ghezzi et al. 2010b; Zieliński et al. 2010; Maldonado et al. 2013) with contradictory results.

Pasquini et al. (2007) suggest that evolved planet-hosting stars are 0.2–0.3 dex more metal-poor than main-sequence planet-hosting stars. Interestingly this is the same difference as between planet hosting and field dwarfs. Takeda et al. (2008) used a sample of late-G giants to show that there is no metallicity enhancement for giant stars hosting a giant planet. This result was confirmed by the preliminary results of Zieliński et al. (2010) and the recent results of Maldonado et al. (2013). Hekker & Meléndez (2007) and Ghezzi et al. (2010b) on the other

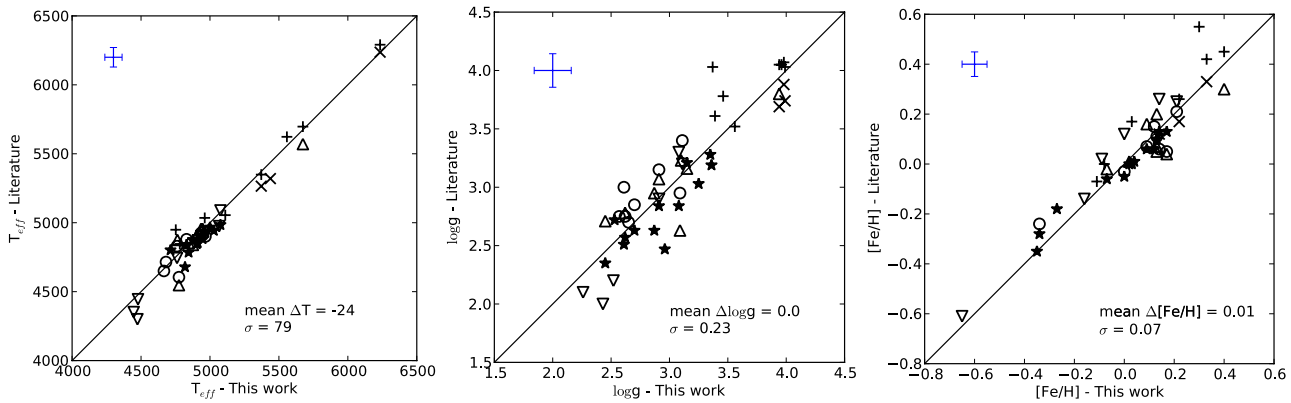

Fig. 3. Comparisons of the adopted spectroscopic results in this work with literature data for effective temperature, surface gravity and metallicity. Different symbols denote different references: circles for Hekker & Meléndez (2007), downward and upward triangles for da Silva et al. (2006, 2011), stars for Takeda et al. (2008), + for Valenti & Fischer (2005) and *x* for Gonzalez et al. (2010).

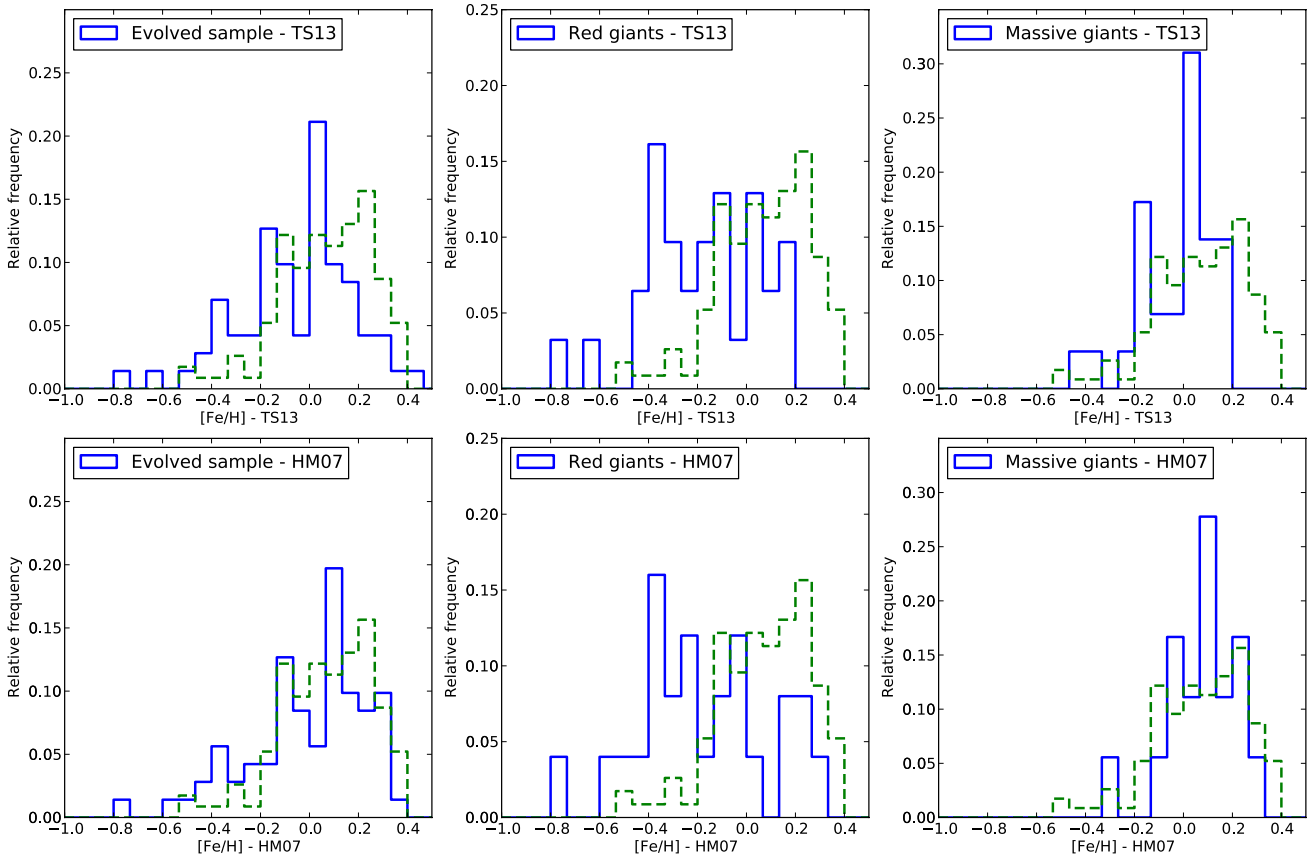

Fig. 4. Metallicity distribution of evolved stars with giant planets (solid line). The metallicity distribution of the giant-planet host CORALIE + HARPS dwarf sample (dashed line) is shown as a reference. The *upper panels* use the metallicities derived with the TS13–SO08 line list set, while the *bottom panels* use the HM07 line list. *From left to right*: the complete sample of evolved stars, the subsample of red giants defined through the log g, and the subsample of the most massive giants.

hand do find a metallicity enhancement of about 0.13–0.21 dex, comparable with what has been found in dwarf stars.

In the following sections we will use the results obtained using the TS13–SO08 line list set to study the giant planet frequency. We will first explore the differences between dwarf and giant stars and discuss a bias in the planet search samples of giant stars. Then, we will compare planet-hosting giant stars with non-planet-hosting giant stars to see if there indeed is a metallicity enhancement for planet-hosting giants. For every comparison, we will also mention the results from the parameters derived using the HM07 line list.

6.1. Giants versus dwarfs

To tackle this problem, we first compared the metallicity distribution for our evolved planet hosts with that for dwarf planet hosts. For this purpose, we used the CORALIE+HARPS dwarf sample (for details see Sousa et al. 2011; Mortier et al. 2013, and references therein). For a full description of these surveys, see Mayor et al. (2011). The metallicities from this sample were derived using either the method described in this work, or the cross correlation function (CCF) calibration when no high-resolution spectra were available. The CCF calibration

Table 7. Atmospheric parameters from the literature for 31 different stars in our sample.

Name	$T_{\rm eff}$ (K)	$\log g_{\rm spec}$ (cm s^{-2})	[Fe/H] (dex)	Reference
11Com	4880	3.00	–0.24	1
	4841	2.51	–0.28	2
18Del	5089	3.30	0.12	3
	4985	2.84	–0.05	2
7CMa	4744	3.20	0.25	3
	4830	3.40	0.21	1
75Cet	4906	2.95	0.01	4
	4846	2.63	0.00	2
81Cet	4785	2.35	–0.06	2
	4853	2.71	–0.02	4
91Aqr	4715	2.70	–0.03	1
epsTau	4910	2.75	0.05	1
	4956	2.78	0.04	4
	4883	2.57	0.13	2
gammaCephei	4875	3.23	0.05	4
HD 104985	4679	2.47	–0.35	2
HD 110014	4445	2.20	0.26	3
HD 11964	5349	4.03	0.12	5
	5265	3.74	0.12	6
HD 11977	4975	2.90	–0.14	3
HD 122430	4300	2.00	0.02	3
HD 148427	5035	3.61	0.17	5
HD 159868	5623	4.05	0.00	5
HD 167042	4943	3.28	0.00	2
HD 175541	5055	3.52	–0.07	5
HD 177830	4949	4.03	0.55	5
HD 210702	4967	3.19	0.01	2
HD 27442	4846	3.78	0.42	5
HD 38529	5697	4.05	0.45	5
	5570	3.80	0.30	4
HD 47536	4352	2.10	–0.61	3
HD 5608	4854	3.03	0.06	2
HD 59686	4650	2.75	0.15	1
HD 62509	4925	3.15	0.07	1
	4955	3.07	0.16	4
	4904	2.84	0.06	2
HD 88133	5320	3.69	0.33	6
HD 89744	6291	4.07	0.26	5
	6237	3.88	0.17	6
HIP75458	4605	2.95	0.11	1
	4547	2.63	0.07	4
kappaCrB	4839	3.16	0.20	4
	4877	3.21	0.10	2
ksiAql	4802	2.72	–0.18	2
nuOph	4900	2.85	0.06	1
	4928	2.63	0.13	2

References. (1) Hekker & Meléndez (2007); (2) Takeda et al. (2008); (3) da Silva et al. (2006); (4) da Silva et al. (2011); (5) Valenti & Fischer (2005); (6) Gonzalez et al. (2010).

was derived by Santos et al. (2004) who also showed that metallicities calculated with this calibration are compatible with the metallicities derived by the method used in this work. Furthermore, the dispersion of the calibration is only 0.06 dex.

These two metallicity distributions are shown in the top-left panel of Fig. 4. For the evolved stars, we use our adopted metallicities derived with the TS13–SO08 line list set. A Kolmogorov-Smirnov test (K-S test) was performed to check whether the two samples follow the same distribution. With a probability of 0.43%, we can say with a 3σ confidence that the evolved sample and the dwarf sample are different in metallicity distribution. All K-S probabilities used in this work are listed in Table 8.

Evolved stars have both lower surface gravities and higher masses than dwarf stars. To test which parameter shows the biggest difference in metallicity distribution for planet hosts, we constructed two subsamples of the evolved sample (where all stars have $\log g < 4.0$). One sample was defined by the surface gravity only ($\log g < 3.0$ – red giants). Another sample was defined by mass only ($M_* > 1.5\ M_\odot$ – massive giants). Figure 5 shows the surface gravity versus stellar mass, derived with the TS13–SO08 line list set. The solid lines represent the boundaries of the two subsamples.

The top-middle and top-right panels of Fig. 4 show the distributions of these two new subsamples for our adopted metallicities. The giant-planet host sample of the CORALIE+HARPS dwarf sample is also shown. We find that the subsample divided by the surface gravity has a different metallicity distribution than the dwarf sample of planet hosts. A K-S test gives a 0.01% probability that the distributions are comparable. When taking the subsample divided by stellar mass only, a K-S test gives a 0.28% probability that the planet host distributions are the same. This result shows that we cannot discard the hypothesis that massive giants with planets and dwarf stars with planets have the same metallicity distribution. Red giants on the other hand do seem to follow a different distribution.

Table 9 lists the mean and median values for all the samples used in this work. Since the samples are not symmetrically distributed in metallicity, we decided to present the trimean[6] as well since it is a very good measure of central tendency for unsymmetric distributions. Here we find that the mean metallicity of the red giants, the massive giants, and the planet host dwarfs are respectively –0.179 dex, –0.024 dex, and 0.07 dex. This shows that red giants with planets are on average 0.24 dex more metal-poor than planet-hosting dwarfs. Using the median or trimean gives similar results.

Figure 4 also clearly shows that the subsample of red giants defined by the surface gravity has no obvious trend in metallicity. This distribution seems rather flat while the distribution for metallicities from planet hosts in dwarf stars shows a clear increasing trend with increasing metallicity. For the massive giants on the other hand we can see a hint of an increasing trend, similar to the one derived for dwarf stars.

From these tests, it seems that surface gravity is the main parameter responsible for giving different metallicity distributions to planet host stars. Stellar mass also plays a role, but it is less important than the surface gravity.

6.1.1. Results for the HM07 values

As discussed in Sect. 4.3, the metallicities derived with the TS13–SO08 line list set may be slightly underestimated for giant stars when compared with other studies. We thus decided to repeat the same analysis presented in the previous section for the metallicities derived with the HM07 line list. The distributions are shown in the bottom panels of Fig. 4. If we perform a K-S test, we find that there is an 11% probability that the evolved planet hosts and the dwarf planet hosts are drawn from the same distribution. As such, we cannot discard the hypothesis that the samples follow the same distribution.

For the subsamples (bottom row, middle and right panels of Fig. 4), we find that the red giants are again differently

[6] $T = (Q1 + 2 \cdot median + Q3)/4$ where Q1 and Q3 are the first and third quartile.

Table 8. Probabilities that the two samples are drawn from the same distribution according to a K-S test.

Sample 1	Sample 2	Probability (%)
Evolved stars ($\log g < 4.0$) – TS13–SO08	Dwarf planet hosts	0.43
Red giants ($\log g < 3.0$) – TS13 – SO08	Dwarf planet hosts	0.01
Massive giants ($M_* > 1.5\ M_\odot$) – TS13 – SO08	Dwarf planet hosts	0.28
Evolved stars ($\log g < 4.0$) – HM07	Dwarf planet hosts	11.49
Red giants ($\log g < 3.0$) – HM07	Dwarf planet hosts	0.01
Massive giants ($M_* > 1.5\ M_\odot$) – HM07	Dwarf planet hosts	66.49
Dwarf field stars	Dwarf planet hosts	8.26×10^{-10}
Evolved stars ($\log g < 4.0$) – TS13 – SO08	Giant comparison stars	0.12
Red giants ($\log g < 3.0$) – TS13 – SO08	Red comparison stars	27.46
Evolved stars ($\log g < 4.0$) – HM07	Giant comparison stars	6.06×10^{-6}
Red giants ($\log g < 3.0$) – HM07	Red comparison stars	13.79

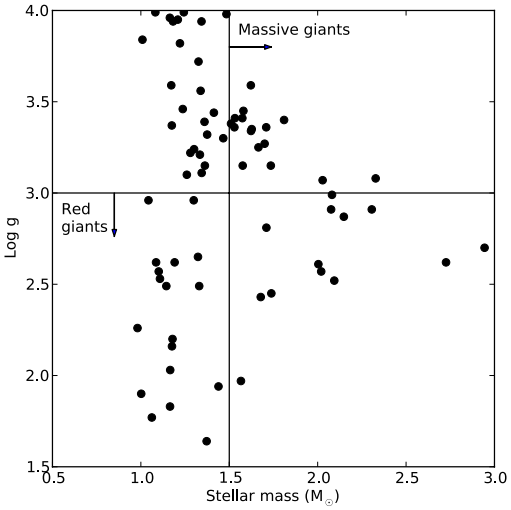

Fig. 5. Surface gravity $\log g$ versus stellar mass. The values were calculated with the TS13–SO08 line list set. Solid lines show the boundaries for the different definitions of the giant subsamples.

distributed with only a 0.01% probability that the distribution is the same as the dwarf sample. The massive giants and the dwarf sample seem to follow the same distribution with a K-S probability of 66.49%.

Here we conclude that surface gravity does seem to play a big role in the different metallicity distributions. For stellar mass, the situation is very dependent on which line list is used, but overall it suggests that stellar mass is not the main factor responsible for the observed different metallicity distributions between dwarf planet hosts and evolved planet hosts.

6.2. Bias in the giant samples

It is important to note that a comparison between dwarf stars and giant stars suffers from a biased sample selection. Most large programs to search for planets around giant or sub-giant stars select the stars for their sample by making a cut-off in the $B - V$ colour ($B - V \leq 1.0$). Examples are the Okayama Planet search program (Sato et al. 2005), the retired A stars program (Johnson et al. 2006), and the Penn State-Toruń Centre for Astronomy Planet Search (Niedzielski & Wolszczan 2008). The ESO FEROS planet search (Setiawan et al. 2003) on the other hand does not perform a $B - V$ cut-off.

In Fig. 6 we plot surface gravity $\log g$ versus metallicity [Fe/H]. The top panel shows the stellar parameters for three

Table 9. Mean, median, and trimean values of the several samples and subsamples used in this work.

Sample	Mean	Median	Trimean
Evolved stars – TS13	–0.055	0.0	–0.020
Red giants ($\log g < 3.0$) – TS13	–0.179	–0.160	–0.166
Massive giants (mass) – TS13	–0.024	0.020	0.004
Evolved stars – HM07	–0.011	0.060	0.040
Red giants ($\log g < 3.0$) – HM07	–0.180	–0.210	–0.198
Massive giants (mass) – HM07	0.072	0.095	0.078
Dwarf stars	–0.106	–0.080	–0.085
Planet-hosting dwarf stars	0.07	0.085	0.082
Evolved comparison stars	–0.13	–0.10	–0.10
Red comparison giants	–0.14	–0.11	–0.12

literature samples. We combined the Okayama Planet search program (parameters from Takeda et al. 2008), the ESO FEROS planet search program (parameters from da Silva et al. 2006) and the Penn State-Toruń Centre for Astronomy Planet Search (parameters from Zieliński et al. 2012). For stars that were present in more than one sample, we preferred the parameters from Takeda et al. (2008) and Zieliński et al. (2012). All stars have surface gravities lower than 4.0 dex, compatible with our definition of evolved stars. In the bottom panel we plot our sample of evolved planet hosts. It can be seen from these plots that higher metallicity stars with low surface gravity are left out in these samples. We drew the dashed lines by eye to emphasize this bias.

For cool stars (which is the case for giant stars), a $B - V$ cut-off results exactly in the lack of high-metallicity, low-gravity stars. The mean temperature of the stars in our evolved sample is about 4850 K. For this temperature, we calculated the $B - V$ with the calibration of Sekiguchi & Fukugita (2000). This calibration depends on temperature, metallicity and surface gravity. Values for different surface gravities and metallicities can be found in Table 10. Clearly, for low-gravity stars the highest metallicity stars are missed because of the a priori cut-off of $B - V \leq 1.0$. In Fig. 7, we plot the metallicity distributions of both the CORALIE+HARPS dwarf sample (solid line) and the comparison sample of giant stars (dashed line). While the distributions are similar at low metallicities, it is clear that there are fewer giant stars with high metallicity. This is probably a reflection of the $B - V$ cut-off.

Since surveys for planets around evolved stars are clearly biased towards lower metallicity, comparisons between evolved stars and dwarf stars with planets should be performed with caution. We found that red giants with planets are on average

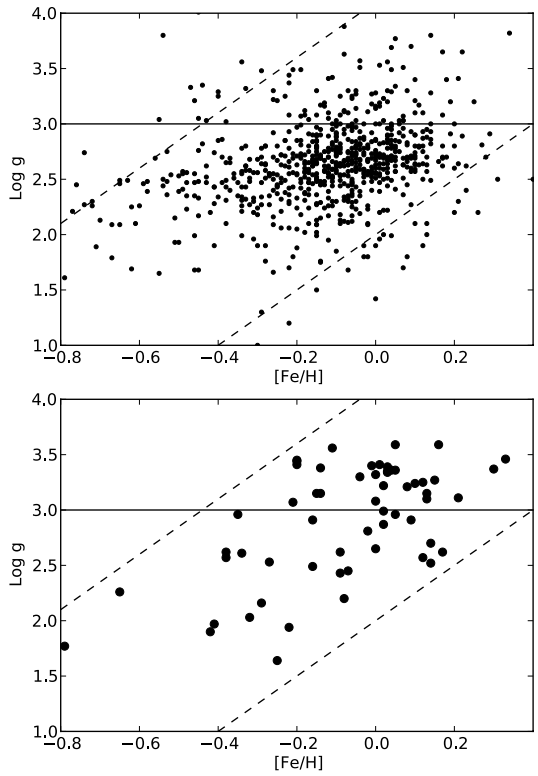

Fig. 6. Surface gravity $\log g$ versus metallicity for the giant comparison sample used in this work (*upper panel*) and for our evolved planet hosts (*lower panel*). The values were calculated with the TS13 line list. The horizontal line denotes the limit in surface gravity for the subsample of red giants. The two dashed lines were drawn by eye and show the biases in the samples due to the $B - V$ cut-off.

Table 10. $B - V$ values for a given temperature of 4850 K, calculated with the calibration of Sekiguchi & Fukugita (2000).

		[Fe/H]			
		–0.2	0.0	0.2	0.4
	1.0	0.985	1.01	1.037	1.066
$\log g$	1.5	0.978	1.003	1.03	1.059
	2.0	0.971	0.996	1.023	1.052
	2.5	0.964	0.989	1.016	1.044

0.24 dex more metal-poor than planet-hosting dwarfs. Given the clear metallicity bias, we recalculated the mean of the planet-hosting dwarfs for stars with metallicities lower than 0.2 dex. The mean metallicity drops then from 0.07 dex to −0.01 dex. Although this mean metallicity is much lower, it is still higher than the mean metallicity for red giants. However, reliable statistics will only be available if we have an unbiased planet search sample of giant stars that includes higher metallicity stars.

6.3. Planet hosts versus non-planet hosts: a tentative, unbiased comparison

To understand whether giant stars with planets also show the metallicity enhancement as observed for dwarf stars with planets, we used the comparison sample of giant stars defined in the previous section. It combines three planet search surveys and consists of 733 giants. Atmospheric parameters were derived with similar methods to this work (da Silva et al. 2006; Takeda et al. 2008; Zieliński et al. 2012). We have 19 stars in common

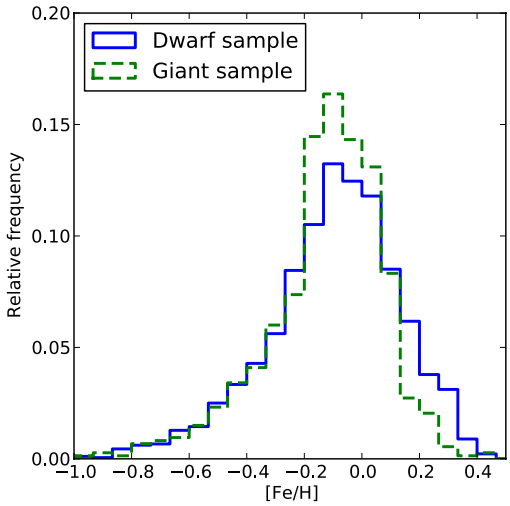

Fig. 7. Metallicity distribution of the CORALIE+HARPS dwarf sample (solid line) and the giant sample of Takeda et al. (2008).

with this sample. The atmospheric parameters for these 19 stars are comparable with our results. Mean differences with our atmospheric parameters are –50 K, –0.11 dex, and 0.01 dex for temperature, surface gravity, and metallicity, respectively (see Sect. 5). The mean, median, and trimean metallicity of this sample is shown in Table 9.

For our adopted metallicities derived with the TS13–SO08 line list set, a K-S test gives a probability of 0.12% that the giant comparison sample and our evolved planet-hosting sample have the same metallicity distribution. In the previous sections, we showed that a different metallicity distribution can be found if we only consider low-gravity stars. In the comparison sample, there are 619 stars with a surface gravity lower than 3 dex. When comparing this subsample with our subsample of low-gravity planet hosts (see top panel of Fig. 8), the probability that the metallicities follow the same distribution is 27.46%. These samples are thus statistically not differently distributed in metallicity. Evolved planet hosts and non-planet hosts follow the same metallicity distribution.

The mean values of the metallicities show that there is a slight metallicity enhancement of about 0.07 dex for evolved stars with planets with respect to non-hosting evolved stars (for dwarf stars, the enhancement is 0.17 dex). If we consider only the red giants, there is no metallicity enhancement present for planet hosts.

6.3.1. Results for the HM07 values

We performed the tests again, also for the parameters derived with the HM07 line list. A K-S test gives a probability of only 6.06×10^{-6}% that the giant comparison sample and this evolved planet-hosting sample have the same metallicity distribution. The lower panel of Fig. 8 shows the distributions for the red giant subsamples. The metallicities of red giants with and without planets cannot be statistically distinguished with a K-S probability of 13.79%, confirming the result we found with the values derived with the TS13–SO08 line list set.

The mean values of the metallicities show that there is a metallicity enhancement of about 0.11 dex for evolved stars with planets with respect to non-hosting evolved stars. If we consider only the red giants, there is again no metallicity enhancement present for planet hosts. It is clear that the results depend on

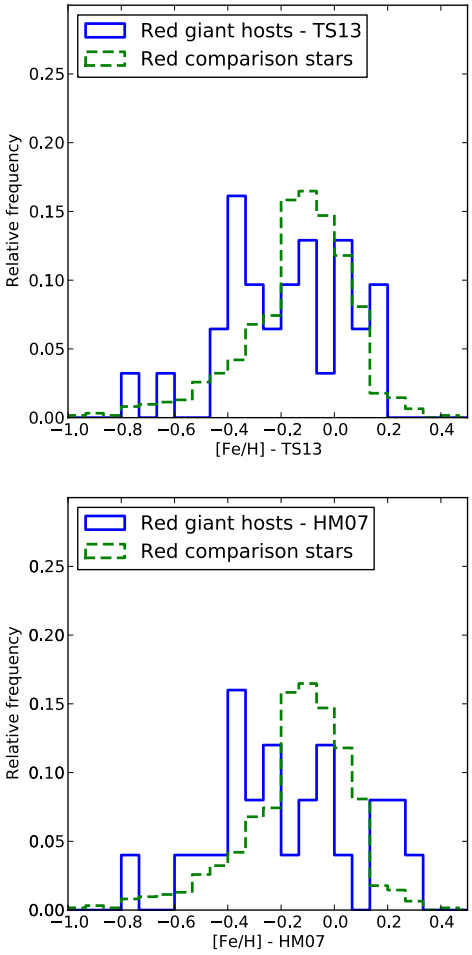

Fig. 8. Metallicity distribution of red giants. A solid line is used for planet hosts while the dashed line represents the comparison sample of Takeda et al. (2008). The *upper panel* uses the metallicities derived with the TS13 line list. Metallicities in *the bottom panel* were derived with the HM07 line list.

the line list used, but for the lower gravity samples there is still agreement. No metallicity enhancement can be found for red giant stars with planets.

7. Discussion

We found that evolved ($\log g < 4.0$ dex) planet hosts are on average 0.24 dex more metal-poor than planet-hosting dwarfs. This confirms the result of Pasquini et al. (2007). However, we also found a huge bias in the evolved stellar samples that are being used for detecting planets. High-metallicity red giants are left out because of a cut-off in the $B - V$ colour at 1.0, applied for most of the surveys in search of planets around giant stars.

We find that stellar mass does not play a role in the metallicity distributions of stars with planets. Massive giants and dwarf stars with planets have the same metallicity distribution where the planet frequency increases with metallicity. This is in line with the recent results of Maldonado et al. (2013) who show that massive giants with planets are more metal-rich.

Furthermore, there seems to be no metallicity enhancement present for red giants with planets. Figure 9 shows the frequency of giant planets as a function of metallicity for the three combined planet-search samples used in this work (Setiawan et al. 2003; Sato et al. 2005; Niedzielski & Wolszczan 2008). We

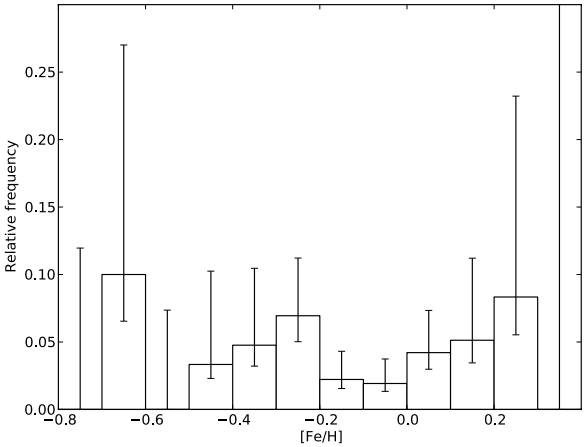

Fig. 9. Frequency of giant planets as a function of metallicity for the combined red giant sample from Setiawan et al. (2003), Sato et al. (2005), and Niedzielski & Wolszczan (2008).

Table 11. Giant-planet frequencies with 1-σ error bars for four subsamples of red giants. The number of stars in each subsample is shown in brackets.

	[Fe/H] < -0.2	[Fe/H] ≥ -0.2
$\log g < 2.5$	$5.55^{+3.09}_{-1.47}$% (108)	$3.39^{+2.55}_{-0.98}$% (118)
$2.5 \leq \log g < 3.0$	$4.16^{+3.78}_{-1.29}$% (72)	$2.80^{+1.25}_{-0.65}$% (321)

limited the sample to red giants, with surface gravity $\log g < 3.0$ dex. This sample consists of 619 giants, among which 22 planet hosts. The plot shows no clear metallicity enhancement for giant stars with planets. The distribution seems rather flat, although a slight dip can also be seen around solar metallicity. This result reinforces our findings that red giant stars with planets have no metallicity preference. This lack of correlation confirms the results of Takeda et al. (2008) and Zieliński et al. (2010). The opposite results from Hekker & Meléndez (2007) and Ghezzi et al. (2010b) could not be confirmed.

The sample of evolved stars with surface gravities between 3.0 and 4.0 dex (i.e. subgiants) does still show a positive correlation with metallicity. This is probably because these stars are, in terms of evolution, still very close to dwarf stars. They are at an intermediate stage and thus better left out of further discussions.

Since surface gravity and metallicity seem closely linked in red giants, we split the red giant sample into four groups divided at [Fe/H] $= -0.2$ and $\log g = 2.5$, and calculated planet frequencies for these four groups (see Table 11). We found that the planet frequency for the low-metallicity, low-gravity stars is 5.55% while the frequency for high-metallicity high-gravity stars is only 2.80%. One should not forget, however, that giant stars with the highest metallicity are not being surveyed for planets. If there were no bias in planet survey samples for giant stars, there might be more planet hosts with high metallicity.

We also caution the reader about these frequency results. We used several survey samples from the literature as a comparison sample. We trust the stellar parameters for the stars in these samples since they compare well with our own results. However, we have no control over the actual survey and the manner in which the search for planets was performed.

Explaining our results is not simple. Several reasons may exist for this lack of metallicity enhancement and for the

importance of the surface gravity on the metallicity distribution of evolved planet hosts.

Pasquini et al. (2007) argues that the factor responsible for this lack of correlation is probably the mass of the convective zone. The high metallicity of main-sequence stars is due to the pollution of their atmospheres. In the extended massive envelopes of giant stars, this metal excess is almost completely diluted. This would explain the lack of correlation seen for evolved planet hosts and also the fact that samples of giant stars have fewer metal-rich stars than dwarf star samples. However, subgiants are also diluted and we do see a metallicity correlation for these stars. Furthermore, it seems that this pollution explanation is in contrast with the primordial scenario explanation, where stars are born in high-metallicity clouds (e.g. Fischer & Valenti 2005).

Evolved stars are on average more massive than dwarf stars. When stars are more massive, they have more massive protoplanetary disks which may make it easier to form giant planets. As such, the metallicity becomes a less important parameter in the formation process and metal-rich stars would not necessarily be preferred. However, when we select only the most massive stars in our sample, the distribution gets closer to the dwarf sample instead of farther away. The trend towards higher metallicities is also present in this massive subsample. Surface gravity clearly plays a role, but low surface gravities do not necessarily mean higher masses. As such, the stellar mass is probably not the reason for this difference in metallicity.

Another important factor may be the periods of the planets. If metal-rich stars have a greater number of low-period planets (e.g. because migration is faster around these stars), these planets would be engulfed by the star when it becomes a giant (and gets a lower surface gravity). This in turn would result in fewer metal-rich giants with planets. However, when we select only the long-period giants in the CORALIE+HARPS sample, the metallicity enhancement can still be seen for dwarf stars, so it should be present in giant stars as well. This engulfment is thus probably not the reason either.

The metallicity correlation seen in dwarf stars with planets can be explained with the core-accretion formation theory (e.g. Ida & Lin 2004; Udry & Santos 2007; Mordasini et al. 2012). Other planet formation theories, such as gravitational instability, do not expect a trend with metallicity (Boss 2002). So, one could argue that planets around evolved stars were formed with another mechanism. However, since all evolved stars were once main-sequence stars, this explanation also seems unfavourable.

To study these giant stars in more depth, there is a need for an unbiased giant sample with no colour cut-off and homogeneously derived parameters that are equally searched for planetary companions.

8. Conclusion

In this paper, we derive atmospheric stellar parameters for a sample of 71 evolved stars with planets. Two different line list sets are considered: a large line list set from TS13 and SO08 for stars cooler and hotter than 5200 K, respectively, and the small line list from HM07, designed to analyse giant stars. These line lists were tested with the reference star Arcturus which gave good results for all line lists.

We can summarize the results as follows:

- Surface gravity, microturbulence, and metallicity are not significantly affected by using different line list sets. All values compare well with other spectroscopic results in the literature. The values derived with the TS13–SO08 line list set are preferred and adopted for further analysis. All these values will be added to SWEET-Cat, a catalogue of stellar parameters for stars with planets (Santos et al. 2013).
- Using different line list sets provides a very small and constant offset for metallicities that affects the planet frequency statistics. Although the offset is small and within errorbars, it still affects the statistics.
- Evolved planet hosts are on average 0.24 dex more metal-poor than planet-hosting dwarfs. There is, however, a strong bias in giant stellar surveys towards lower metallicities. Comparing dwarf stars with giant stars should be done with caution.
- Only a slight metallicity enhancement is found for evolved stars with planets with respect to evolved stars without planets (depending on the line list used). This enhancement is smaller than the one seen in dwarf stars.
- No metallicity enhancement is found for red giants with planets with respect to red giants without planets. The metallicity distribution seems flat. Furthermore, the lowest gravity, lowest metallicity stars are slightly preferred for giant planet formation.
- The reasons for this lack of metallicity enhancement and the preference for lower surface gravities are still unclear. Sample biases cannot be discarded, and a fully uniform study is critical to disentangle the causes of the observed discrepancy.

Acknowledgements. We thank the anonymous referee for the useful comments. This research has made use of the SIMBAD database, operated at CDS, Strasbourg, France. This work was supported by the European Research Council/European Community under the FP7 through Starting Grant agreement number 239953. E.D.M, S.G.S, and V.Zh.A. acknowledge the support from the Fundação para a Ciência e Tecnologia, FCT (Portugal) in the form of the grants SFRH/BPD/76606/2011, SFRH/BPD/47611/2008, and SFRH/BPD/70574/2010, respectively. G.I. acknowledges financial support from the Spanish Ministry project MICINN AYA2011-29060.

References

Bergemann, M., Lind, K., Collet, R., Magic, Z., & Asplund, M. 2012, MNRAS, 427, 27
Bonfils, X., Delfosse, X., Udry, S., et al. 2005, A&A, 442, 635
Boss, A. P. 2002, ApJ, 567, L149
Boss, A. P. 2011, ApJ, 731, 74
Buchhave, L. A., Latham, D. W., Johansen, A., et al. 2012, Nature, 486, 375
Cohen, J. G., Huang, W., Udalski, A., Gould, A., & Johnson, J. A. 2008, ApJ, 682, 1029
da Silva, L., Girardi, L., Pasquini, L., et al. 2006, A&A, 458, 609
da Silva, R., Milone, A. C., & Reddy, B. E. 2011, A&A, 526, A71
Endl, M., Cochran, W. D., Kürster, M., et al. 2006, ApJ, 649, 436
Fischer, D. A., & Valenti, J. 2005, ApJ, 622, 1102
Flower, P. J. 1996, ApJ, 469, 355
Ghezzi, L., Cunha, K., Schuler, S. C., & Smith, V. V. 2010a, ApJ, 725, 721
Ghezzi, L., Cunha, K., Smith, V. V., et al. 2010b, ApJ, 720, 1290
Gonzalez, G. 1997, MNRAS, 285, 403
Gonzalez, G., Carlson, M. K., & Tobin, R. W. 2010, MNRAS, 403, 1368
Hekker, S., & Meléndez, J. 2007, A&A, 475, 1003
Ida, S., & Lin, D. N. C. 2004, ApJ, 616, 567
Johnson, J. A., Marcy, G. W., Fischer, D. A., et al. 2006, ApJ, 647, 600
Johnson, J. A., Fischer, D. A., Marcy, G. W., et al. 2007, ApJ, 665, 785
Kurucz, R. 1993, ATLAS9 Stellar Atmosphere Programs and 2 km s^{-1} grid. Kurucz CD-ROM No. 13 (Cambridge, Mass.: Smithsonian Astrophysical Observatory)
Lind, K., Bergemann, M., & Asplund, M. 2012, MNRAS, 427, 50
Lovis, C., & Mayor, M. 2007, A&A, 472, 657
Luck, R. E., & Heiter, U. 2007, AJ, 133, 2464
Maldonado, J., Villaver, E., & Eiroa, C. 2013, A&A, 554, A84
Mayer, L., Quinn, T., Wadsley, J., & Stadel, J. 2002, Science, 298, 1756
Mayor, M., & Queloz, D. 1995, Nature, 378, 355

Mayor, M., Marmier, M., Lovis, C., et al. 2011, A&A, submitted [arXiv:1109.2497]
Mordasini, C., Alibert, Y., Benz, W., & Naef, D. 2009, A&A, 501, 1161
Mordasini, C., Alibert, Y., Benz, W., Klahr, H., & Henning, T. 2012, A&A, 541, A97
Mortier, A., Santos, N. C., Sozzetti, A., et al. 2012, A&A, 543, A45
Mortier, A., Santos, N. C., Sousa, S., et al. 2013, A&A, 551, A112
Moutou, C., Mayor, M., Lo Curto, G., et al. 2011, A&A, 527, A63
Neves, V., Bonfils, X., Santos, N. C., et al. 2013, A&A, 551, A36
Niedzielski, A., & Wolszczan, A. 2008, in Extreme Solar Systems, eds. D. Fischer, F. A. Rasio, S. E. Thorsett, & A. Wolszczan, ASP Conf. Ser., 398, 71
Pasquini, L., Döllinger, M. P., Weiss, A., et al. 2007, A&A, 473, 979
Pollack, J. B., Hubickyj, O., Bodenheimer, P., et al. 1996, Icarus, 124, 62
Ramírez, I., & Allende Prieto, C. 2011, ApJ, 743, 135
Santos, N. C., Israelian, G., & Mayor, M. 2001, A&A, 373, 1019
Santos, N. C., Israelian, G., & Mayor, M. 2004, A&A, 415, 1153
Santos, N. C., Israelian, G., Mayor, M., et al. 2005, A&A, 437, 1127
Santos, N. C., Lovis, C., Pace, G., Melendez, J., & Naef, D. 2009, A&A, 493, 309
Santos, N. C., Mayor, M., Benz, W., et al. 2010, A&A, 512, A47
Santos, N. C., Sousa, S. G., Mortier, A., et al. 2013, A&A, 556, A150
Sato, B., Kambe, E., Takeda, Y., et al. 2005, PASJ, 57, 97
Sekiguchi, M., & Fukugita, M. 2000, AJ, 120, 1072
Setiawan, J., Pasquini, L., da Silva, L., von der Lühe, O., & Hatzes, A. 2003, A&A, 397, 1151
Sneden, C. A. 1973, Ph.D. Thesis, The University of Texas at Austin
Soubiran, C., Le Campion, J.-F., Cayrel de Strobel, G., & Caillo, A. 2010, A&A, 515, A111
Sousa, S. G., Santos, N. C., Israelian, G., Mayor, M., & Monteiro, M. J. P. F. G. 2006, A&A, 458, 873
Sousa, S. G., Santos, N. C., Israelian, G., Mayor, M., & Monteiro, M. J. P. F. G. 2007, A&A, 469, 783
Sousa, S. G., Santos, N. C., Mayor, M., et al. 2008, A&A, 487, 373
Sousa, S. G., Santos, N. C., Israelian, G., Mayor, M., & Udry, S. 2011, A&A, 533, A141
Takeda, Y., Sato, B., & Murata, D. 2008, PASJ, 60, 781
Tsantaki, M., Sousa, S. G., Adibekyan, V. Z., et al. 2013, A&A, 555, A150
Udry, S., & Santos, N. C. 2007, ARA&A, 45, 397
Valenti, J. A., & Fischer, D. A. 2005, ApJS, 159, 141
van Leeuwen, F. 2007, A&A, 474, 653
Zieliński, P., Niedzielski, A., Adamów, M., & Wolszczan, A. 2010, in EAS Pub. Ser. 42, eds. K. Gożdziewski, A. Niedzielski, & J. Schneider, 201
Zieliński, P., Niedzielski, A., Wolszczan, A., Adamów, M., & Nowak, G. 2012, A&A, 547, A91

Pages 13 to 19 are available in the electronic edition of the journal at http://www.aanda.org

Table 1. Data log.

Name	Instrument	Reference
11Com	UVES	This work
18Del	UVES	This work
24Sex	FEROS	This work
7CMa	FEROS	This work
75Cet	FEROS	This work
81Cet	FEROS	This work
91Aqr	UVES	Santos et al. (2005)
alfAri	FEROS	This work
BD+202457	FEROS	This work
BD+20274	FEROS	This work
BD+48738	SOPHIE	This work
epsCrB	UVES	This work
epsTau	UVES	This work
gam01Leo	FEROS	This work
gammaCephei	SARG	Santos et al. (2004)
HD 100655	FEROS	This work
HD 102272	UVES	This work
HD 102329	FEROS	This work
HD 104985	SARG	Santos et al. (2005)
HD 106270	FIES	This work
HD 108863	FEROS	This work
HD 110014	FEROS	This work
HD 116029	FEROS	This work
HD 11964	FEROS	Sousa et al. (2006)
HD 11977	CORALIE	Sousa et al. (2006)
HD 122430	FEROS	This work
HD 13189	SARG	Sousa et al. (2006)
HD 148427	FEROS	This work
HD 1502	FEROS	This work
HD 156411	HARPS	Sousa et al. (2011)
HD 159868	HARPS	Sousa et al. (2008)
HD 167042	SOPHIE	This work
HD 1690	HARPS	Moutou et al. (2011)
HD 171028	HARPS	Sousa et al. (2011)
HD 175541	UVES	This work
HD 177830	SARG	Santos et al. (2004)
HD 180902	FEROS	This work
HD 181342	FEROS	This work
HD 18742	FEROS	This work
HD 192699	UVES	This work
HD 200964	FEROS	This work
HD 206610	FEROS	This work
HD 210702	UVES	This work
HD 212771	FEROS	This work
HD 27442	FEROS	Santos et al. (2004)
HD 28678	FEROS	This work
HD 30856	FEROS	This work
HD 33142	FEROS	This work
HD 38529	FEROS	Santos et al. (2004)
HD 38801	FEROS	This work
HD 4313	FEROS	This work
HD 47536	FEROS	Santos et al. (2004)
HD 48265	UVES	This work
HD 5319	UVES	This work
HD 5608	FEROS	This work
HD 5891	FEROS	This work
HD 59686	UVES	Santos et al. (2005)
HD 62509	UVES	This work
HD 66141	UVES	This work
HD 73534	FEROS	This work
HD 88133	UVES	Santos et al. (2005)
HD 89744	UES	Santos et al. (2004)
HD 95089	FEROS	This work
HD 96063	FEROS	This work
HD 98219	FEROS	This work
HIP 75458	SARG	Santos et al. (2004)
kappaCrB	UVES	This work
ksiAql	UVES	This work
NGC 2423 No3	UVES	Santos et al. (2009)
NGC 4349 No127	UVES	Santos et al. (2009)
nuOph	FEROS	This work

Table 5. Stellar parameters derived with the TS13 line list for the stars cooler than 5200 K, and the SO08 line list for the hotter stars (marked with ∗).

Name	$T_{\rm eff}$ (K)	$\log g_{\rm spec}$ (cm s^{-2})	[Fe/H] (dex)	ξ (km s^{-1})	M_* ($M_\odot$)
11Com	4830 ± 79	2.61 ± 0.13	–0.34 ± 0.06	1.70 ± 0.10	2.04 ± 0.29
18Del	5076 ± 38	3.08 ± 0.10	0.00 ± 0.03	1.32 ± 0.04	2.33 ± 0.05
24Sex	5069 ± 62	3.40 ± 0.13	–0.01 ± 0.05	1.27 ± 0.07	1.81 ± 0.08
75Cet	4904 ± 47	2.87 ± 0.14	0.02 ± 0.04	1.41 ± 0.05	2.15 ± 0.18
7CMa	4761 ± 79	3.11 ± 0.22	0.21 ± 0.05	1.19 ± 0.08	1.34 ± 0.13
81Cet	4845 ± 51	2.45 ± 0.19	–0.07 ± 0.04	1.58 ± 0.05	1.74 ± 0.21
91Aqr	4681 ± 92	2.65 ± 0.22	0.00 ± 0.05	1.59 ± 0.09	1.32 ± 0.23
alfAri	4513 ± 72	2.49 ± 0.21	–0.16 ± 0.03	1.50 ± 0.07	1.33 ± 0.22
BD+202457	4259 ± 64	1.77 ± 0.19	–0.79 ± 0.03	1.98 ± 0.07	1.06 ± 0.21
BD+20274	4391 ± 79	2.03 ± 0.21	–0.32 ± 0.04	1.80 ± 0.08	1.17 ± 0.23
BD+48738	4658 ± 118	2.62 ± 0.26	–0.09 ± 0.08	1.70 ± 0.12	1.19 ± 0.24
epsCrB	4436 ± 56	1.94 ± 0.15	–0.22 ± 0.03	1.68 ± 0.06	1.44 ± 0.18
epsTau	4946 ± 70	2.62 ± 0.15	0.17 ± 0.06	1.48 ± 0.07	2.73 ± 0.10
gam01Leo	4428 ± 53	1.97 ± 0.17	–0.41 ± 0.03	1.74 ± 0.05	1.57 ± 0.18
gammaCephei	4764 ± 112	3.10 ± 0.27	0.13 ± 0.06	1.06 ± 0.12	1.26 ± 0.14
HD 100655	4801 ± 60	2.81 ± 0.18	–0.02 ± 0.04	1.50 ± 0.06	1.71 ± 0.33
HD 102329	4745 ± 71	2.96 ± 0.16	0.05 ± 0.04	1.39 ± 0.07	1.30 ± 0.15
HD 102272	4807 ± 34	2.57 ± 0.13	–0.38 ± 0.03	1.53 ± 0.04	1.10 ± 0.20
HD 104985	4819 ± 161	2.96 ± 0.27	–0.35 ± 0.11	2.00 ± 0.22	1.04 ± 0.27
HD 106270∗	5601 ± 24	3.72 ± 0.05	0.06 ± 0.02	1.32 ± 0.02	1.33 ± 0.05
HD 108863	4919 ± 44	2.99 ± 0.13	0.02 ± 0.03	1.31 ± 0.04	2.08 ± 0.14
HD 110014	4478 ± 106	2.52 ± 0.31	0.14 ± 0.05	1.90 ± 0.11	2.09 ± 0.39
HD 116029	4811 ± 57	3.21 ± 0.17	0.08 ± 0.04	1.11 ± 0.06	1.33 ± 0.11
HD 11964∗	5372 ± 35	3.99 ± 0.04	0.14 ± 0.05	1.09 ± 0.04	1.08 ± 0.02
HD 11977	5067 ± 42	2.91 ± 0.15	–0.16 ± 0.04	1.59 ± 0.05	2.31 ± 0.12
HD 122430	4474 ± 102	2.43 ± 0.29	–0.09 ± 0.05	1.81 ± 0.1	1.68 ± 0.32
HD 13189∗∗	4337 ± 133	1.83 ± 0.31	–0.39 ± 0.19	1.99 ± 0.12	1.17 ± 0.23
HD 148427	4962 ± 45	3.39 ± 0.12	0.03 ± 0.03	1.06 ± 0.05	1.36 ± 0.06
HD 1502	4984 ± 46	3.30 ± 0.10	–0.04 ± 0.03	1.21 ± 0.05	1.47 ± 0.11
HD 156411∗	5910 ± 16	3.99 ± 0.01	–0.11 ± 0.01	1.31 ± 0.01	1.24 ± 0.02
HD 159868∗	5558 ± 15	3.96 ± 0.02	–0.08 ± 0.01	1.02 ± 0.01	1.16 ± 0.04
HD 167042	5028 ± 53	3.35 ± 0.18	0.03 ± 0.04	1.26 ± 0.06	1.63 ± 0.06
HD 1690	4364 ± 111	2.16 ± 0.27	–0.29 ± 0.06	1.75 ± 0.12	1.18 ± 0.23
HD 171028∗	5671 ± 16	3.84 ± 0.03	–0.48 ± 0.01	1.24 ± 0.02	1.01 ± 0.06
HD 175541	5111 ± 38	3.56 ± 0.08	–0.11 ± 0.03	1.13 ± 0.05	1.34 ± 0.08
HD 177830	4752 ± 79	3.37 ± 0.20	0.30 ± 0.05	0.99 ± 0.12	1.17 ± 0.10
HD 180902	5040 ± 47	3.41 ± 0.18	0.01 ± 0.04	1.15 ± 0.05	1.53 ± 0.09
HD 181342	4965 ± 56	3.27 ± 0.19	0.15 ± 0.04	1.25 ± 0.06	1.70 ± 0.09
HD 18742	5016 ± 32	3.15 ± 0.08	–0.15 ± 0.03	1.23 ± 0.04	1.73 ± 0.19
HD 192699	5141 ± 20	3.45 ± 0.07	–0.20 ± 0.02	1.11 ± 0.02	1.58 ± 0.04
HD 200964	5082 ± 38	3.41 ± 0.08	–0.20 ± 0.03	1.28 ± 0.05	1.57 ± 0.06
HD 206610	4821 ± 55	3.24 ± 0.16	0.10 ± 0.03	1.14 ± 0.06	1.30 ± 0.12
HD 210702	5000 ± 44	3.36 ± 0.08	0.04 ± 0.03	1.15 ± 0.05	1.71 ± 0.06
HD 212771	5091 ± 39	3.38 ± 0.07	–0.14 ± 0.03	1.20 ± 0.04	1.51 ± 0.08
HD 27442	4781 ± 76	3.46 ± 0.19	0.33 ± 0.05	1.09 ± 0.11	1.24 ± 0.10
HD 28678	5052 ± 29	3.07 ± 0.09	–0.21 ± 0.02	1.31 ± 0.03	2.03 ± 0.20
HD 30856	4973 ± 29	3.15 ± 0.11	–0.14 ± 0.02	1.19 ± 0.03	1.36 ± 0.07
HD 33142	5049 ± 41	3.34 ± 0.14	0.03 ± 0.03	1.17 ± 0.04	1.62 ± 0.09
HD 38529∗	5674 ± 40	3.94 ± 0.12	0.40 ± 0.06	1.38 ± 0.05	1.34 ± 0.02
HD 38801∗	5314 ± 43	3.82 ± 0.08	0.25 ± 0.03	1.29 ± 0.06	1.22 ± 0.07
HD 4313	4966 ± 40	3.36 ± 0.17	0.05 ± 0.03	1.17 ± 0.05	1.53 ± 0.09
HD 47536	4447 ± 70	2.26 ± 0.17	–0.65 ± 0.04	1.70 ± 0.07	0.98 ± 0.08
HD 48265∗	5798 ± 29	3.95 ± 0.14	0.36 ± 0.02	1.36 ± 0.03	1.21 ± 0.04
HD 5319	4869 ± 51	3.22 ± 0.10	0.02 ± 0.03	1.11 ± 0.05	1.28 ± 0.10
HD 5608	4911 ± 51	3.25 ± 0.16	0.12 ± 0.03	1.18 ± 0.06	1.66 ± 0.08
HD 5891	4825 ± 47	2.62 ± 0.10	–0.38 ± 0.04	1.69 ± 0.05	1.09 ± 0.19
HD 59686	4666 ± 76	2.57 ± 0.21	0.12 ± 0.04	1.49 ± 0.07	2.02 ± 0.29
HD 62509	4935 ± 49	2.91 ± 0.13	0.09 ± 0.04	1.34 ± 0.05	2.08 ± 0.09

Notes. We adopt these parameters for all future analyses of these stars. (∗∗) For HD 13189, the SO08 parameters are mentioned and adopted, even though the star is cooler than 5200 K.

Table 5. continued

Name	$T_{\rm eff}$ (K)	$\log g_{\rm spec}$ (cm s^{-2})	[Fe/H] (dex)	ξ (km s^{-1})	M_* ($M_\odot$)
HD 66141	4320 ± 50	1.90 ± 0.15	–0.42 ± 0.03	1.59 ± 0.05	1.00 ± 0.06
HD 73534	4884 ± 63	3.59 ± 0.20	0.16 ± 0.04	1.00 ± 0.08	1.17 ± 0.07
HD 88133*	5438 ± 34	3.94 ± 0.11	0.33 ± 0.05	1.16 ± 0.03	1.18 ± 0.06
HD 89744*	6234 ± 45	3.98 ± 0.05	0.22 ± 0.05	1.62 ± 0.08	1.48 ± 0.02
HD 95089	4950 ± 68	3.32 ± 0.18	0.00 ± 0.05	1.27 ± 0.08	1.37 ± 0.12
HD 96063	5131 ± 26	3.44 ± 0.06	–0.20 ± 0.02	1.14 ± 0.03	1.41 ± 0.09
HD 98219	5046 ± 71	3.59 ± 0.14	0.05 ± 0.05	1.07 ± 0.08	1.62 ± 0.11
HIP 75458	4528 ± 111	2.49 ± 0.26	–0.16 ± 0.06	1.64 ± 0.12	1.14 ± 0.16
kappaCrB	4876 ± 46	3.15 ± 0.14	0.13 ± 0.03	1.10 ± 0.06	1.58 ± 0.08
ksiAql	4714 ± 49	2.53 ± 0.11	–0.27 ± 0.04	1.55 ± 0.05	1.11 ± 0.25
NGC 2423 No3	4545 ± 71	2.20 ± 0.20	–0.08 ± 0.05	1.55 ± 0.07	1.18 ± 0.26
NGC 4349 No127	4445 ± 87	1.64 ± 0.23	–0.25 ± 0.06	1.84 ± 0.08	1.37 ± 0.37
nuOph	4967 ± 61	2.70 ± 0.13	0.14 ± 0.05	1.61 ± 0.06	2.94 ± 0.08

Table 6. Stellar parameters derived with the HM07 line list.

Name	$T_{\rm eff}$ (K)	$\log g_{\rm spec}$ (cm s^{-2})	[Fe/H] (dex)	ξ (km s^{-1})	M_* ($M_\odot$)
11Com	4811 ± 76	2.70 ± 0.14	–0.29 ± 0.06	1.59 ± 0.10	2.09 ± 0.29
18Del	5090 ± 71	3.23 ± 0.11	0.07 ± 0.06	1.25 ± 0.09	2.11 ± 0.13
24Sex*	5061 ± 88	3.65 ± 0.15	0.12 ± 0.08	1.12 ± 0.20	1.86 ± 0.11
75Cet*	4853 ± 128	2.84 ± 0.23	0.15 ± 0.13	1.23 ± 0.20	1.88 ± 0.40
7CMa*	4790 ± 138	3.37 ± 0.28	0.28 ± 0.09	1.26 ± 0.20	1.30 ± 0.16
81Cet	4858 ± 97	2.63 ± 0.26	0.01 ± 0.09	1.56 ± 0.11	1.77 ± 0.39
91Aqr	4637 ± 62	2.50 ± 0.13	–0.05 ± 0.05	1.57 ± 0.07	1.17 ± 0.16
alfAri	4614 ± 94	2.80 ± 0.21	–0.05 ± 0.06	1.46 ± 0.10	1.58 ± 0.24
BD+202457	4196 ± 103	1.59 ± 0.26	–0.77 ± 0.05	1.90 ± 0.12	1.07 ± 0.22
BD+20274	4254 ± 170	1.80 ± 0.46	–0.36 ± 0.08	1.84 ± 0.16	1.17 ± 0.25
BD+48738	4493 ± 154	2.41 ± 0.35	–0.03 ± 0.10	1.53 ± 0.15	1.19 ± 0.25
epsCrB	4272 ± 220	1.81 ± 0.54	–0.21 ± 0.11	1.73 ± 0.19	1.23 ± 0.27
epsTau*	4812 ± 178	2.54 ± 0.33	0.24 ± 0.16	1.25 ± 0.20	2.63 ± 0.22
gam01Leo	4373 ± 76	1.87 ± 0.18	–0.41 ± 0.05	1.72 ± 0.08	1.41 ± 0.24
gammaCephei*	4932 ± 259	3.63 ± 0.48	0.31 ± 0.13	1.18 ± 0.20	1.30 ± 0.19
HD 100655	4869 ± 70	3.05 ± 0.14	0.13 ± 0.05	1.44 ± 0.08	2.08 ± 0.15
HD 102329	4751 ± 69	3.07 ± 0.15	0.11 ± 0.05	1.42 ± 0.08	1.29 ± 0.13
HD 102272	4790 ± 56	2.75 ± 0.10	–0.36 ± 0.05	1.61 ± 0.09	1.09 ± 0.16
HD 104985	4750 ± 71	2.78 ± 0.13	–0.26 ± 0.05	1.51 ± 0.10	1.01 ± 0.16
HD 106270	5611 ± 76	4.08 ± 0.08	0.09 ± 0.07	1.48 ± 0.19	1.33 ± 0.06
HD 108863	4906 ± 89	3.29 ± 0.16	0.14 ± 0.06	1.27 ± 0.11	1.42 ± 0.15
HD 110014	4430 ± 233	2.45 ± 0.54	0.20 ± 0.14	1.83 ± 0.24	1.82 ± 0.60
HD 116029	4846 ± 82	3.35 ± 0.16	0.13 ± 0.05	1.24 ± 0.09	1.38 ± 0.14
HD 11964	5375 ± 79	4.17 ± 0.12	0.16 ± 0.06	1.01 ± 0.12	1.08 ± 0.02
HD 11977	5048 ± 78	3.17 ± 0.11	–0.08 ± 0.06	1.58 ± 0.10	2.32 ± 0.16
HD 122430	4264 ± 174	2.06 ± 0.46	–0.11 ± 0.10	1.75 ± 0.18	1.26 ± 0.29
HD 13189	4228 ± 242	2.09 ± 0.61	–0.52 ± 0.14	1.88 ± 0.30	1.08 ± 0.16
HD 148427*	5024 ± 107	3.68 ± 0.18	0.14 ± 0.08	1.14 ± 0.20	1.37 ± 0.11
HD 1502	5002 ± 73	3.44 ± 0.12	0.01 ± 0.06	1.31 ± 0.10	1.36 ± 0.11
HD 156411	5892 ± 80	4.16 ± 0.07	–0.06 ± 0.07	1.30 ± 0.31	1.27 ± 0.05
HD 159868	5514 ± 92	4.08 ± 0.08	–0.10 ± 0.08	1.32 ± 0.23	1.16 ± 0.05
HD 167042*	5061 ± 101	3.74 ± 0.17	0.20 ± 0.10	1.12 ± 0.20	1.68 ± 0.10
HD 1690	4157 ± 186	1.54 ± 0.48	–0.27 ± 0.07	1.46 ± 0.13	1.20 ± 0.29
HD 171028	5697 ± 89	4.18 ± 0.08	–0.44 ± 0.07	1.74 ± 0.66	0.89 ± 0.02
HD 175541	5093 ± 88	3.66 ± 0.13	–0.09 ± 0.07	1.2 ± 0.12	1.20 ± 0.08
HD 177830*	4881 ± 204	3.91 ± 0.38	0.39 ± 0.11	1.21 ± 0.20	1.22 ± 0.12
HD 180902*	5001 ± 99	3.48 ± 0.18	0.08 ± 0.10	1.15 ± 0.20	1.41 ± 0.16
HD 181342*	4930 ± 122	3.39 ± 0.22	0.24 ± 0.11	1.19 ± 0.20	1.49 ± 0.19
HD 18742	5007 ± 79	3.37 ± 0.13	–0.14 ± 0.07	1.35 ± 0.12	1.28 ± 0.12
HD 192699	5126 ± 72	3.56 ± 0.11	–0.20 ± 0.06	1.27 ± 0.13	1.48 ± 0.10
HD 200964	5078 ± 68	3.53 ± 0.10	–0.04 ± 0.06	1.06 ± 0.10	1.67 ± 0.10
HD 206610*	4830 ± 125	3.42 ± 0.23	0.14 ± 0.10	1.24 ± 0.20	1.20 ± 0.12
HD 210702	4996 ± 81	3.50 ± 0.14	0.06 ± 0.06	1.21 ± 0.10	1.63 ± 0.13
HD 212771	5080 ± 78	3.63 ± 0.13	–0.11 ± 0.06	1.31 ± 0.11	1.22 ± 0.08
HD 27442*	4768 ± 136	3.50 ± 0.31	0.21 ± 0.11	1.27 ± 0.20	1.19 ± 0.12
HD 28678	5088 ± 68	3.41 ± 0.10	–0.09 ± 0.06	1.27 ± 0.10	1.40 ± 0.12
HD 30856	4964 ± 79	3.41 ± 0.13	–0.11 ± 0.06	1.29 ± 0.10	1.30 ± 0.13
HD 33142	5029 ± 86	3.60 ± 0.14	0.08 ± 0.06	1.22 ± 0.10	1.56 ± 0.14
HD 38529	5547 ± 52	3.69 ± 0.12	0.28 ± 0.05	1.29 ± 0.08	1.37 ± 0.02
HD 38801	5241 ± 90	3.98 ± 0.14	0.27 ± 0.07	1.22 ± 0.13	1.24 ± 0.07
HD 4313	4993 ± 86	3.49 ± 0.14	0.08 ± 0.07	1.33 ± 0.11	1.35 ± 0.11
HD 47536	4500 ± 194	2.54 ± 0.39	–0.58 ± 0.10	1.83 ± 0.19	1.18 ± 0.25
HD 48265	5683 ± 81	4.07 ± 0.08	0.32 ± 0.07	1.33 ± 0.16	1.21 ± 0.04
HD 5319*	4886 ± 104	3.43 ± 0.17	0.04 ± 0.10	1.21 ± 0.20	1.24 ± 0.14
HD 5608*	4874 ± 122	3.34 ± 0.23	0.16 ± 0.10	1.21 ± 0.20	1.41 ± 0.19
HD 5891	4827 ± 80	2.84 ± 0.13	–0.34 ± 0.07	1.75 ± 0.13	1.12 ± 0.16
HD 59686*	4592 ± 228	2.59 ± 0.49	0.28 ± 0.14	1.36 ± 0.20	2.04 ± 0.46
HD 62509	4992 ± 235	3.46 ± 0.39	0.11 ± 0.17	1.61 ± 0.28	1.61 ± 0.54
HD 66141	4260 ± 117	1.93 ± 0.31	–0.40 ± 0.06	1.65 ± 0.12	1.06 ± 0.12
HD 73534*	5003 ± 129	4.06 ± 0.25	0.26 ± 0.08	1.15 ± 0.20	1.20 ± 0.07
HD 88133	5473 ± 22	3.83 ± 0.22	0.30 ± 0.02	1.17 ± 0.03	1.18 ± 0.06
HD 89744	6095 ± 97	3.77 ± 0.13	0.09 ± 0.08	1.66 ± 0.28	1.44 ± 0.05

Notes. For stars with an asterisk, the microturbulences were derived with a calibration formula.

Table 6. continued.

Name	$T_{\rm eff}$ (K)	$\log g_{\rm spec}$ (cm s^{-2})	[Fe/H] (dex)	ξ (km s^{-1})	M_* ($M_\odot$)
HD 95089*	4956 ± 90	3.51 ± 0.15	0.12 ± 0.09	1.17 ± 0.20	1.30 ± 0.11
HD 96063	5142 ± 62	3.74 ± 0.09	–0.10 ± 0.05	1.12 ± 0.10	1.16 ± 0.07
HD 98219	4970 ± 94	3.65 ± 0.16	0.08 ± 0.07	1.17 ± 0.12	1.47 ± 0.16
HIP 75458	4950 ± 202	3.92 ± 0.36	–0.03 ± 0.11	2.92 ± 0.62	1.57 ± 0.42
kappaCrB	4853 ± 132	3.41 ± 0.25	0.12 ± 0.08	1.27 ± 0.13	1.32 ± 0.17
ksiAql	4719 ± 80	2.83 ± 0.16	–0.18 ± 0.06	1.58 ± 0.09	0.97 ± 0.17
NGC 2423 No3	4337 ± 144	1.69 ± 0.36	–0.11 ± 0.07	1.36 ± 0.09	1.16 ± 0.34
NGC 4349 No127	4258 ± 160	1.52 ± 0.43	–0.22 ± 0.07	1.80 ± 0.11	1.27 ± 0.30
nuOph	4919 ± 105	2.88 ± 0.18	0.14 ± 0.08	1.72 ± 0.12	2.91 ± 0.11

Appendix A: Results from the SO08 line list for cool stars

Table A.1 lists the results from the SO08 line list for the stars cooler than 5200 K. Figure A.1 shows the comparisons of these results with the results from the TS13 and the HM07 line lists.

Effective temperatures for cool stars determined with the SO08 line list have resulted in overestimated values. Because of heavy line blending in the spectra, the equivalent widths of many lines are incorrectly measured, causing incorrect spectroscopic parameters and, specifically, overestimated temperatures (Tsantaki et al. 2013). The TS13 line list has been carefully chosen to resolve this issue. As can be seen in the left panels of Fig. A.1, the effective temperatures derived with the SO08 line list are overestimated with respect to the temperatures derived with the TS13 line list and HM07 with a mean difference of −80 K and −95 K, respectively. This difference is higher for the cooler objects, as expected.

The surface gravities determined with the three line lists are comparable with mean differences of −0.11 and 0.03 dex for TS13–SO08 and HM07–SO08, respectively (see second column in Fig. A.1). Microturbulences also compare very well with each other (last column in Fig. A.1) with mean differences of −0.10 and −0.07 km s^{-1}, respectively.

Considering metallicities, TS13 found no difference in the results from their line list and the SO08 line list for dwarf stars. Our values confirm these results for evolved stars with a mean difference of −0.04 dex (Col. 3 in Fig. 1). The metallicities derived with the HM07 line list also compare well with the SO08 metallicities, with a mean difference of 0.02 dex.

In general, we confirm the results from Tsantaki et al. (2013).

Table A.1. Stellar parameters derived with the SO08 line list.

Name	$T_{\rm eff}$ (K)	$\log g_{\rm spec}$ (cm s^{-2})	[Fe/H] (dex)	ξ (km s^{-1})
11Com	4847 ± 25	2.63 ± 0.05	–0.28 ± 0.02	1.52 ± 0.03
18Del	5147 ± 30	3.22 ± 0.05	0.04 ± 0.03	1.36 ± 0.03
24Sex	5070 ± 35	3.38 ± 0.09	–0.01 ± 0.03	1.27 ± 0.04
75Cet	4941 ± 48	2.81 ± 0.11	–0.01 ± 0.04	1.63 ± 0.05
7CMa	4962 ± 69	3.25 ± 0.16	0.21 ± 0.05	1.44 ± 0.07
81Cet	4864 ± 45	2.64 ± 0.12	–0.05 ± 0.04	1.68 ± 0.05
91Aqr	4757 ± 102	2.71 ± 0.25	0.05 ± 0.14	1.71 ± 0.09
alfAri	4635 ± 49	2.49 ± 0.12	–0.13 ± 0.03	1.50 ± 0.04
BD+202457	4479 ± 74	2.36 ± 0.16	–0.65 ± 0.05	2.24 ± 0.08
BD+20274	4592 ± 71	2.47 ± 0.16	–0.27 ± 0.04	2.21 ± 0.08
BD+48738	4610 ± 92	2.47 ± 0.21	–0.06 ± 0.04	1.55 ± 0.08
epsCrB	4532 ± 55	2.10 ± 0.14	–0.23 ± 0.04	1.87 ± 0.06
epsTau	5024 ± 49	2.80 ± 0.09	0.21 ± 0.04	1.55 ± 0.05
gam01Leo	4586 ± 55	2.38 ± 0.14	–0.34 ± 0.04	1.95 ± 0.05
gammaCephei	4916 ± 70	3.36 ± 0.21	0.16 ± 0.08	1.27 ± 0.06
HD 100655	4906 ± 55	2.88 ± 0.11	0.00 ± 0.05	1.66 ± 0.06
HD 102272	4858 ± 28	2.63 ± 0.07	–0.35 ± 0.02	1.58 ± 0.03
HD 102329	4898 ± 62	3.10 ± 0.13	0.06 ± 0.05	1.62 ± 0.06
HD 104985	4773 ± 62	2.76 ± 0.14	–0.28 ± 0.09	1.71 ± 0.07
HD 108863	4966 ± 45	3.06 ± 0.10	0.03 ± 0.04	1.45 ± 0.05
HD 110014	4702 ± 122	2.53 ± 0.25	0.21 ± 0.06	1.92 ± 0.11
HD 116029	4984 ± 50	3.37 ± 0.12	0.08 ± 0.04	1.4 ± 0.06
HD 11977	5020 ± 30	2.86 ± 0.04	–0.09 ± 0.06	1.46 ± 0.03
HD 122430	4588 ± 97	2.53 ± 0.22	–0.07 ± 0.04	1.96 ± 0.09
HD 13189	4337 ± 133	1.83 ± 0.31	–0.39 ± 0.19	1.99 ± 0.12
HD 148427	5036 ± 43	3.44 ± 0.10	0.03 ± 0.03	1.25 ± 0.05
HD 1502	5038 ± 36	3.28 ± 0.08	–0.01 ± 0.03	1.27 ± 0.04
HD 167042	5086 ± 38	3.48 ± 0.11	0.10 ± 0.03	1.17 ± 0.04
HD 1690	4393 ± 85	2.12 ± 0.17	–0.32 ± 0.06	1.86 ± 0.07
HD 175541	5134 ± 23	3.5 ± 0.04	–0.1 ± 0.02	1.08 ± 0.03
HD 177830	4804 ± 77	3.57 ± 0.17	0.33 ± 0.09	1.14 ± 0.09

Table A.1. continued.

Name	$T_{\rm eff}$ (K)	$\log g_{\rm spec}$ (cm s^{-2})	[Fe/H] (dex)	ξ (km s^{-1})
HD 180902	5098 ± 41	3.41 ± 0.10	0.03 ± 0.03	1.24 ± 0.05
HD 181342	5074 ± 62	3.34 ± 0.13	0.18 ± 0.05	1.41 ± 0.06
HD 18742	5047 ± 30	3.23 ± 0.07	–0.13 ± 0.03	1.29 ± 0.03
HD 192699	5143 ± 19	3.42 ± 0.03	–0.21 ± 0.02	1.13 ± 0.02
HD 200964	5113 ± 29	3.37 ± 0.07	–0.17 ± 0.02	1.28 ± 0.03
HD 206610	5008 ± 56	3.44 ± 0.13	0.12 ± 0.04	1.38 ± 0.07
HD 210702	5016 ± 32	3.31 ± 0.05	0.04 ± 0.02	1.15 ± 0.03
HD 212771	5132 ± 33	3.42 ± 0.07	–0.11 ± 0.03	1.24 ± 0.04
HD 27442	4825 ± 107	3.55 ± 0.32	0.39 ± 0.13	1.18 ± 0.12
HD 28678	5101 ± 27	3.16 ± 0.06	–0.18 ± 0.02	1.36 ± 0.03
HD 30856	4994 ± 35	3.23 ± 0.07	–0.13 ± 0.03	1.28 ± 0.04
HD 33142	5057 ± 45	3.38 ± 0.09	0.03 ± 0.03	1.24 ± 0.04
HD 4313	5029 ± 49	3.31 ± 0.11	0.03 ± 0.04	1.36 ± 0.05
HD 47536	4554 ± 85	2.48 ± 0.23	–0.54 ± 0.12	1.82 ± 0.08
HD 5319	4937 ± 34	3.33 ± 0.06	0.05 ± 0.03	1.13 ± 0.05
HD 5608	4971 ± 58	3.22 ± 0.13	0.1 ± 0.04	1.34 ± 0.06
HD 5891	4810 ± 36	2.53 ± 0.08	–0.35 ± 0.03	1.62 ± 0.04
HD 59686	4871 ± 135	3.15 ± 0.41	0.28 ± 0.18	1.85 ± 0.12
HD 62509	4996 ± 44	3.09 ± 0.09	0.12 ± 0.03	1.37 ± 0.05
HD 66141	4466 ± 58	2.26 ± 0.15	–0.37 ± 0.04	1.85 ± 0.07
HD 73534	5072 ± 69	3.67 ± 0.15	0.16 ± 0.05	1.30 ± 0.07
HD 95089	4997 ± 46	3.35 ± 0.11	0.04 ± 0.04	1.30 ± 0.05
HD 96063	5151 ± 24	3.43 ± 0.06	–0.17 ± 0.02	1.15 ± 0.03
HD 98219	5063 ± 49	3.58 ± 0.09	0.05 ± 0.03	1.21 ± 0.05
HIP 75458	4775 ± 113	3.09 ± 0.40	0.13 ± 0.14	1.78 ± 0.11
kappaCrB	4968 ± 48	3.37 ± 0.10	0.15 ± 0.04	1.22 ± 0.06
ksiAql	4808 ± 41	2.72 ± 0.08	–0.17 ± 0.03	1.51 ± 0.04
NGC 2423 No3	4703 ± 49	2.48 ± 0.40	0.00 ± 0.15	1.67 ± 0.05
NGC 4349 No127	4569 ± 69	2.08 ± 0.35	–0.13 ± 0.18	1.93 ± 0.06
nuOph	5000 ± 51	2.80 ± 0.12	0.12 ± 0.04	1.83 ± 0.05

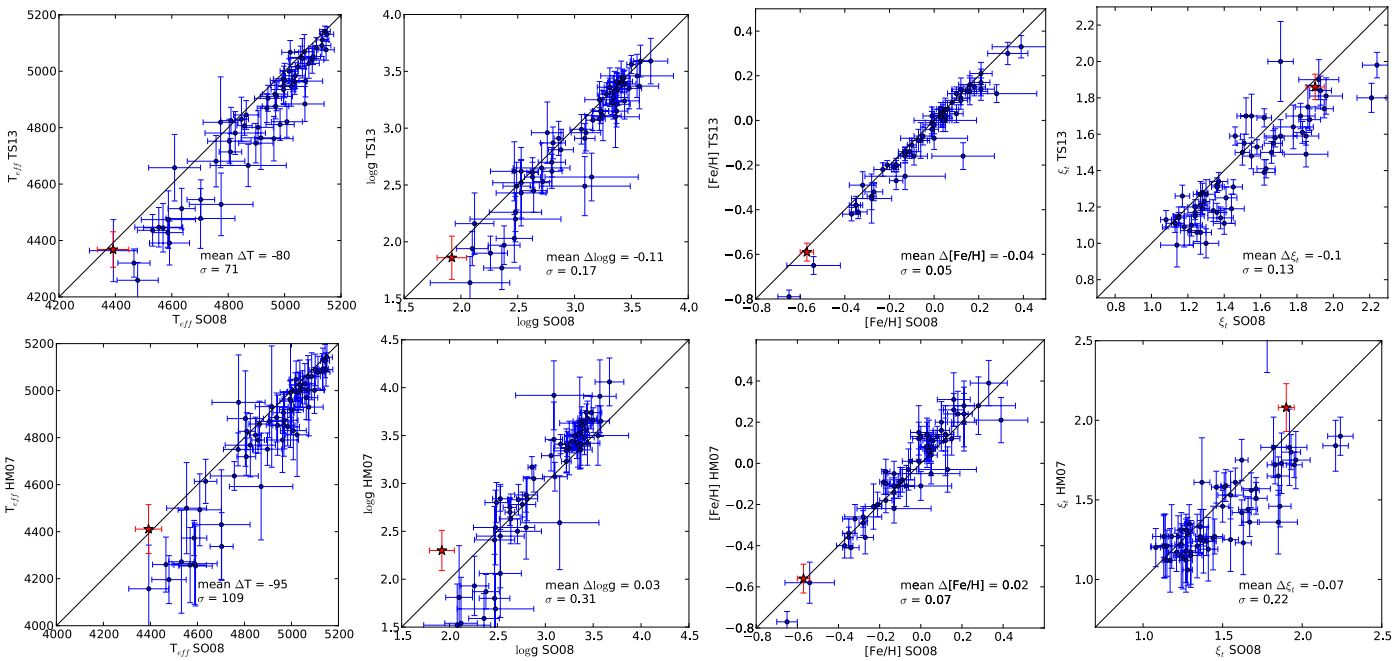

Fig. A.1. Comparisons of the spectroscopic results from the different line lists for effective temperature, surface gravity, metallicity, and microturbulence. In the *left panels*, the results from the TS13 line list are plotted versus the results from SO08. The *middle panels* are HM07 versus SO08 and the right panels HM07 versus TS13. The measurements for the reference star Arcturus are overplotted with a star symbol. The dashed line in the *top-right panel* represents a second degree polynomial fit.

Chapter 5

The effect of the surface gravity for transit hosts

Foreword

As mentioned in section 1.3, my colleagues and me have recently developed the largest catalogue of uniformly analysed planet hosts (SWEETCat - Santos et al. 2013). In order to expand this catalogue, several observations were carried out (by me or my colleagues) to obtain high-resolution spectra of planet hosts. Combined with data from the ESO archive, I had a sample of 90 transit hosts with high-resolution spectra.

From the transit light curve, an independent measurement of the stellar density can be obtained. Combining this with the temperature and metallicity, derived from the spectra, the surface gravity can be calculated. As such, the surface gravity can be derived in two independent manners for transit hosts. Torres et al. (2012) showed that surface gravities can differ significantly, depending on the derivation method. For this work, I looked into the effect of these different surface gravities for the large sample of 90 trasit hosts on the derivation of stellar mass and radius, the key parameters for planetary mass and radius determinations. Additionally, the high-resolution spectra were used to derive abundances of other elements in the stars' atmosphere. This work was peer-reviewed and accepted for publicatin in Astronomy & Astrophysics.

A&A 558, A106 (2013)
DOI: 10.1051/0004-6361/201322240

Astronomy & Astrophysics

New and updated stellar parameters for 90 transit hosts

The effect of the surface gravity⋆,⋆⋆,⋆⋆⋆

A. Mortier[1,2], N. C. Santos[1,2], S. G. Sousa[1,3], J. M. Fernandes[4], V. Zh. Adibekyan[1], E. Delgado Mena[1], M. Montalto[1], and G. Israelian[3,5]

[1] Centro de Astrofísica, Universidade do Porto, Rua das Estrelas, 4150-762 Porto, Portugal
e-mail: amortier@astro.up.pt
[2] Departamento de Física e Astronomia, Faculdade de Ciências, Universidade do Porto, 4169-007 Porto, Portugal
[3] Instituto de Astrofísica de Canarias, 38200 La Laguna, Tenerife, Spain
[4] CGUC, Departement of Mathematics and Astronomical Observatory, University of Coimbra, 3004-531 Coimbra, Portugal
[5] Departamento de Astrofísica, Universidad de La Laguna, 38206 La Laguna, Tenerife, Spain

Received 9 July 2013 / Accepted 27 August 2013

ABSTRACT

Context. Precise stellar parameters are crucial in exoplanet research for correctly determining the planetary parameters. For stars hosting a transiting planet, determining the planetary mass and radius depends on the stellar mass and radius, which in turn depend on the atmospheric stellar parameters. Different methods can provide different results, which leads to different planet characteristics.
Aims. In this paper, we use a uniform method to spectroscopically derive stellar atmospheric parameters, chemical abundances, stellar masses, and stellar radii for a sample of 90 transit hosts. Surface gravities are also derived photometrically using the stellar density as derived from the light curve. We study the effect of using these different surface gravities on the determination of the chemical abundances and the stellar mass and radius.
Methods. A spectroscopic analysis based on Kurucz models in local thermodynamical equilibrium was performed through the MOOG code to derive the atmospheric parameters and the chemical abundances. The photometric surface gravity was determined through isochrone fitting and the use of the stellar density, directly determined from the light curve. Stellar masses and radii are determined through calibration formulae.
Results. Spectroscopic and photometric surface gravities differ, but this has very little effect on the precise determination of the stellar mass in our spectroscopic analysis. The stellar radius, and hence the planetary radius, is most affected by the surface gravity discrepancies. For the chemical abundances, the difference is, as expected, only noticable for the abundances derived from analyzing lines of ionized species.

Key words. stars: fundamental parameters – stars: abundances – planets and satellites: fundamental parameters – techniques: spectroscopic

1. Introduction

Since the discovery of the first extrasolar planet around a solar-like star in 1995 (51 Peg b, Mayor & Queloz 1995), the search for extrasolar planetary systems has accelerated. Today, more than 900 planets have been announced[1]. Most of them were detected using the radial velocity technique, but in the past few years, the photometric transit technique has started to produce a large number of results thanks to big space and ground missions, such as *Kepler*, CoRoT, and WASP (e.g. Anderson et al. 2010; Léger et al. 2009; Batalha et al. 2013). Over 200 stars have been confirmed so far to be transited by one or more planets.

Transiting extrasolar planets have been found orbiting different types of stars, and the planets themselves also turn out to be very diverse. The large number of discoveries combined with this diversity in the planets and their hosts opens the possibility of comparing the observed properties with those predicted by theoretical models (e.g. Miguel et al. 2011; Mordasini et al. 2012a,b). This will put constraints on the models and help in our understanding of planet formation.

However, derivation of the planetary properties (mass, radius, and mean density) depends considerably on the deduced parameters for the stellar hosts (e.g. Bouchy et al. 2004; Torres et al. 2012). For a transiting planet, analysis of the lightcurve only determines the planetary radius relative to the stellar radius

⋆ The data presented herein are based on observations collected at the La Silla Paranal Observatory, ESO (Chile) with the FEROS spectrograph at the 2.2-m telescope (ESO runs ID 088.C-0892, 089.C-0444, 090.C-0146) and the HARPS spectrograph at the 3.6-m telescope (ESO archive), the Paranal Observatory, ESO (Chile) with the UVES spectrograph at the VLT Kueyen telescope (ESO run ID 083.C-0174), at the Spanish Observatorio del Roque de los Muchachos of the Instituto de Astrofísica de Canarias with the FIES spectrograph at the Nordic Optical Telescope, operated on the island of La Palma jointly by Denmark, Finland, Iceland, Norway, and Sweden (program ID 40-203), and at the Observatoire de Haute-Provence (OHP, CNRS/OAMP), France with the SOPHIE spectrographs at the 1.93-m telescope (program ID 11B.DISC.SOUS).
⋆⋆ Table 4 is available in electronic form at http://www.aanda.org
⋆⋆⋆ Full Table 5 is only available at the CDS via anonymous ftp to cdsarc.u-strasbg.fr (130.79.128.5) or via http://cdsarc.u-strasbg.fr/viz-bin/qcat?J/A+A/558/A106

[1] www.exoplanet.eu for an updated number

(R_p/R_*). Also, the planetary mass depends on the stellar mass ($M_p \propto M_*^{2/3}$), as derived from the radial velocity curve. Deriving the stellar radius and mass in turn depends on the effective temperature, surface gravity, and the metallicity of the star.

It is thus extremely important to use high-quality data to refine the values for these stellar properties to obtain more precise stellar masses and radii and therefore more precise planetary masses and radii. Furthermore, to minimize the errors, a uniform analysis is required (Torres et al. 2008, 2012) to guarantee the best possible homogeneity in the results. Using different methods to derive stellar properties leads to discrepancies in the results, which in turn leads to less significance for the statistical analyses of the data. If, for example, stellar radii were underestimated, the planetary radii would be underestimated. The occurrence rate of small planets (e.g. Dressing & Charbonneau 2013) in our Galaxy will be affected by this underestimation.

By homogeneously deriving precise stellar parameters for planet hosts, we gain more than just improving the planetary parameters. Observational and theoretical evidence shows that the presence of a planet seems to depend on several stellar properties, such as mass and metallicity (Udry & Santos 2007; Sousa et al. 2011; Mayor et al. 2011; Mortier et al. 2013a). Several other correlations have come to light with the increasing discoveries of extrasolar planets, like the radius anomaly. There is evidence for a possible correlation between planetary effective temperature, metallicity, and the radius anomaly (between the observed radius and the one expected from planetary models) for giant planets (Guillot et al. 2006; Burrows et al. 2007; Laughlin et al. 2011). According to basic core accretion theory, higher metallicities lead to larger planet cores, and such planets would have smaller radii than similar-mass planets with small or no cores. If this is true, the metallicity should be a determining factor in the observed radius anomaly and in the chemical composition and structure of the planets. Precise metallicities are thus crucial for understanding these possible correlations.

In this paper, we homogeneously derive stellar parameters and chemical abundances for a large sample of transit hosts. We also take a closer look at the surface gravity and its effect on the stellar mass and radius determinations. In Sect. 2, we present the sample that has been used and the observations. Section 3 describes the spectroscopic analysis that was performed, as well as the results. Section 4 handles the effect of the surface gravity on the stellar mass and radius and on the chemical abundances. In Sect. 5, we compare our results with the literature. We discuss in Sect. 6 and conclude in Sect. 7.

2. The sample

For this analysis, we used a sample of 90 stars. All these stars are of spectral type F, G or K and are known to be orbited by a transiting planet (according to the online catalog `www.exoplanet.eu`). From this sample, 28 stars were previously analyzed and published by members of our team. The references can be found in Table 1. For the 62 remaining stars, we gathered spectra through observations made by our team and the use of the ESO archive (see Table 2).

In total, ten different high-resolution spectrographs were used (see Table 3): UVES (VLT Kueyen telescope, Paranal, Chile), FEROS (2.2 m ESO/MPI telescope, La Silla, Chile), HARPS (3.6 m ESO telescope, La Silla, Chile), CORALIE (1.2 m Swiss telescope, La Silla, Chile), SOPHIE (1.93 m telescope, OHP, France), SARG (TNG Telescope, La Palma, Spain), FIES (Nordic Optical Telescope, La Palma, Spain), NARVAL (2 m Télescope *Bernard Lyot*, OPM, France), HIRES (Keck-I, Paranal, Chile) and UES (*William Herschel* Telescope, La Palma, Spain). The spectra were reduced using the available pipelines and IRAF[2]. The spectra were corrected for radial velocity with the IRAF task `DOPCOR`, to put the lines in their rest frame. To correct for this, we used the very recognizable Fe I line at 6705.11 Å. Individual exposures of multiple observed stars with the same instrument were added using the task `SCOMBINE` in IRAF. The data logs can be found in Tables 1 and 2.

So far, 234 FGK planet hosts have been discovered, that are orbited by at least one transiting planet[3]. With our sample of 90 stars, we thus analyze ~40% of all known transit hosts. Our analysis requires high-resolution and high signal-to-noise (S/N) spectra, which is, unfortunately, not always easy to acquire for these transit hosts, since they are, on average, fainter than radial velocity hosts. Our spectra have a S/N between 100 and 300.

Table 1. Observation log of the transit hosts analyzed previously with the same method used in this work.

Name	Instrument	Reference
HAT-P-1	SARG	1
HAT-P-4	SOPHIE	1
HAT-P-6	SOPHIE	1
HAT-P-7	SOPHIE	1
HD 149026	SARG	1
HD 17156	SOPHIE	1
HD 189733	CORALIE	2
HD 209458	HARPS	3
HD 80606	UES	4
HD 97658	UVES	5
Kepler-17	SOPHIE	6
Kepler-21	NARVAL	7
KOI-135	SOPHIE	6
KOI-204	SOPHIE	6
OGLE-TR-10	UVES	8
OGLE-TR-111	UVES	8
OGLE-TR-113	UVES	8
OGLE-TR-132	UVES	9
OGLE-TR-182	UVES	10
OGLE-TR-211	UVES	11
OGLE-TR-56	UVES	8
TrES-1	UVES	8
TrES-2	SARG	1
TrES-3	SARG	1
TrES-4	SOPHIE	1
WASP-13	HIRES	12
XO-1	SARG	1
XO-2	SOPHIE	1

References. (1) Ammler-von Eiff et al. (2009); (2) Sousa et al. (2006); (3) Sousa et al. (2008); (4) Santos et al. (2004); (5) Sousa (in prep.); (6) Bonomo et al. (2012); (7) Molenda-Żakowicz et al. (2013); (8) Santos et al. (2006); (9) Gillon et al. (2007); (10) Pont et al. (2008); (11) Udalski et al. (2008); (12) Gómez Maqueo Chew et al. (2013).

3. Spectroscopic analysis

3.1. Atmospheric parameters

From the spectra, we derived the following atmospheric stellar parameters: the effective temperature $T_{\rm eff}$, the surface gravity

[2] IRAF is distributed by National Optical Astronomy Observatories, operated by the Association of Universities for Research in Astronomy, Inc., under contract with the National Science Foundation, USA.

[3] According to `exoplanet.eu` on 8 July 2013.

Table 2. Observation log of the transit hosts analyzed in this work.

Name	Instrument
HAT-P-17, HAT-P-20, HAT-P-26, HAT-P-30, HAT-P-35, WASP-12, WASP-18, WASP-21, WASP-26, WASP-29, WASP-32, WASP-34, WASP-35, WASP-42, WASP-45, WASP-47, WASP-50, WASP-54, WASP-55, WASP-56, WASP-62, WASP-63, WASP-66, WASP-67, WASP-71, WASP-77A, WASP-78, WASP-79, WASP-8	FEROS
HAT-P-8	FIES
CoRoT-1, CoRoT-10, CoRoT-12, CoRoT-4, CoRoT-5, CoRoT-7, CoRoT-8, CoRoT-9, HAT-P-27, WASP-15, WASP-16, WASP-17, WASP-19, WASP-22, WASP-23, WASP-24, WASP-25, WASP-28, WASP-31, WASP-36, WASP-38, WASP-41, WASP-6	HARPS
HAT-P-11	SOPHIE
CoRoT-2, WASP-1, WASP-10, WASP-11, WASP-2, WASP-4, WASP-5, WASP-7	UVES

Table 3. Spectrograph details: resolving power and spectral ranges.

Instrument	Resolving power $\lambda/\Delta\lambda$	Spectral range Å	Stars
CORALIE	50 000	3800–6800	1
FEROS	48 000	3600–9200	29
FIES	67 000	3700–7300	1
HARPS	100 000	3800–7000	24
HIRES	72 000	4800–8000	1
NARVAL	75 000	3700–10 500	2
SOPHIE	75 000	3820–6920	10
SARG	57 000–86 000	5100–10 100	5
UES	55 000	4000–10 000	1
UVES	110 000	3000–6800	16

log g, the metallicity [Fe/H], and the microturbulence ξ. The procedure we followed is described in Santos et al. (2004) and is based on the equivalent widths of Fe I and Fe II lines and on iron excitation and ionization equilibrium, assumed in local thermodynamic equilibrium (LTE). The 2010 version of MOOG[4] (Sneden 1973), a grid of ATLAS plane-parallel model atmospheres (Kurucz 1993), and the iron linelist of Sousa et al. (2008) are therefore used.

To measure the equivalent widths of the iron lines, the code ARES was used (Automatic Routine for line Equivalent widths in stellar Spectra – Sousa et al. 2007). The input parameters for ARES, are the same as in Sousa et al. (2008), except for the *rejt* parameter, which determines the calibration of the continuum position. Since this parameter strongly depends on the S/N of the spectra, different values are needed for each spectrum. A uniform S/N value is derived for the spectra with the IRAF routine BPLOT. Therefore, three spectral regions are used: [5744 Å, 5747 Å], [6047 Å, 6053 Å], and [6068 Å, 6076 Å].

Then, the *rejt* parameter was set by eye for a couple of spectra with different S/N (representable for the whole sample). Afterwards, all the *rejt* parameters were derived by a simple interpolation of these values. This method ensures uniform use of the *rejt* parameter, since we otherwise do not have access to a uniform source for the S/N through the headers of the spectra as in Sousa et al. (2008). The dependence of the *rejt* parameter on the S/N is the same as in Mortier et al. (2013b).

For cool stars, the results from using the linelist from Sousa et al. (2008) have shown to be unsatisfactory. The derived temperatures were higher than values from other methods, like the InfraRed flux Method (Casagrande et al. 2006). Therefore a new linelist was built, specifically for these cooler stars (Tsantaki et al. 2013), based on the linelist of Sousa et al. (2008). Only weak and isolated lines were left, since blending effects play a huge role in cool stars. Tsantaki et al. (2013) show that their new results are in very good agreement with the results from the InfraRed flux Method (IRFM). For the 13 stars in our sample with temperatures lower than 5200 K, as obtained with the Sousa et al. (2008) linelist, we rederived the parameters with this new linelist from Tsantaki et al. (2013). All atmospheric parameters can be found in Table 4.

3.2. Abundances

Chemical abundances were determined for 12 refractory elements (Na, Mg, Al, Si, Ca, Ti, Cr, Ni, Co, Sc, Mn, and V), and lithium. For chromium, scandium, and titanium, we also calculated the abundance of the ions. The analysis for the refractory elements was again done in LTE, which is a good approximation for this stellar sample (Bergemann et al. 2012; Serenelli et al. 2013). We derived the abundances with the 2010 version of MOOG (Sneden 1973) and a grid of ATLAS plane-parallel model atmospheres (Kurucz 1993), using the EWs of the lines. For all elements these EWs were calculated with ARES. The final abundance for each element was calculated as the average value of the abundances given by each detected line of that element. The Li abundances, $A(\mathrm{Li}) = \log(\mathrm{N(Li)/N(H)}) + 12$, were derived by a standard LTE analysis using spectral synthesis with the revised version of the spectral synthesis code MOOG2010 (Sneden 1973), a grid of Kurucz ATLAS9 atmospheres with overshooting (Kurucz 1993), and the linelist from Ghezzi et al. (2009). More details about these methods can be found in the works of Adibekyan et al. (2012) and Delgado Mena et al. (2013).

All abundances can be found in Table 5. Several lithium abundances present upper limits since the lines are at the same level as the noise. The typical error for A(Li) is 0.1 dex.

3.3. Masses and radii

Stellar masses and radii were computed with the calibration of Torres et al. (2010). This calibration is based on effective temperature, surface gravity and metallicity. For stellar mass, we applied a small quadratic correction. Torres et al. (2010) and Santos et al. (2013) show that there is a small offset between masses obtained through this calibration and masses obtained through isochrones. Santos et al. (2013) fit this offset with a quadratic function that we use to correct the masses obtained through the calibration of Torres et al. (2010):

$$M_{\mathrm{cor}} = 0.791 \cdot M_T^2 - 0.575 \cdot M_T + 0.701 \quad (1)$$

[4] http://www.as.utexas.edu/~chris/moog.html

Table 5. Abundances for the transit hosts in this sample.

Name	Al I (dex)	Ca I (dex)	Co I (dex)	Cr I (dex)	Cr II (dex)	Mg I (dex)	Mn I (dex)	...
CoRoT-9	–0.03 ± 0.04	0.01 ± 0.06	0.00 ± 0.05	0.01 ± 0.06	–0.08 ± 0.07	–0.02 ± 0.02	–0.04 ± 0.03	...
WASP-31	–0.30 ± 0.22	–0.06 ± 0.19	0.00 ± 0.19	–0.01 ± 0.10	–0.10 ± 0.12	–0.13 ± 0.08	–0.22 ± 0.14	...
...								
Name	Al I_{LC} (dex)	Ca I_{LC} (dex)	Co I_{LC} (dex)	Cr I_{LC} (dex)	Cr II_{LC} (dex)	Mg I_{LC} (dex)	Mn I_{LC} (dex)	...
CoRoT-9	–0.03 ± 0.04	–0.03 ± 0.06	0.01 ± 0.05	0.00 ± 0.07	–0.04 ± 0.07	–0.04 ± 0.03	–0.05 ± 0.03	...
WASP-31	–0.29 ± 0.22	–0.02 ± 0.20	0.00 ± 0.19	0.00 ± 0.10	–0.26 ± 0.13	–0.10 ± 0.11	–0.21 ± 0.14	...
...								

Notes. The complete table is provided in electronic form at the CDS.

where $M_{\rm cor}$ and M_T denote the corrected stellar masses and the mass from the Torres et al. (2010) calibration, respectively. Table 4 lists all stellar parameters for the stars in this sample.

4. Photometric surface gravity

Over the years, it has become clear that determining surface gravities spectroscopically is not well constrained (e.g. Sozzetti et al. 2007; Torres et al. 2012). Luckily, for stars with a transiting planet, the photometric light curve can be used independently to determine the surface gravity with much better precision. This can improve the precision of the stellar mass and radius and consequently also the precision of the planetary mass and radius. Good precision is necessary for a correct classification of the exoplanets. Purely from transit photometry, the stellar density can be calculated from Kepler's third law (Seager & Mallén-Ornelas 2003):

$$\rho_* + k^3\rho_{\rm p} = \frac{3\pi}{GP^2}\left(\frac{a}{R_*}\right)^3 \quad (2)$$

where ρ_* and $\rho_{\rm p}$ are the stellar and planetary density, P the period of the planet, a the orbital separation, G the gravitational constant, and R_* the stellar radius. Since the constant coefficient k is usually small, the second term on the left is negligible. All parameters on the right come directly from analyzing the transit light curve.

With this stellar density, combined with the effective temperature and metallicity from the spectroscopic analysis, the surface gravity can be determined through isochrone fitting, as described in Sozzetti et al. (2007). For this work, we used the stellar densities from the discovery papers, PARSEC isochrones (Bressan et al. 2012), a χ^2 minimization process for the fitting, and the individual metallicity and effective temperature from our spectroscopic analysis. The one-sigma error bars were computed using all solutions where $\chi^2 < 3$. From all these solutions, we computed the standard deviation of all surface gravities.

All values can be found in Table 4. For WASP-45, WASP-56, and XO-2, no photometric surface gravity could be calculated owing to the high metallicity and the uncertainties of the models at these high metallicities (Valle et al. 2013). In the top panel of Fig. 1, we compare the spectroscopic and the photometric surface gravity. It can be seen that they do not always compare well. The differences in surface gravity also depend on the temperature as can be seen in the bottom panel of Fig. 1, where a decreasing linear trend is noticeable. The same trend is found for the microturbulence, which is closely related to the temperature. Comparing the log g differences with metallicities reveals

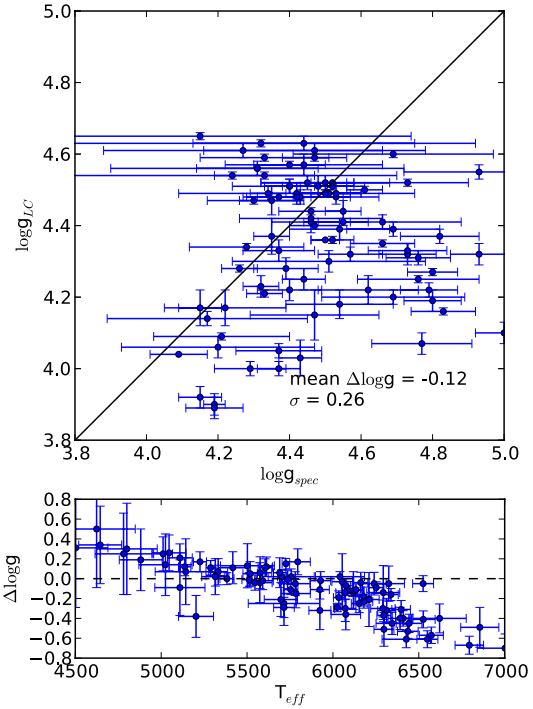

Fig. 1. *Top panel*: comparison of the spectroscopic and the photometric surface gravity. *Bottom panel*: differences in log g (defined as "photometric – spectroscopic") as a function of the effective temperature.

no additional trends. These trends and the possible causes will be discussed in a forthcoming work.

Photometric surface gravities are generally more precise than spectroscopic surface gravities. This higher precision, however, does not guarantee higher accuracy. To determine the stellar density, which is used to derive the photometric surface gravity, the ratio a/R_* is used. This value comes from fitting the light curve, which depends on a correct limb darkening coefficient. This limb darkening coefficient can be fixed using the dependence on the effective temperature. An incorrect effective temperature will thus lead to an incorrect fixed limb darkening coefficient and thus an incorrect fitting of the light curve. However, the limb darkening coefficient can also be left as a free parameter in the fit. The determination of a/R_* also depends on the orbital eccentricity. This eccentricity is determined from a radial velocity curve and is thus unfortunately not always known for transiting planets and fixed to a standard value in the transit light curve fit. Furthermore, the photometric surface gravities depend on theoretical stellar evolution models. The spectroscopic surface gravities are poorly constrained and thus not necessarily

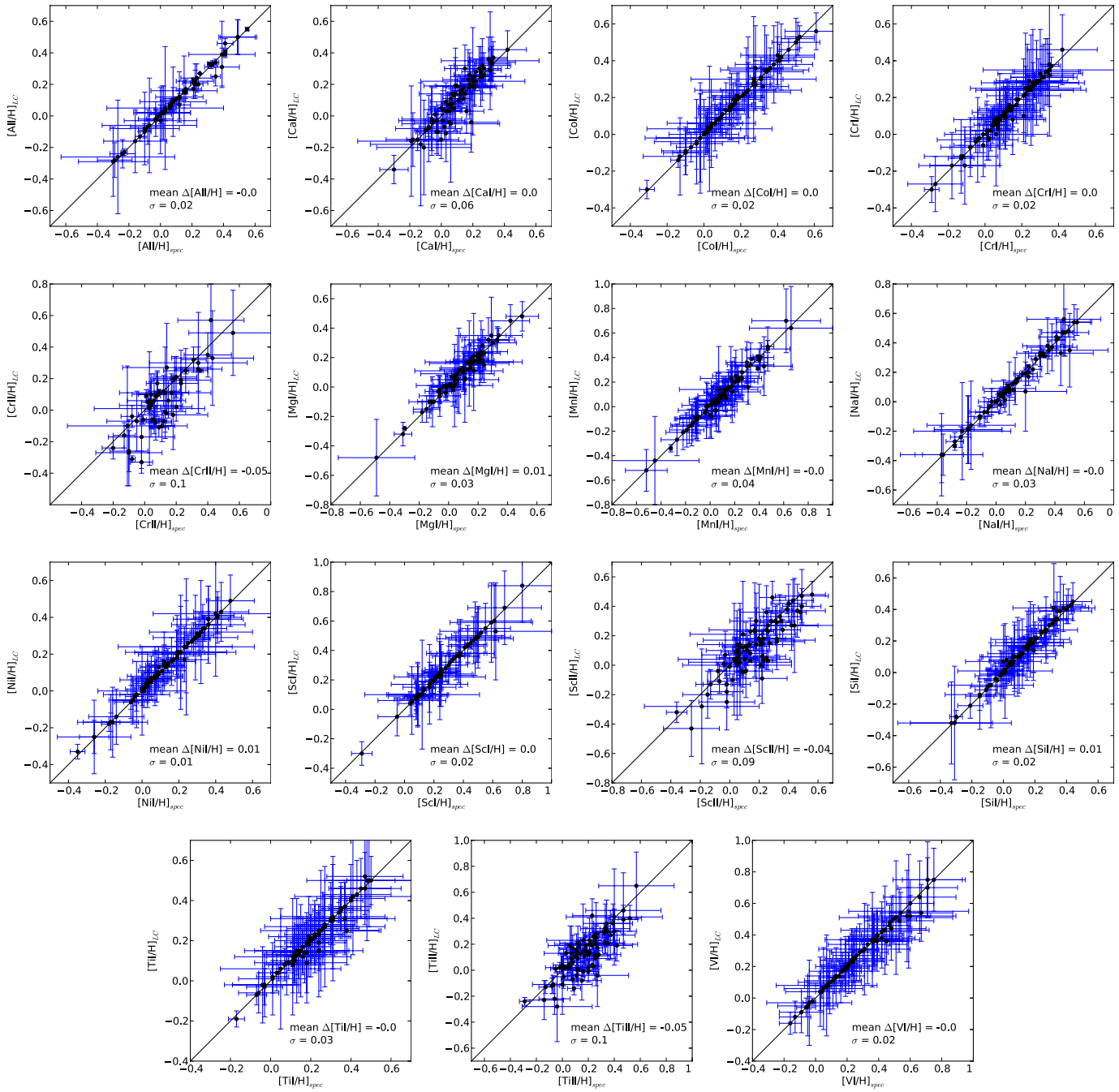

Fig. 2. Comparisons of the chemical abundances, obtained with the spectroscopic and photometric surface gravity.

accurate either. Since both methods have their pros and cons, we provide the reader with both values.

The other atmospheric parameters that are spectroscopically determined are much better constrained, so we adopt these parameters for the continuation of this work. Effective temperatures derived with our method, have shown to compare well with well established methods, such as the IRFM (e.g. Tsantaki et al. 2013; Santos et al. 2013). Torres et al. (2012) explored the impact of using different surface gravities on the other atmospheric parameters. They show that by using the method that we use in this work, the impact is minimal, compared with other methods. However, small trends are still present. These trends and their possible corrections will be explored in a forthcoming paper.

4.1. Chemical abundances

The derivation of the chemical abundances is based on all atmospheric parameters and thus also depends on the surface gravity. We recalculated the abundances of the refractory elements (see Table 5) with the photometric surface gravity. For all atomic elements, there is virtually no difference between the two abundances, as can be seen in Fig. 2. Since the atom abundances do not differ, we did not redo the spectral synthesis to derive the lithium abundances A(Li) again. For the three ions, on the other hand, the differences are greater. However, they are still within the error bars. Since ions are more sensitive to the surface gravity (Gray 1992), these larger differences are as expected.

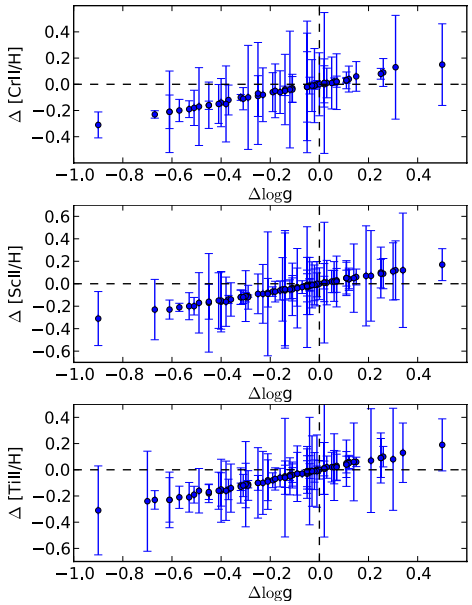

Fig. 3. Differences between the ion abundances as a function of the difference in logg (defined as "constrained – unconstrained").

Figure 3 shows the differences between these ion abundances as a function of the surface gravity difference. There are clear, visible linear trends with small slopes of 0.34, 0.37, and 0.37 for Cr II, Sc II, and Ti II, respectively.

4.2. Stellar mass and radius

With the new photometric surface gravity, we also recalculated the mass and radius of every star, using the calibrations from Torres et al. (2010). Results are listed in Table 4. Figure 4 shows the comparisons between these values. The masses compare well with a mean difference of 0.06 $M_{\odot}$. The greatest differences are found for higher mass stars. The radii, on the other hand, do not compare so well. In the righthand panel of Fig. 4, we plot the differences in masses and radii with respect to the surface gravity difference (all defined as "photometric – spectroscopic log g"). Clear linear trends are visible.

For the radii, the effect of using different surface gravities is greatest with absolute differences up to 1.0 $R_{\odot}$. These large discrepancies in stellar radii can lead to large discrepancies in planetary radii (see Sect. 6). Since the photometric surface gravity is generally more precise than the spectroscopic one, the resulting stellar masses and radii will also be more precise.

5. Comparison with the literature

Recently, another homogeneous spectroscopic analysis has been done for transiting planet hosts by Torres et al. (2012). Their analysis of the temperature and metallicity is based primarily on the spectral classification technique, as described in Buchhave et al. (2012). They also use the spectroscopy made easy (SME) technique (Valenti & Fischer 2005) and MOOG. We have 28 stars in common with their sample. The comparisons are shown in the top panels of Fig. 5. Both the temperature and the metallicity compare well with a mean difference of −64 K and −0.03 dex, respectively. For the effective temperature, a slight deviation for higher temperatures can be seen. We do not compare with their surface gravities since they have taken them from external sources.

We also compared with all the values listed in the TEPCat catalog (Southworth 2011) where we have 88 stars in common. In the bottom panels we compare our spectroscopic results for the effective temperature, metallicity, and surface gravity with their results. The temperatures compare well, with a mean difference of −93 K. The same slight deviation for higher temperatures can be seen. The metallicities show a mean difference of −0.09. There is also a wide spread present in this comparison. This shows again that a homogeneous analysis of stellar parameters is very important. As expected it can be seen that the spectroscopic surface gravities do not compare well. In the top righthand panel, we compare our light curve surface gravities with the values in the TEPCat catalog. It is immediately clear that these compare extremely well. On average, there is no difference between these surface gravities.

6. Discussion

We found that stellar masses and radii are affected by using different surface gravities. Especially for stellar radii, the differences can go up to 1.0 $R_{\odot}$. Planetary radii are linearly affected by the stellar radius (the transit depth provides the radius ratio $R_{\rm p}/R_{*}$). Caution should thus be placed when calculating planetary radii.

With our stellar radii, we recalculated all planetary radii for the planets from this sample. We used the radius ratios from the same works we used to get the stellar densities. The top panel of Fig. 6 compares the new planetary radii calculated with our photometric stellar radius with the planetary radii from the literature works. Most planetary radii, especially the small ones, agree very well, within one sigma. Since most transit discovery papers calculate stellar radii based on a photometric surface gravity, this could be expected. However, there are still several planets where the difference in radius is more than two sigma (CoRoT-1, HD 149026, WASP-11, WASP-12, WASP-13, WASP-32, WASP-50, WASP-8). If one used stellar radii, which are calculated with spectroscopic surface gravities, the differences would be much greater.

For the planet hosts that we have in common with the homogeneous part of the TEPCat Catalogue (Southworth 2010), we also recalculated the planetary masses using our photometric stellar masses. In the bottom panel of Fig. 6, we plot the planetary radius versus the planetary mass. We use both our newly calculated values and the values from the TEPCat catalog. Since the stellar radius is more affected than the stellar mass by using a different surface gravity, the planetary radius is also more affected than the planetary mass. As already seen, most planetary values agree well, but for some planets, the radii differ a lot. This can influence theoretical composition models for these extrasolar planets. Overplotted in Fig. 6 are isodensity curves for some planets from the solar system. A large difference in stellar and thus planetary radius can lead to incorrectly classifying a planet. Caution should thus be used on planetary radius determinations since precise stellar radius determinations are very dependent on a precise determination of the atmospheric stellar parameters. In a forthcoming work, we will focus more on these planets for which we find very different parameters.

7. Conclusions

In this work, we spectroscopically derived stellar atmospheric parameters (effective temperature, surface gravity, metallicity, and microturbulent velocity), stellar masses and radii, and chemical abundances for 90 transiting planet hosts, of which 28 were

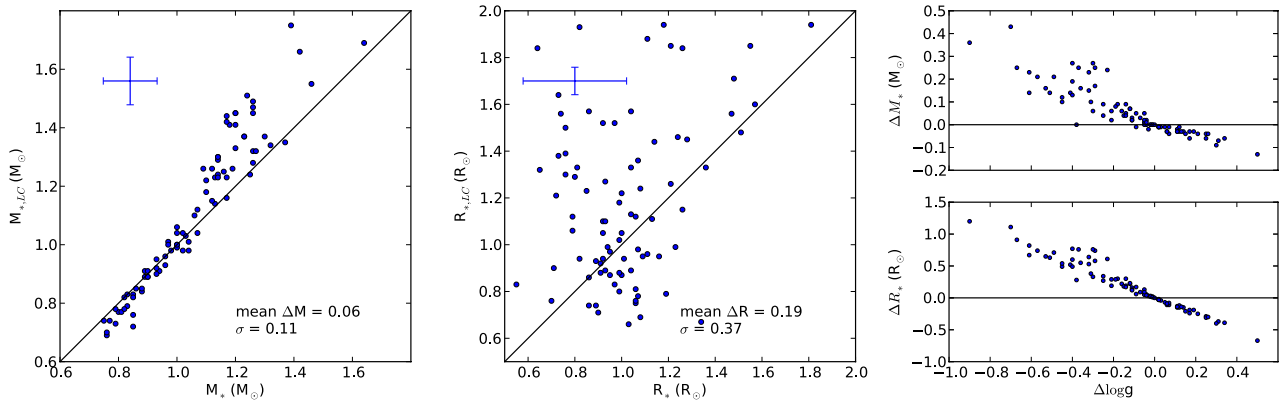

Fig. 4. Comparisons of the masses and radii, obtained with the spectroscopic and photometric surface gravity. The *right panel* shows the differences as a function of the difference in surface gravity (all defined as "photometric – spectroscopic").

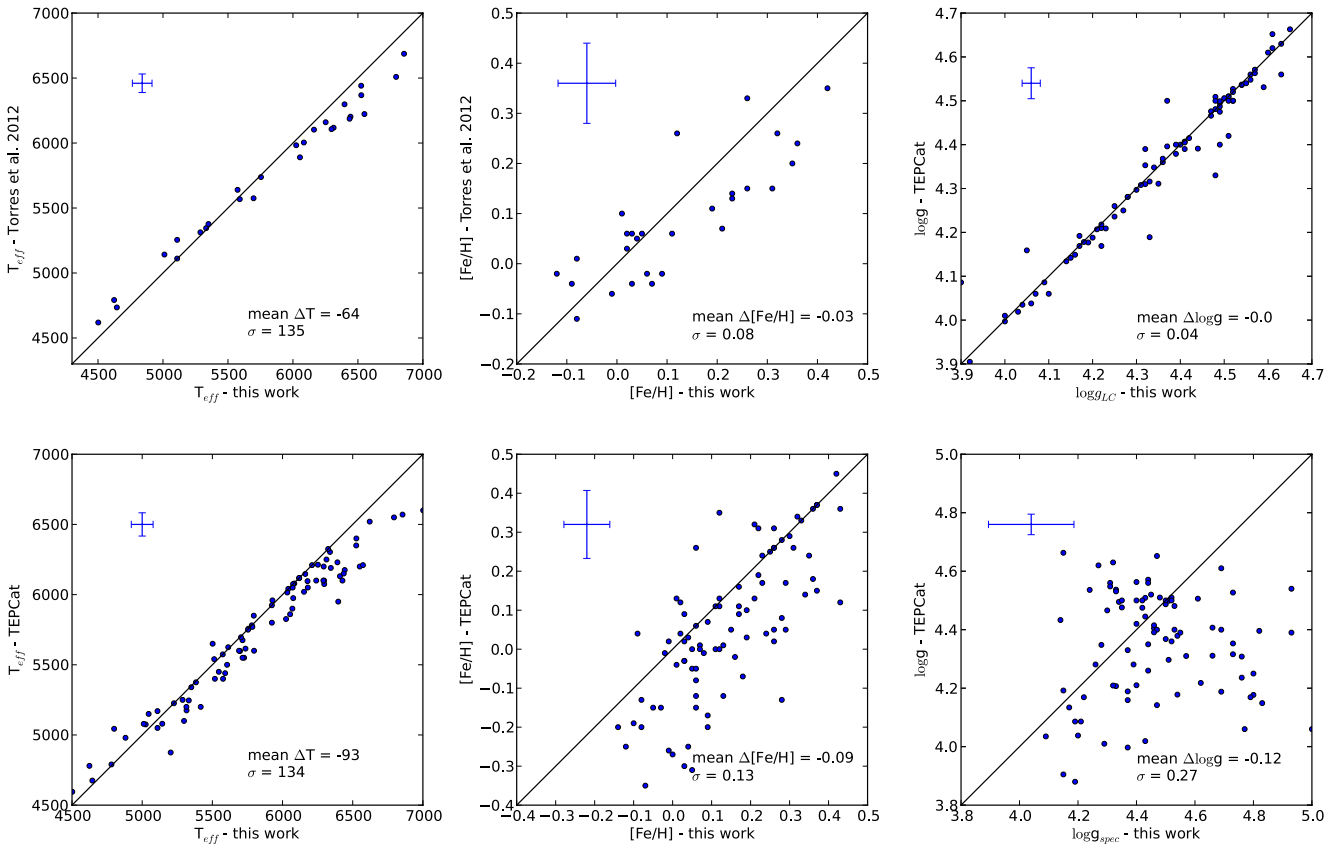

Fig. 5. Comparisons of the spectroscopic results in this work with the results of Torres et al. (2012) (*top left* and *midddle panels*) and the results of the TEPCat catalog (*bottom panels*).

previously presented in works by members of our team. We used the ARES+MOOG method with carefully selected iron linelists. All values, calculated in this work, are added to the online SWEET-Cat catalog[5] (Santos et al. 2013).

We can summarize the results as follows.

- Temperatures and metallicities in general compare well with different literature sources.
- Spectroscopically derived surface gravities are very poorly constrained. They were independently derived from the photometric light curve, using the spectroscopic temperatures and metallicities and stellar densities from the discovery papers. These new photometric surface gravities are much more precise and match, in general, the literature data very well.
- The chemical abundances were derived again using the photometric surface gravity. The abundances of the atoms are not affected by using different surface gravities. Abundances of ions, however, are slightly affected, as predicted by Gray (1992).
- Stellar masses and radii were derived through calibration formulae based on the effective temperature, metallicity, and surface gravity. The different values of the surface gravity

[5] https://www.astro.up.pt/resources/sweet-cat/

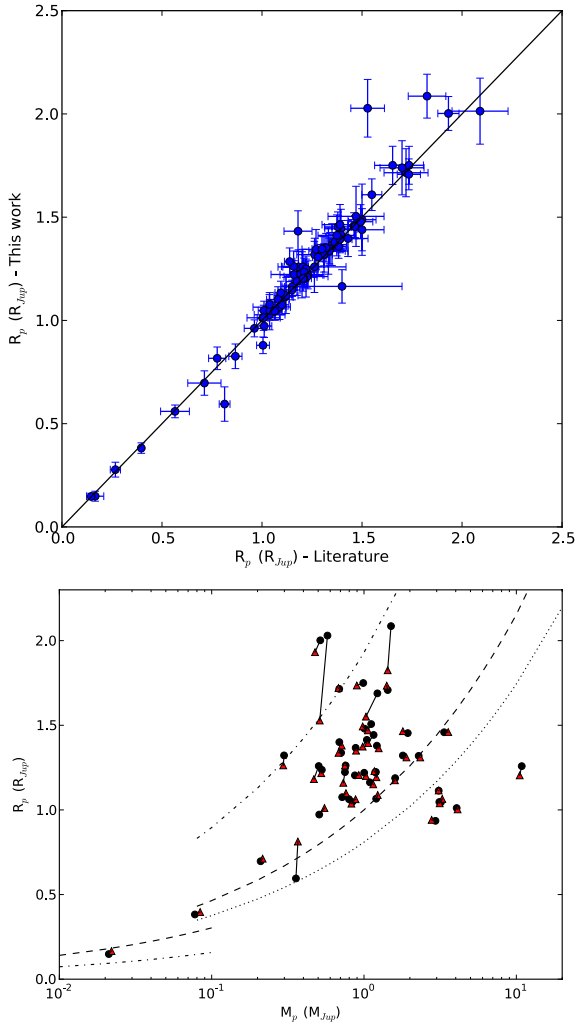

Fig. 6. *Top panel*: comparison of the planetary radii, calculated with our photometric stellar radius, with literature values. *Bottom panel*: planetary radii are plotted against their masses. Circles denote the values calculated with the stellar radius and mass from this work, using the photometric surface gravity, while the triangles are the values from the homogenous TEPCat Catalogue. Isodensity curves are overplotted for Saturn (dash-dotted), Jupiter (dashed), Neptune (dotted), Mars (dash-dotted), and Pluto (dashed).

do not have any strong effect on the mass determination with only a mean difference of 0.06 $M_{\odot}$, but it does on the radius determination where the comparison shows a large spread. Using the more precise photometric surface gravity also results in more precise stellar mass and radius determinations.

– Planetary radii and masses were recalculated using the photometric stellar radii and masses. Most values agree within error bars, but eight planets show differences of more than two sigma.

Acknowledgements. This work made use of the ESO archive and the Simbad Database. This work was supported by the European Research Council/European Community under the FP7 through Starting Grant agreement number 239953. N.C.S. acknowledges the support of the Fundação para a Ciência e a Tecnologia (FCT) in the form of grant reference PTDC/CTE-AST/098528/2008. V.Zh.A., S.G.S. and E.D.M are supported by grants SFRH/BPD/70574/2010, SFRH/BPD/47611/2008 and SFRH/BPD/76606/2011, respectively , also from FCT. GI acknowledges financial support from the Spanish Ministry project MICINN AYA2011-29060.

References

Adibekyan, V. Z., Sousa, S. G., Santos, N. C., et al. 2012, A&A, 545, A32
Ammler-von Eiff, M., Santos, N. C., Sousa, S. G., et al. 2009, A&A, 507, 523
Anderson, D. R., Hellier, C., Gillon, M., et al. 2010, ApJ, 709, 159
Anderson, D. R., Collier Cameron, A., Hellier, C., et al. 2011, A&A, 531, A60
Anderson, D. R., Collier Cameron, A., Gillon, M., et al. 2012, MNRAS, 422, 1988
Bakos, G. Á., Hartman, J., Torres, G., et al. 2011, ApJ, 742, 116
Bakos, G. Á., Hartman, J. D., Torres, G., et al. 2012, AJ, 144, 19
Barros, S. C. C., Faedi, F., Collier Cameron, A., et al. 2011, A&A, 525, A54
Batalha, N. M., Rowe, J. F., Bryson, S. T., et al. 2013, ApJS, 204, 24
Béky, B., Bakos, G. Á., Hartman, J., et al. 2011, ApJ, 734, 109
Bergemann, M., Lind, K., Collet, R., Magic, Z., & Asplund, M. 2012, MNRAS, 427, 27
Bonomo, A. S., Hébrard, G., Santerne, A., et al. 2012, A&A, 538, A96
Bouchy, F., Pont, F., Santos, N. C., et al. 2004, A&A, 421, L13
Bressan, A., Marigo, P., Girardi, L., et al. 2012, MNRAS, 427, 127
Buchhave, L. A., Latham, D. W., Johansen, A., et al. 2012, Nature, 486, 375
Burrows, A., Hubeny, I., Budaj, J., & Hubbard, W. B. 2007, ApJ, 661, 502
Casagrande, L., Portinari, L., & Flynn, C. 2006, MNRAS, 373, 13
Delgado Mena et al., E. 2013, A&A, submitted
Dressing, C. D., & Charbonneau, D. 2013, ApJ, 767, 95
Enoch, B., Anderson, D. R., Barros, S. C. C., et al. 2011a, AJ, 142, 86
Enoch, B., Cameron, A. C., Anderson, D. R., et al. 2011b, MNRAS, 410, 1631
Faedi, F., Pollacco, D., Barros, S. C. C., et al. 2013, A&A, 551, A73
Ghezzi, L., Cunha, K., Smith, V. V., et al. 2009, ApJ, 698, 451
Gillon, M., Pont, F., Moutou, C., et al. 2007, A&A, 466, 743
Gillon, M., Anderson, D. R., Triaud, A. H. M. J., et al. 2009, A&A, 501, 785
Gillon, M., Doyle, A. P., Lendl, M., et al. 2011, A&A, 533, A88
Gómez Maqueo Chew, Y., Faedi, F., Cargile, P., et al. 2013, ApJ, 768, 79
Gray, D. F. 1992, The observation and analysis of stellar photospheres, Camb. Astrophys. Ser., 20
Guillot, T., Santos, N. C., Pont, F., et al. 2006, A&A, 453, L21
Hartman, J. D., Bakos, G. Á., Kipping, D. M., et al. 2011, ApJ, 728, 138
Hebb, L., Collier-Cameron, A., Triaud, A. H. M. J., et al. 2010, ApJ, 708, 224
Hellier, C., Anderson, D. R., Collier Cameron, A., et al. 2010, ApJ, 723, L60
Hellier, C., Anderson, D. R., Collier Cameron, A., et al. 2012, MNRAS, 426, 739
Henry, G. W., Howard, A. W., Marcy, G. W., Fischer, D. A., & Johnson, J. A. 2011 [arXiv:1109.2549]
Howard, A. W., Bakos, G. Á., Hartman, J., et al. 2012, ApJ, 749, 134
Howell, S. B., Rowe, J. F., Bryson, S. T., et al. 2012, ApJ, 746, 123
Johnson, J. A., Winn, J. N., Bakos, G. Á., et al. 2011, ApJ, 735, 24
Kurucz, R. 1993, ATLAS9 Stellar Atmosphere Programs and 2 km s^{-1} grid. Kurucz CD-ROM No. 13 (Cambridge, Mass.: Smithsonian Astrophysical Observatory)
Laughlin, G., Crismani, M., & Adams, F. C. 2011, ApJ, 729, L7
Léger, A., Rouan, D., Schneider, J., et al. 2009, A&A, 506, 287
Lendl, M., Anderson, D. R., Collier-Cameron, A., et al. 2012, A&A, 544, A72
Lister, T. A., Anderson, D. R., Gillon, M., et al. 2009, ApJ, 703, 752
Maxted, P. F. L., Anderson, D. R., Collier Cameron, A., et al. 2010a, PASP, 122, 1465
Maxted, P. F. L., Anderson, D. R., Gillon, M., et al. 2010b, AJ, 140, 2007
Maxted, P. F. L., Anderson, D. R., Collier Cameron, A., et al. 2011, PASP, 123, 547
Maxted, P. F. L., Anderson, D. R., Collier Cameron, A., et al. 2013, PASP, 125, 48
Mayor, M., & Queloz, D. 1995, Nature, 378, 355
Mayor, M., Marmier, M., Lovis, C., et al. 2011, A&A, submitted [arXiv:1109.2497]
Miguel, Y., Guilera, O. M., & Brunini, A. 2011, MNRAS, 417, 314
Molenda-Żakowicz, J., Sousa, S. G., Frasca, A., et al. 2013, MNRAS, 434, 1422
Mordasini, C., Alibert, Y., Benz, W., Klahr, H., & Henning, T. 2012a, A&A, 541, A97
Mordasini, C., Alibert, Y., Georgy, C., et al. 2012b, A&A, 547, A112
Mortier, A., Santos, N. C., Sousa, S., et al. 2013a, A&A, 551, A112
Mortier, A., Santos, N. C., Sousa, S. G., et al. 2013b, A&A, 557, A70
Pont, F., Tamuz, O., Udalski, A., et al. 2008, A&A, 487, 749
Queloz, D., Anderson, D., Collier Cameron, A., et al. 2010, A&A, 517, L1
Santos, N. C., Israelian, G., & Mayor, M. 2004, A&A, 415, 1153
Santos, N. C., Ecuvillon, A., Israelian, G., et al. 2006, A&A, 458, 997
Santos, N. C., Sousa, S. G., Mortier, A., et al. 2013, A&A, 556, A150
Seager, S., & Mallén-Ornelas, G. 2003, ApJ, 585, 1038
Serenelli, A. M., Bergemann, M., Ruchti, G., & Casagrande, L. 2013, MNRAS, 429, 3645
Smalley, B., Anderson, D. R., Collier Cameron, A., et al. 2010, A&A, 520, A56

Smalley, B., Anderson, D. R., Collier Cameron, A., et al. 2011, A&A, 526, A130
Smalley, B., Anderson, D. R., Collier-Cameron, A., et al. 2012, A&A, 547, A61
Smith, A. M. S., Anderson, D. R., Collier Cameron, A., et al. 2012, AJ, 143, 81
Smith, A. M. S., Anderson, D. R., Bouchy, F., et al. 2013, A&A, 552, A120
Sneden, C. A. 1973, Ph.D. Thesis, The University of Texas at Austin
Sousa, S. G., Santos, N. C., Israelian, G., Mayor, M., & Monteiro, M. J. P. F. G. 2006, A&A, 458, 873
Sousa, S. G., Santos, N. C., Israelian, G., Mayor, M., & Monteiro, M. J. P. F. G. 2007, A&A, 469, 783
Sousa, S. G., Santos, N. C., Mayor, M., et al. 2008, A&A, 487, 373
Sousa, S. G., Santos, N. C., Israelian, G., Mayor, M., & Udry, S. 2011, A&A, 533, A141
Southworth, J. 2010, MNRAS, 408, 1689
Southworth, J. 2011, MNRAS, 417, 2166
Southworth, J. 2012, MNRAS, 426, 1291
Sozzetti, A., Torres, G., Charbonneau, D., et al. 2007, ApJ, 664, 1190
Street, R. A., Simpson, E., Barros, S. C. C., et al. 2010, ApJ, 720, 337
Todorov, K. O., Deming, D., Knutson, H. A., et al. 2012, ApJ, 746, 111
Torres, G., Winn, J. N., & Holman, M. J. 2008, ApJ, 677, 1324
Torres, G., Andersen, J., & Giménez, A. 2010, A&ARv, 18, 67
Torres, G., Fischer, D. A., Sozzetti, A., et al. 2012, ApJ, 757, 161
Triaud, A. H. M. J., Queloz, D., Hellier, C., et al. 2011, A&A, 531, A24
Tsantaki, M., Sousa, S. G., Adibekyan, V. Z., et al. 2013, A&A, 555, A150
Udalski, A., Pont, F., Naef, D., et al. 2008, A&A, 482, 299
Udry, S., & Santos, N. C. 2007, ARA&A, 45, 397
Valenti, J. A., & Fischer, D. A. 2005, ApJS, 159, 141
Valle, G., Dell'Omodarme, M., Prada Moroni, P. G., & Degl'Innocenti, S. 2013, A&A, 554, A68
West, R. G., Anderson, D. R., Gillon, M., et al. 2009a, AJ, 137, 4834
West, R. G., Collier Cameron, A., Hebb, L., et al. 2009b, A&A, 502, 395
West, R. G., Anderson, D. R., Gillon, M., et al. 2013, submitted

Pages 10 to 12 are available in the electronic edition of the journal at http://www.aanda.org

Table 4. Stellar parameters for the transit hosts in this sample.

Name	$T_{\rm eff}$ (K)	log $g_{\rm spec}$ (dex)	[Fe/H] (dex)	ξ (km s^{-1})	M_* ($M_\odot$)	R_* ($R_\odot$)	ρ_* ($\rho_\odot$)	Ref.	log $g_{\rm LC}$ (dex)	$M_{*,\rm LC}$ ($M_\odot$)	$R_{*,\rm LC}$ ($R_\odot$)
CoRoT-1	6397 ± 54	4.66 ± 0.09	0.03 ± 0.04	1.68 ± 0.09	1.13 ± 0.08	0.85 ± 0.10	0.66 ± 0.02	1	4.35 ± 0.01	1.23 ± 0.08	1.23 ± 0.04
CoRoT-10	5025 ± 155	4.47 ± 0.31	0.06 ± 0.09	1.26 ± 0.34	0.80 ± 0.10	0.89 ± 0.41	2.20 ± 0.47	1	4.61 ± 0.02	0.77 ± 0.07	0.74 ± 0.04
CoRoT-12	5715 ± 208	4.66 ± 0.22	0.17 ± 0.14	1.07 ± 0.31	0.97 ± 0.10	0.79 ± 0.23	0.89 ± 0.08	1	4.41 ± 0.02	1.01 ± 0.10	1.06 ± 0.06
CoRoT-2	5697 ± 97	4.73 ± 0.17	–0.09 ± 0.07	1.64 ± 0.16	0.89 ± 0.07	0.71 ± 0.15	1.36 ± 0.06	2	4.52 ± 0.01	0.91 ± 0.07	0.90 ± 0.04
CoRoT-4	6344 ± 93	4.82 ± 0.11	0.15 ± 0.06	1.74 ± 0.14	1.14 ± 0.08	0.72 ± 0.09	0.79 ± 0.11	1	4.37 ± 0.02	1.24 ± 0.09	1.21 ± 0.05
CoRoT-5	6240 ± 70	4.46 ± 0.11	0.04 ± 0.05	1.28 ± 0.09	1.13 ± 0.09	1.06 ± 0.16	0.88 ± 0.18	1	4.41 ± 0.03	1.14 ± 0.08	1.12 ± 0.06
CoRoT-7	5288 ± 27	4.40 ± 0.07	0.02 ± 0.02	0.90 ± 0.05	0.85 ± 0.06	1.00 ± 0.10	1.00 ± 0.48	1	4.51 ± 0.02	0.83 ± 0.06	0.87 ± 0.04
CoRoT-8	5143 ± 178	4.42 ± 0.33	0.22 ± 0.11	0.61 ± 0.40	0.88 ± 0.12	0.99 ± 0.51	1.21 ± 0.32	1	4.49 ± 0.03	0.84 ± 0.08	0.88 ± 0.05
CoRoT-9	5613 ± 36	4.35 ± 0.09	-0.02 ± 0.03	0.90 ± 0.05	0.94 ± 0.07	1.11 ± 0.14	1.16 ± 0.24	1	4.47 ± 0.04	0.91 ± 0.07	0.96 ± 0.05
HAT-P-1	6076 ± 27	4.47 ± 0.07	0.21 ± 0.03	1.17 ± 0.05	1.12 ± 0.08	1.04 ± 0.10	0.82 ± 0.07	3	4.40 ± 0.01	1.15 ± 0.08	1.13 ± 0.04
HAT-P-11	4624 ± 225	4.15 ± 0.59	0.26 ± 0.08	0.39 ± 0.39	0.85 ± 0.27	1.34 ± 1.34	2.42 ± 0.10	1	4.65 ± 0.01	0.72 ± 0.08	0.67 ± 0.04
HAT-P-17	5332 ± 55	4.45 ± 0.13	0.05 ± 0.03	0.82 ± 0.10	0.86 ± 0.07	0.95 ± 0.17	1.46 ± 0.09	4	4.52 ± 0.02	0.85 ± 0.06	0.87 ± 0.03
HAT-P-20	4502 ± 188	4.32 ± 0.60	0.12 ± 0.15	0.73 ± 0.60	0.76 ± 0.20	1.03 ± 1.03	2.27 ± 0.18	5	4.63 ± 0.01	0.69 ± 0.07	0.66 ± 0.04
HAT-P-26	5011 ± 55	4.31 ± 0.17	0.01 ± 0.04	0.48 ± 0.16	0.81 ± 0.08	1.07 ± 0.27	1.69 ± 0.32	6	4.56 ± 0.02	0.77 ± 0.06	0.78 ± 0.03
HAT-P-27	5316 ± 55	4.48 ± 0.10	0.30 ± 0.03	0.82 ± 0.09	0.90 ± 0.07	0.93 ± 0.12	1.32 ± 0.19	7	4.51 ± 0.03	0.89 ± 0.07	0.89 ± 0.04
HAT-P-30	6338 ± 42	4.52 ± 0.06	0.12 ± 0.03	1.40 ± 0.05	1.17 ± 0.08	1.00 ± 0.08	0.70 ± 0.07	8	4.36 ± 0.01	1.23 ± 0.08	1.22 ± 0.05
HAT-P-35	6178 ± 45	4.40 ± 0.09	0.12 ± 0.03	1.34 ± 0.06	1.16 ± 0.08	1.14 ± 0.14	0.42 ± 0.06	9	4.22 ± 0.03	1.25 ± 0.08	1.44 ± 0.08
HAT-P-4	6054 ± 60	4.17 ± 0.28	0.35 ± 0.08	1.59 ± 0.09	1.37 ± 0.18	1.57 ± 0.71	0.31 ± 0.03	1	4.14 ± 0.02	1.35 ± 0.09	1.60 ± 0.07
HAT-P-6	6855 ± 111	4.69 ± 0.20	-0.08 ± 0.11	2.85 ± 1.15	1.26 ± 0.10	0.86 ± 0.22	0.37 ± 0.04	2	4.20 ± 0.02	1.47 ± 0.11	1.57 ± 0.08
HAT-P-7	6525 ± 61	4.09 ± 0.08	0.31 ± 0.07	1.78 ± 0.14	1.64 ± 0.11	1.81 ± 0.22	0.20 ± 0.01	1	4.04 ± 0.01	1.69 ± 0.10	1.94 ± 0.07
HAT-P-8	6550 ± 61	4.80 ± 0.08	0.07 ± 0.04	1.93 ± 0.09	1.18 ± 0.08	0.74 ± 0.07	0.37 ± 0.04	10	4.19 ± 0.03	1.41 ± 0.09	1.56 ± 0.08
HD 149026	6162 ± 41	4.37 ± 0.10	0.36 ± 0.05	1.41 ± 0.07	1.26 ± 0.09	1.21 ± 0.17	0.59 ± 0.11	3	4.33 ± 0.03	1.28 ± 0.09	1.26 ± 0.07
HD 17156	6084 ± 29	4.33 ± 0.05	0.23 ± 0.04	1.47 ± 0.05	1.19 ± 0.08	1.24 ± 0.09	0.40 ± 0.02	1	4.21 ± 0.01	1.26 ± 0.08	1.46 ± 0.05
HD 189733	5109 ± 146	4.69 ± 0.28	0.03 ± 0.08	0.78 ± 0.33	0.79 ± 0.08	0.70 ± 0.26	1.98 ± 0.17	3	4.60 ± 0.01	0.78 ± 0.07	0.76 ± 0.03
HD 209458	6118 ± 25	4.50 ± 0.04	0.03 ± 0.02	1.21 ± 0.03	1.07 ± 0.07	0.99 ± 0.06	0.73 ± 0.01	3	4.36 ± 0.01	1.12 ± 0.08	1.18 ± 0.04
HD 80606	5574 ± 72	4.46 ± 0.20	0.32 ± 0.09	1.14 ± 0.09	1.00 ± 0.09	1.00 ± 0.28	0.91 ± 0.06	1	4.42 ± 0.02	1.00 ± 0.08	1.05 ± 0.04
HD 97658	5137 ± 36	4.47 ± 0.09	–0.35 ± 0.02	0.63 ± 0.08	0.75 ± 0.06	0.86 ± 0.11	1.38 ± 0.45	11	4.59 ± 0.01	0.74 ± 0.05	0.74 ± 0.03
Kepler-17	5781 ± 85	4.53 ± 0.12	0.26 ± 0.10	1.73 ± 0.14	1.03 ± 0.08	0.94 ± 0.15	1.12 ± 0.02	2	4.48 ± 0.01	1.03 ± 0.08	0.99 ± 0.04
Kepler-21	6409 ± 44	4.43 ± 0.06	–0.03 ± 0.03	1.86 ± 0.07	1.17 ± 0.08	1.11 ± 0.09	0.20 ± 0.01	12	4.03 ± 0.05	1.44 ± 0.10	1.88 ± 0.15
KOI-135	6041 ± 143	4.26 ± 0.05	0.33 ± 0.11	1.85 ± 0.26	1.25 ± 0.10	1.36 ± 0.11	0.52 ± 0.02	2	4.28 ± 0.01	1.24 ± 0.10	1.33 ± 0.06
KOI-204	5757 ± 134	4.15 ± 0.06	0.26 ± 0.10	1.75 ± 0.19	1.17 ± 0.10	1.51 ± 0.14	0.39 ± 0.07	2	4.17 ± 0.05	1.16 ± 0.10	1.48 ± 0.11
OGLE-TR-10	6075 ± 86	4.54 ± 0.15	0.28 ± 0.10	1.45 ± 0.14	1.14 ± 0.09	0.97 ± 0.19	0.36 ± 0.06	3	4.18 ± 0.04	1.30 ± 0.10	1.52 ± 0.10
OGLE-TR-111	4800 ± 177	4.24 ± 0.46	0.22 ± 0.15	0.30 ± 0.30	0.85 ± 0.19	1.19 ± 0.97	1.52 ± 0.10	2	4.54 ± 0.01	0.76 ± 0.08	0.79 ± 0.04

Notes. The last 4 columns show the surface gravity, derived from the photometric lightcurve (LC) and the mass and radius, obtained with this surface gravity. Columns 8 and 12 show the radius, obtained through the Newton's law of gravitation.

References. (1) Southworth (2011); (2) Southworth (2012); (3) Southworth (2010); (4) Howard et al. (2012); (5) Bakos et al. (2011); (6) Hartman et al. (2011); (7) Béky et al. (2011); (8) Johnson et al. (2011); (9) Bakos et al. (2012); (10) Todorov et al. (2012); (11) Henry et al. (2011); (12) Howell et al. (2012); (13) West et al. (2009b); (14) West et al. (2009a); (15) Lister et al. (2009); (16) Hebb et al. (2010); (17) Maxted et al. (2010b); (18) Triaud et al. (2011); (19) Street et al. (2010); (20) Enoch et al. (2011b); (21) Smalley et al. (2010); (22) West et al. (2013); (23) Hellier et al. (2010); (24) Anderson et al. (2011); (25) Maxted et al. (2010a); (26) Smalley et al. (2011); (27) Enoch et al. (2011a); (28) Smith et al. (2012); (29) Barros et al. (2011); (30) Maxted et al. (2011); (31) Lendl et al. (2012); (32) Anderson et al. (2012); (33) Hellier et al. (2012); (34) Gillon et al. (2011); (35) Faedi et al. (2013); (36) Gillon et al. (2009); (37) Smith et al. (2013); (38) Maxted et al. (2013); (39) Smalley et al. (2012); (40) Queloz et al. (2010).

Table 4. continued.

Name	$T_{\rm eff}$ (K)	log $g_{\rm spec}$ (dex)	[Fe/H] (dex)	ξ (km s^{-1})	M_* ($M_\odot$)	R_* ($R_\odot$)	ρ_* ($\rho_\odot$)	Ref.	log $g_{\rm LC}$ (dex)	$M_{*,\rm LC}$ ($M_\odot$)	$R_{*,\rm LC}$ ($R_\odot$)
OGLE-TR-113	4781 ± 166	4.31 ± 0.41	0.03 ± 0.06	1.24 ± 0.29	0.79 ± 0.14	1.06 ± 0.73	1.68 ± 0.06	2	4.56 ± 0.01	0.73 ± 0.07	0.75 ± 0.04
OGLE-TR-132	6210 ± 59	4.51 ± 0.27	0.37 ± 0.07	1.23 ± 0.09	1.26 ± 0.12	1.04 ± 0.40	0.54 ± 0.06	2	4.30 ± 0.03	1.32 ± 0.09	1.33 ± 0.06
OGLE-TR-182	5924 ± 64	4.47 ± 0.18	0.37 ± 0.08	0.91 ± 0.09	1.14 ± 0.10	1.04 ± 0.26	0.33 ± 0.10	3	4.15 ± 0.07	1.29 ± 0.10	1.57 ± 0.16
OGLE-TR-211	6325 ± 91	4.22 ± 0.17	0.11 ± 0.10	1.63 ± 0.21	1.32 ± 0.13	1.47 ± 0.37	0.34 ± 0.08	3	4.17 ± 0.05	1.34 ± 0.10	1.56 ± 0.13
OGLE-TR-56	6119 ± 62	4.21 ± 0.19	0.25 ± 0.08	1.48 ± 0.11	1.30 ± 0.13	1.48 ± 0.43	0.26 ± 0.01	2	4.09 ± 0.01	1.37 ± 0.09	1.71 ± 0.07
TrES-1	5226 ± 38	4.40 ± 0.10	0.06 ± 0.05	0.90 ± 0.05	0.85 ± 0.07	0.99 ± 0.14	1.63 ± 0.09	3	4.57 ± 0.01	0.82 ± 0.06	0.80 ± 0.03
TrES-2	5795 ± 73	4.30 ± 0.13	0.06 ± 0.08	0.79 ± 0.12	1.04 ± 0.09	1.23 ± 0.23	1.10 ± 0.01	1	4.47 ± 0.01	0.98 ± 0.07	0.99 ± 0.04
TrES-3	5502 ± 157	4.44 ± 0.22	–0.10 ± 0.19	1.00 ± 0.30	0.88 ± 0.10	0.97 ± 0.31	1.65 ± 0.04	1	4.57 ± 0.03	0.85 ± 0.09	0.83 ± 0.05
TrES-4	6293 ± 96	4.20 ± 0.27	0.34 ± 0.10	2.01 ± 0.17	1.46 ± 0.18	1.55 ± 0.67	0.22 ± 0.03	2	4.06 ± 0.03	1.55 ± 0.11	1.85 ± 0.10
WASP-1	6252 ± 45	4.32 ± 0.05	0.23 ± 0.03	1.42 ± 0.05	1.27 ± 0.09	1.28 ± 0.10	0.40 ± 0.05	2	4.23 ± 0.03	1.32 ± 0.09	1.45 ± 0.07
WASP-10	4645 ± 125	4.27 ± 0.39	0.04 ± 0.05	0.58 ± 0.47	0.76 ± 0.13	1.08 ± 0.71	2.16 ± 0.31	3	4.61 ± 0.02	0.70 ± 0.06	0.69 ± 0.03
WASP-11	4881 ± 125	4.44 ± 0.31	0.01 ± 0.05	0.64 ± 0.24	0.77 ± 0.09	0.90 ± 0.42	2.12 ± 0.46	13	4.63 ± 0.02	0.74 ± 0.06	0.71 ± 0.03
WASP-12	6313 ± 52	4.37 ± 0.12	0.21 ± 0.04	1.65 ± 0.07	1.26 ± 0.10	1.21 ± 0.21	0.22 ± 0.02	2	4.05 ± 0.02	1.49 ± 0.10	1.85 ± 0.08
WASP-13	6025 ± 21	4.19 ± 0.03	0.11 ± 0.05	1.28 ± 0.10	1.20 ± 0.08	1.46 ± 0.08	0.13 ± 0.02	2	3.90 ± 0.03	1.45 ± 0.10	2.20 ± 0.13
WASP-15	6573 ± 70	4.79 ± 0.08	0.09 ± 0.04	1.72 ± 0.09	1.20 ± 0.08	0.76 ± 0.07	0.39 ± 0.03	14	4.22 ± 0.02	1.41 ± 0.09	1.50 ± 0.06
WASP-16	5726 ± 22	4.34 ± 0.05	0.13 ± 0.02	0.97 ± 0.03	1.02 ± 0.07	1.16 ± 0.09	1.21 ± 0.15	15	4.49 ± 0.02	0.98 ± 0.07	0.95 ± 0.04
WASP-17	6794 ± 83	4.83 ± 0.09	–0.12 ± 0.05	2.57 ± 0.22	1.20 ± 0.08	0.73 ± 0.08	0.32 ± 0.01	2	4.16 ± 0.01	1.45 ± 0.10	1.64 ± 0.06
WASP-18	6526 ± 69	4.73 ± 0.08	0.19 ± 0.05	1.83 ± 0.10	1.23 ± 0.08	0.81 ± 0.08	0.69 ± 0.06	2	4.32 ± 0.03	1.37 ± 0.09	1.33 ± 0.07
WASP-19	5591 ± 62	4.46 ± 0.09	0.26 ± 0.05	1.23 ± 0.09	0.98 ± 0.08	0.99 ± 0.12	0.99 ± 0.04	16	4.44 ± 0.01	0.98 ± 0.07	1.02 ± 0.04
WASP-2	5109 ± 72	4.33 ± 0.14	0.02 ± 0.05	0.57 ± 0.12	0.83 ± 0.07	1.06 ± 0.21	1.52 ± 0.07	2	4.54 ± 0.01	0.79 ± 0.06	0.81 ± 0.03
WASP-21	5924 ± 55	4.39 ± 0.09	–0.22 ± 0.04	1.06 ± 0.08	0.97 ± 0.07	1.08 ± 0.14	0.59 ± 0.06	2	4.28 ± 0.03	1.00 ± 0.07	1.24 ± 0.06
WASP-22	6153 ± 46	4.57 ± 0.09	0.26 ± 0.03	1.36 ± 0.06	1.14 ± 0.08	0.93 ± 0.11	0.61 ± 0.06	17	4.32 ± 0.02	1.23 ± 0.08	1.27 ± 0.05
WASP-23	5046 ± 99	4.33 ± 0.18	0.05 ± 0.06	0.64 ± 0.23	0.82 ± 0.08	1.06 ± 0.28	1.84 ± 0.03	18	4.59 ± 0.01	0.78 ± 0.06	0.76 ± 0.03
WASP-24	6297 ± 58	4.76 ± 0.17	0.09 ± 0.04	1.41 ± 0.08	1.12 ± 0.08	0.76 ± 0.16	0.47 ± 0.03	19	4.25 ± 0.01	1.26 ± 0.09	1.39 ± 0.05
WASP-25	5736 ± 35	4.52 ± 0.09	0.06 ± 0.03	1.11 ± 0.05	0.96 ± 0.07	0.92 ± 0.11	1.29 ± 0.10	20	4.51 ± 0.01	0.96 ± 0.07	0.94 ± 0.03
WASP-26	6034 ± 31	4.44 ± 0.06	0.16 ± 0.02	1.28 ± 0.04	1.10 ± 0.08	1.07 ± 0.09	0.47 ± 0.06	21	4.25 ± 0.03	1.18 ± 0.08	1.36 ± 0.07
WASP-28	6134 ± 38	4.55 ± 0.05	–0.12 ± 0.03	1.17 ± 0.06	1.02 ± 0.07	0.92 ± 0.06	0.93 ± 0.13	22	4.44 ± 0.03	1.04 ± 0.07	1.05 ± 0.06
WASP-29	5203 ± 102	4.93 ± 0.21	0.17 ± 0.05	1.77 ± 0.22	0.83 ± 0.07	0.55 ± 0.13	1.56 ± 0.21	23	4.55 ± 0.02	0.83 ± 0.07	0.83 ± 0.04
WASP-31	6443 ± 75	4.76 ± 0.09	–0.08 ± 0.05	1.62 ± 0.11	1.10 ± 0.08	0.76 ± 0.08	0.59 ± 0.04	24	4.31 ± 0.02	1.22 ± 0.08	1.30 ± 0.05
WASP-32	6427 ± 141	4.93 ± 0.08	0.28 ± 0.10	1.20 ± 0.21	1.23 ± 0.10	0.65 ± 0.06	0.80 ± 0.10	25	4.32 ± 0.03	1.37 ± 0.10	1.32 ± 0.07
WASP-34	5704 ± 26	4.35 ± 0.05	0.08 ± 0.02	0.97 ± 0.03	1.00 ± 0.07	1.13 ± 0.08	0.83 ± 0.21	26	4.37 ± 0.05	0.99 ± 0.07	1.11 ± 0.08
WASP-35	6072 ± 62	4.69 ± 0.13	–0.05 ± 0.05	1.26 ± 0.09	1.00 ± 0.07	0.79 ± 0.13	0.83 ± 0.07	27	4.39 ± 0.02	1.06 ± 0.08	1.12 ± 0.05
WASP-36	5928 ± 59	4.51 ± 0.09	–0.01 ± 0.05	0.89 ± 0.09	1.00 ± 0.07	0.95 ± 0.12	1.21 ± 0.05	28	4.49 ± 0.01	1.00 ± 0.07	0.97 ± 0.03

Table 4. continued.

Name	$T_{\rm eff}$ (K)	log $g_{\rm spec}$ (dex)	[Fe/H] (dex)	ξ (km s^{-1})	M_* ($M_\odot$)	R_* ($R_\odot$)	ρ_* ($\rho_\odot$)	Ref.	log $g_{\rm LC}$ (dex)	$M_{*,\rm LC}$ ($M_\odot$)	$R_{*,\rm LC}$ ($R_\odot$)
WASP-38	6436 ± 60	4.80 ± 0.07	0.06 ± 0.04	1.75 ± 0.09	1.14 ± 0.08	0.73 ± 0.06	0.51 ± 0.02	29	4.27 ± 0.01	1.30 ± 0.09	1.38 ± 0.05
WASP-4	5513 ± 43	4.50 ± 0.07	0.03 ± 0.03	0.86 ± 0.07	0.89 ± 0.07	0.91 ± 0.09	1.23 ± 0.02	2	4.49 ± 0.01	0.89 ± 0.06	0.92 ± 0.03
WASP-41	5546 ± 33	4.53 ± 0.07	0.06 ± 0.02	1.08 ± 0.05	0.90 ± 0.07	0.89 ± 0.08	1.27 ± 0.14	30	4.49 ± 0.03	0.91 ± 0.06	0.93 ± 0.04
WASP-42	5315 ± 79	4.50 ± 0.18	0.29 ± 0.05	1.16 ± 0.13	0.90 ± 0.08	0.91 ± 0.23	1.37 ± 0.14	31	4.52 ± 0.02	0.89 ± 0.07	0.88 ± 0.04
WASP-45	5298 ± 95	4.43 ± 0.18	0.43 ± 0.06	1.10 ± 0.13	0.95 ± 0.09	1.00 ± 0.25	1.08 ± 0.25	32			
WASP-47	5576 ± 68	4.28 ± 0.16	0.36 ± 0.05	1.25 ± 0.09	1.07 ± 0.10	1.26 ± 0.30	0.71 ± 0.03	33	4.34 ± 0.01	1.04 ± 0.08	1.15 ± 0.04
WASP-5	5785 ± 83	4.54 ± 0.14	0.17 ± 0.06	0.96 ± 0.12	1.00 ± 0.08	0.92 ± 0.17	0.80 ± 0.08	2	4.39 ± 0.03	1.04 ± 0.08	1.10 ± 0.05
WASP-50	5518 ± 42	4.43 ± 0.12	0.13 ± 0.03	1.25 ± 0.06	0.93 ± 0.07	1.01 ± 0.17	1.48 ± 0.10	34	4.48 ± 0.02	0.92 ± 0.07	0.94 ± 0.04
WASP-54	6296 ± 40	4.37 ± 0.06	0.00 ± 0.03	1.45 ± 0.05	1.17 ± 0.08	1.18 ± 0.10	0.20 ± 0.03	35	4.00 ± 0.02	1.42 ± 0.09	1.94 ± 0.08
WASP-55	6070 ± 53	4.55 ± 0.07	0.09 ± 0.04	1.10 ± 0.06	1.06 ± 0.08	0.93 ± 0.09	0.85 ± 0.03	33	4.41 ± 0.01	1.10 ± 0.08	1.10 ± 0.04
WASP-56	5797 ± 52	4.44 ± 0.09	0.43 ± 0.04	1.19 ± 0.06	1.11 ± 0.08	1.06 ± 0.13	0.74 ± 0.04	35			
WASP-6	5383 ± 41	4.52 ± 0.06	–0.14 ± 0.03	0.80 ± 0.07	0.82 ± 0.06	0.86 ± 0.07	1.34 ± 0.11	36	4.52 ± 0.01	0.82 ± 0.06	0.86 ± 0.03
WASP-62	6391 ± 70	4.73 ± 0.11	0.24 ± 0.05	1.50 ± 0.09	1.20 ± 0.08	0.80 ± 0.11	0.59 ± 0.06	33	4.33 ± 0.02	1.33 ± 0.09	1.29 ± 0.05
WASP-63	5715 ± 60	4.29 ± 0.10	0.28 ± 0.05	1.28 ± 0.07	1.09 ± 0.09	1.26 ± 0.18	0.20 ± 0.02	33	4.00 ± 0.02	1.26 ± 0.09	1.84 ± 0.09
WASP-66	7051 ± 79	5.00 ± 0.08	0.05 ± 0.05	3.07 ± 0.27	1.39 ± 0.09	0.64 ± 0.06	0.24 ± 0.03	33	4.10 ± 0.03	1.75 ± 0.11	1.84 ± 0.10
WASP-67	5417 ± 85	4.40 ± 0.16	0.18 ± 0.06	1.16 ± 0.12	0.93 ± 0.08	1.04 ± 0.23	1.32 ± 0.15	33	4.51 ± 0.02	0.90 ± 0.07	0.89 ± 0.04
WASP-7	6621 ± 155	4.62 ± 0.14	0.12 ± 0.09	3.00 ± 0.83	1.26 ± 0.10	0.92 ± 0.17	0.41 ± 0.07	2	4.22 ± 0.04	1.45 ± 0.11	1.52 ± 0.09
WASP-71	6180 ± 52	4.15 ± 0.06	0.37 ± 0.04	1.69 ± 0.06	1.42 ± 0.10	1.61 ± 0.15	0.13 ± 0.02	37	3.92 ± 0.03	1.66 ± 0.10	2.22 ± 0.12
WASP-77A	5605 ± 41	4.37 ± 0.09	0.07 ± 0.03	1.09 ± 0.06	0.96 ± 0.07	1.09 ± 0.14	1.16 ± 0.02	38	4.48 ± 0.01	0.93 ± 0.07	0.95 ± 0.03
WASP-78	6291 ± 71	4.19 ± 0.08	–0.07 ± 0.05	1.63 ± 0.10	1.24 ± 0.09	1.49 ± 0.18	0.12 ± 0.02	39	3.89 ± 0.03	1.51 ± 0.10	2.25 ± 0.13
WASP-79	7002 ± 162	4.77 ± 0.14	0.19 ± 0.10	2.64 ± 0.24	1.43 ± 0.11	0.82 ± 0.14	0.22 ± 0.03	39	4.07 ± 0.03	1.86 ± 0.13	1.93 ± 0.11
WASP-8	5690 ± 36	4.42 ± 0.15	0.29 ± 0.03	1.25 ± 0.05	1.04 ± 0.08	1.07 ± 0.23	1.22 ± 0.16	40	4.48 ± 0.01	1.01 ± 0.07	0.98 ± 0.04
XO-1	5754 ± 42	4.61 ± 0.05	–0.01 ± 0.05	1.07 ± 0.09	0.93 ± 0.07	0.82 ± 0.06	1.24 ± 0.08	3	4.50 ± 0.01	0.95 ± 0.07	0.94 ± 0.04
XO-2	5350 ± 72	4.14 ± 0.22	0.42 ± 0.07	1.10 ± 0.08	1.08 ± 0.13	1.48 ± 0.51	1.03 ± 0.09	2			

Chapter 6

Discussion and future work

Below I will summarize the most important conclusions of this thesis. I will link the different studies I've performed and include a discussion of the results. Finally, I will outline some possibilities for future work that can be done.

6.1 Giant planet frequency

Due to the rapid growth of the exoplanet population, and the variety in fundamental parameters, the samples lend themselves excellently to performing thorough statistical analyses. With every new discovery of an exoplanet, the ideas on planet formation and evolution are either confirmed or refuted. By providing significant correlations, certain formation theories that don't match the observations can be discarded while the remaining theories can be finetuned.

During my PhD, I focused mainly on studying the correlation between giant planet frequency and various stellar parameters, such as metallicity and stellar mass. When it was first discovered that giant planets are more frequent around metal-rich hosts (e.g. Gonzalez 1997; Santos et al. 2001), dedicated surveys were conducted for planet searches, using metal-rich stars (e.g. N2K described in Fischer & Valenti 2005). Large volume-limited surveys (e.g. CORALIE and Lick-Keck) made it clear that it was not as straightforward to describe giant planet frequency around metal-poor stars (Udry & Santos 2007) as it is for metal-rich stars, showing the need for dedicated surveys of metal-poor stars in search of planets.

To understand the behaviour of giant planet frequency around these metal-poor stars, I used two different approaches. First, as described in Chapter 2, I looked solely at metal-poor stars. Similarly to the dedicated planet searches around metal-rich stars, surveys were conducted with metal-poor stars (Sozzetti et al. 2009; Santos et al. 2011). These surveys, with 234 stars

in total, revealed only 3 giant planets, of which no hot Jupiters. By calculating the inherent detection limits in the data, it was clear that giant planets, and especially hot Jupiters, should have been detected if present around these stars.

While this work confirmed that giant planets are indeed rare around metal-poor stars (4.48% for stars with $-0.7 \leq$[Fe/H]≤ 0.0 with a sensitivity to periods up to 1800 days), they may be more frequent than what is expected based on a strictly exponential correlation with metallicity. According to several studies that use an exponential fit to the data (e.g. Fischer & Valenti 2005; Sousa et al. 2011), 3% is the frequency of giant planets around stars of solar metallicity. Given that I derived a higher number for metal-poor stars, this may mean that a different correlation with metallicity could exist for these stars (e.g. a constant as already suggested by Santos et al. 2004; Udry & Santos 2007).

An exponential dependence on metallicity is expected if giant planet formation follows the core-accretion model. The lack of such a trend can be explained more easily with the theory of gravitational instability. In recent works (e.g. Meru & Bate 2010; Rogers & Wadsley 2012), simulations have shown that planet formation induced by gravitational instability is more likely to occur around metal-poor stars than around metal-rich ones. This could explain the existence of two different regimes (with an exponential dependence for metal-rich stars and a constant one for metal-poor stars). While gravitational instability is the preferred scenario for very long period planets (see section 1.2), short period planets may also be formed from through this mechanism. Baruteau et al. (2011) suggest that planets formed by gravitational instability may migrate very rapidly inwards.

Moreover, it seems that giant planets are not formed around stars where the metallicity is very low. A theoretical study based on a synthetic planet population formed by core-accretion revealed that giant planets are not formed around stars with metallicities lower than -0.5 dex (Mordasini et al. 2012a). No planets were discovered in the samples I studied around stars with metallicity lower than -0.7 despite the fact that half of the stars in the samples have lower metallicities. In this regard, it is worth mentioning that at the time of this work, only one (giant) planet had been detected (by RV or transit) around a main-sequence star with metallicity lower than -0.6 dex (HD155358 with [Fe/H] $= -0.68$ dex Cochran et al. 2007). However, recently these authors have derived a new and higher metallicity for this star (-0.51 dex Robertson et al. 2012), strenghtening the idea of a lower limit. No new planets were found in the mean time around FGK dwarfs with metallicities below -0.6 dex. Very recently, a new planet was discovered around a star with [Fe/H] $= -0.6$ dex (WASP-98 Hellier et al. 2013), however it must be noted that their errorbar on the metallicity is rather large (0.19 dex).

All this work showed that a purely exponential dependence on metallicity is not enough to describe giant planet frequency. As a different approach to this issue, I then investigated dif-

ferent functional forms to describe giant planet frequency as a function of stellar parameters, as described in Chapter 3. This study made use of three volume-limited samples that were searched for planets using the radial velocity technique from measurements with CORALIE and HARPS. The previous study showed that giant planet frequency can be either exponentially or constantly correlated with metallicity for metal-poor stars. Furthermore, a lower limit in metallicity may exist below which no giant planets are formed.

Next to metallicity, it has been suggested that disk properties play a role in giant planet formation. Since these properties are not easily determined and they are connected with the stellar mass, the role of stellar mass on giant planet formation has been studied (e.g. Johnson et al. 2010). I thus also included a possible dependence of stellar mass. Using a Bayesian statistical analysis, I was able to distinguish between the different functional forms. The test concluded that giant planet frequency is definitely not a function of stellar mass alone. This result was as expected, as the dependence on metallicity is fairly obvious. An additional dependence on stellar mass next to metallicity could neither be confirmed nor discarded. It has to be noted, however, that the used samples consist solely of FGK dwarfs. As such the mass range is very narrow. Including A and M stars in the analysis (as is the case in Johnson et al. 2010) could still reveal a stellar mass dependence. Regarding this issue it should be noted that there is currently a debate in the literature whether the 'retired A stars' from Johnson et al. (2010) are indeed as massive as they claim (for the discussion see Lloyd 2011; Johnson et al. 2013; Lloyd 2013).

All the remaining functional forms turned out to be statistically indistinguishable. The Bayesfactors, used to compare between the functions, are all between 1.0 and 4.12. According to Kass & Raftery (1995), this means that the difference is not worth more than a bare mention. A factor of at least 20, and preferably 100, is needed to have strong evidence in favour of a function. Larger samples or a more clever way of relating the parameters can help in resolving this issue (see Section 6.3).

The above-mentioned studies always used FGK dwarfs. Several planets are, however, also found around subgiant and giant stars. SWEETCat (Santos et al. 2013) shows that $\sim 18\%$ of the FGKM host stars have a surface gravity $\log g$ lower than 4.0 dex, suggesting the star is a (sub)giant. This inspired me to look into giant planet frequency for these evolved stars, as described in Chapter 4. Using a sample of 71 evolved stars (of which 31 are red giants with $\log g \leq 3.0$ dex), I found that evolved planet hosts are on average 0.24 dex more metal-poor than planet-hosting dwarfs, confirming the result of Pasquini et al. (2007).

When comparing planet hosts with non-hosts for evolved stars, only a slight metallicity enhancement is found. This enhancement is much smaller than the one seen in dwarf stars. By only considering red giants ($\log g < 3.0$ dex), no metallicity enhancement is found and the metallicity distribution seems flat. This lack of correlation confirms the results of Takeda

et al. (2008) and Zieliński et al. (2010). The opposite results from Hekker & Meléndez (2007) and Ghezzi et al. (2010b) could thus not be confirmed.

There is, however, a strong bias in giant stellar surveys that are used for planet searches. High-metallicity, low-gravity stars are left out from these samples, most likely due to a $B-V$ colour cut-off at 1.0 in creating the sample, which is a standard procedure for dwarf stars. Comparing dwarf stars with giant stars should thus be done with caution. This bias towards lower metallicities can also affect the frequency studies.

Regarding stellar mass, it is found that it does not play a role in the metallicity distributions of stars with planets. Massive giants (with $M_* > 1.5M_\odot$) and dwarf stars with planets have the same metallicity distribution where the planet frequency increases with metallicity. This is in line with the recent results of Maldonado et al. (2013) who show that massive giants with planets are more metal-rich.

This lack of correlation with metallicity for red giants, is not easily explained. Since red giants are simply the evolutionary result of dwarf stars, one should naively expect the same behaviour for both stellar groups. Different scenarios have been put forward, like planet engulfment, pollution, formation by gravitational instability, etc to explain the difference between dwarf planet hosts and evolved planet hosts. However, all these scenarios can easily be discarded also. A clear explanation on this issue is still being investigated. It must be noted though that the sample of evolved hosts is 4 times smaller than the dwarf sample and all analyses are thus based on low number statistics.

6.2 Precise parameters

Statistical methods are powerful tools to practice modern day astronomy. However, the significance of the results is subject to the accuracy and precision of the used parameters. Precise stellar parameters are thus key in performing statistical analyses to investigate possible correlations between stellar and planetary parameters. Since the main subject of my PhD thesis is planet frequency as a function of stellar parameters, I have focused part of my research on the derivation of precise stellar parameters. More details on the methods for parameter derivation and the physics behind it are described in section 1.3.

The method described in section 1.3 makes use of a list of iron lines (both Fe I and Fe II). Since these lines, and especially the Fe II lines, are affected by changes in the temperature and surface gravity, it is important to use an appropriate list of lines for each type of star. For dwarf stars, I use the line list from Sousa et al. (2008) and Tsantaki et al. (2013) for stars hotter and cooler than 5200 K, respectively. For (sub)giant stars, I investigated if another line list would produce more precise and accurate parameters. Herefor, I used the line list

proposed by Hekker & Meléndez (2007) compiled specifically for giant stars.

The two line list sets were first tested on the well known giant star Arcturus (using a high resolution spectrum with high S/N) for which the results agreed well with each other and with literature data, confirming that they are appropriate line lists for giant stars. By applying both line list sets on the sample of 71 evolved planet hosts (see Chapter 4), I found that surface gravity, microturbulence, and metallicity are not significantly different when using different line list sets. All values compare well with each other and other spectroscopic results in the literature. Temperatures agree very well for stars hotter than 4700 K. For lower temperature stars, however, the differences start to grow a bit larger. Since giant stars tend to be cooler than dwarf stars, this should be taken into account for the coolest giants. The remarkable agreement with literature data and each other for the bulk of the sample made me conclude that the same lists can be used for dwarf stars and evolved stars. The line list set from Sousa et al. (2008) and Tsantaki et al. (2013) is preferred since it contains much more lines than the line list of Hekker & Meléndez (2007) and thus produces more precise parameters.

The spectroscopic method I use to derive parameters delivers very precise and accurate parameters (see e.g. Sousa et al. 2011; Neves et al. 2012; Tsantaki et al. 2013; Santos et al. 2013; Mortier et al. 2013b). However, the surface gravity is not that well constrained. Using spectral synthesis instead of spectral line analysis will also result in badly constrained surface gravities (e.g. Torres et al. 2012). Since surface gravity is an important parameter for the determination of stellar mass and radius, this issue needs investigating. Luckily, the surface gravity can be determined independently by using asteroseismology (Huber et al. 2013) or photometric transits, in the case of a planet hosts. I studied the latter method using a large sample of 90 transit hosts, as described in Chapter 5.

Using the stellar density from the transit light curve and the spectroscopically derived temperature and metallicity, surface gravities were rederived. A large discrepancy was found between the photometric and spectroscopic surface gravities. In general, the photometric ones match best with literature data, where most values were also based on a photometric approach. As a side note, I would like to point out that Huber et al. (2013) found that surface gravities derived photometrically, using the planetary transit, are in half of the cases in significant disagreement with the values derived from asteroseismology. They argue that the reason for this lies in the systematic mismodeling of the impact parameter or the disregard of the eccentricity of the planetary orbit. According to Huber et al. (2013), the differences are greater than 50% for more than half of the studied stars.

I also studied the effect of the surface gravity on chemical abundances, stellar mass, and stellar radius and found that the chemical abundances of atoms (using 12 refractory elements and lithium) are not affected by using different surface gravities. Abundances of ions (using 3 ions of refractory elements), however, are slightly affected, as predicted already theoretically by

Gray (2008). The mass determination is also not strongly affected by using different surface gravities. Stellar radii calculated with the spectroscopic and photometric surface gravity, on the other hand, show a large spread (with differencecs up to 1.0 $R_{\odot}$). Planetary radii and masses are thus affected by these different gravity values. In the sample of 90 transit hosts, 8 planets show differences in their planet parameters of more than 2 sigma compared to literature data, when using the photometric values. This can influence theoretical composition models for these extrasolar planets.

6.3 Future work

The research I have been doing during my PhD is far from finished and there are still many open questions and interesting studies that can be performed to continue this work. I will here only name a few research opportunities that I find interesting to pursue next.

Surface gravity

As shown in Mortier et al. (2013c), there are discrepancies in the determination of the surface gravity. I've showed that spectroscopic surface gravities are significantly different than the ones calculated through the precise stellar density from the transit light curve. Furthermore Huber et al. (2013) show that stellar densities derived from asteroseismic data and from the transit light curve can differ as well, especially for systems where the spin-orbit misalignment is large. The differences in surface gravity for their sample are greater than 50% for more than half of the sample.

Surface gravity is an important stellar parameters for the determination of stellar mass and radius, and thus planetary mass and radius. Additionally, spectroscopically, surface gravity is constrained together with the effective temperature and metallicity. A wrong determination of the gravity may thus have an impact on the determination of the other atmospheric parameters of the star.

This issue can be investigated in several ways. By fixing the surface gravity in the analysis with MOOG, the effect on the other atmospheric parameters can be seen. Using different methods to determine temperature (e.g. the InfraRed Flux Method or TMCalc) and surface gravity can bring to light possible dependences of the atmospheric parameters to the wrong determination of the surface gravity. If possible, corrections can be applied to factor in these dependences.

Extend and homogenize planet samples

Any analysis of planet host samples requires homogeneously derived and precise stellar parameters. Only then can one truely draw conclusion from possible correlations (see e.g. Mortier et al. 2013a,b). The catalogue, SWEETCat, created and maintained by my colleagues and me (Santos et al. 2013) collects all planet hosts. We strive for homogeneously derived parameters for all these planet hosts. Currently, about 30% of the listed planet hosts show literature data. This is mostly due to the fact that our team has no access to high-resolution spectra of these stars.

Continuing the effort of gathering high-resolution spectra for planet hosts and derive the stellar parameters, is a work that will never end as new planets are discovered on a regular basis. New spectrographs like HARPS-North or ESPRESSO, will help in getting high-resolution spectra even for the fainter targets.

Additionally, the planet characteristics can be refined. Upcoming missions like Gaia (Perryman et al. 2001) or ESPRESSO (Pepe et al. 2010) will provide high-quality data of current and new planets from spectroscopy, photometry and astrometry. The combination of these three datasets will prove to be invaluable for the precise characterization of stars and their planets. Combining the radial-velocity technique with either the photometric-transit technique or the astrometry technique enables one to characterize the stars and planets completely whereas using just one method always results in unknown parameters.

Narrowing down planet formation theories

The main part of the work in this thesis was focused on the correlation between giant planet frequency and metallicity. I showed in Mortier et al. (2012, 2013a) that there can still be a correlation with stellar mass. The exact dependence for metal-poor stars is also still unclear. Furthermore, Adibekyan et al. (2012a) showed that metal-poor stars with planets are enhanced in aplha-elements. With more planets available and better data of the planet hosts, the connection between planet frequency and stellar parameters can be explored more deeply.

Other interesting correlations between stellar parameters and planetary parameters can also be investigated. Relating these results with the expected results from theoretical modelling will shed lights on the theories of planet formation and evolution and help in the understanding of the Universe.

Bibliography

Adibekyan, V. Z., Delgado Mena, E., Sousa, S. G., et al. 2012a, A&A, 547, A36

Adibekyan, V. Z., Sousa, S. G., Santos, N. C., et al. 2012b, A&A, 545, A32

Alibert, Y., Mordasini, C., & Benz, W. 2004, A&A, 417, L25

Alibert, Y., Mordasini, C., & Benz, W. 2011, A&A, 526, A63

Alibert, Y., Mordasini, C., Benz, W., & Winisdoerffer, C. 2005, A&A, 434, 343

Angel, J. R. P. 1994, Nature, 368, 203

Bakos, G. Á., Hartman, J. D., Torres, G., et al. 2012, AJ, 144, 19

Ballard, S., Fabrycky, D., Fressin, F., et al. 2011, ApJ, 743, 200

Baranne, A., Queloz, D., Mayor, M., et al. 1996, A&AS, 119, 373

Baruteau, C., Meru, F., & Paardekooper, S.-J. 2011, MNRAS, 416, 1971

Bary, J. S., Weintraub, D. A., & Kastner, J. H. 2003, ApJ, 586, 1136

Batalha, N. M., Rowe, J. F., Bryson, S. T., et al. 2013, ApJS, 204, 24

Beaugé, C. & Nesvorný, D. 2012, ApJ, 751, 119

Benedict, G. F., McArthur, B. E., Bean, J. L., et al. 2010, AJ, 139, 1844

Benedict, G. F., McArthur, B. E., Forveille, T., et al. 2002, ApJ, 581, L115

Bertelli, G., Girardi, L., Marigo, P., & Nasi, E. 2008, A&A, 484, 815

Boisse, I., Bouchy, F., Hébrard, G., et al. 2011, A&A, 528, A4

Bonfils, X., Mayor, M., Delfosse, X., et al. 2007, A&A, 474, 293

Boss, A. P. 1997, Science, 276, 1836

Boss, A. P. 2002, ApJ, 567, L149

Boss, A. P. 2006, ApJ, 643, 501

Bouchy, F., Pepe, F., & Queloz, D. 2001, A&A, 374, 733

Bouchy, F., Udry, S., Mayor, M., et al. 2005, A&A, 444, L15

Bouvier, J., Forestini, M., & Allain, S. 1997, A&A, 326, 1023

Bowler, B. P., Johnson, J. A., Marcy, G. W., et al. 2010, ApJ, 709, 396

Brauer, F., Dullemond, C. P., & Henning, T. 2008, A&A, 480, 859

Bressan, A., Marigo, P., Girardi, L., et al. 2012, MNRAS, 427, 127

Brogi, M., Keller, C. U., de Juan Ovelar, M., et al. 2012, A&A, 545, L5

Brown, T. M. 2003, ApJ, 593, L125

Bruntt, H., Bedding, T. R., Quirion, P.-O., et al. 2010, MNRAS, 405, 1907

Buchhave, L. A., Latham, D. W., Johansen, A., et al. 2012, Nature, 486, 375

Butler, R. P., Johnson, J. A., Marcy, G. W., et al. 2006, PASP, 118, 1685

Butler, R. P., Marcy, G. W., Fischer, D. A., et al. 1999, ApJ, 526, 916

Butler, R. P., Marcy, G. W., Williams, E., Hauser, H., & Shirts, P. 1997, ApJ, 474, L115

Cai, K., Durisen, R. H., Michael, S., et al. 2006, ApJ, 636, L149

Carson, J., Thalmann, C., Janson, M., et al. 2013, ApJ, 763, L32

Casagrande, L., Portinari, L., & Flynn, C. 2006, MNRAS, 373, 13

Castelli, F. 2005, Memorie della Societa Astronomica Italiana Supplementi, 8, 44

Chambers, J. 2006, Icarus, 180, 496

Chambers, J. 2011, Terrestrial Planet Formation, ed. S. Seager, 297–317

Chauvin, G., Lagrange, A.-M., Zuckerman, B., et al. 2005, A&A, 438, L29

Claret, A. 2004, A&A, 428, 1001

Cochran, W. D., Endl, M., Wittenmyer, R. A., & Bean, J. L. 2007, ApJ, 665, 1407

Cochran, W. D., Hatzes, A. P., Butler, R. P., & Marcy, G. W. 1997, ApJ, 483, 457

Cumming, A., Marcy, G. W., & Butler, R. P. 1999, ApJ, 526, 890

da Silva, L., Girardi, L., Pasquini, L., et al. 2006, A&A, 458, 609

D'Angelo, G., Durisen, R. H., & Lissauer, J. J. 2011, Giant Planet Formation, ed. S. Seager, 319–346

Delgado Mena et al., E. 2013, submitted to A&A

Delorme, P., Gagné, J., Girard, J. H., et al. 2013, A&A, 553, L5

Dullemond, C. P. & Dominik, C. 2008, A&A, 487, 205

Dumusque, X., Pepe, F., Lovis, C., et al. 2012, Nature, 491, 207

Dumusque, X., Udry, S., Lovis, C., Santos, N. C., & Monteiro, M. J. P. F. G. 2011, A&A, 525, A140

Endl, M., Robertson, P., Cochran, W. D., et al. 2012, ApJ, 759, 19

Fabrycky, D. & Tremaine, S. 2007, ApJ, 669, 1298

Figueira, P., Santos, N. C., Pepe, F., Lovis, C., & Nardetto, N. 2013, A&A, 557, A93

Fischer, D. A., Laughlin, G., Butler, P., et al. 2005, ApJ, 620, 481

Fischer, D. A., Marcy, G. W., Butler, R. P., Vogt, S. S., & Apps, K. 1999, PASP, 111, 50

Fischer, D. A. & Valenti, J. 2005, ApJ, 622, 1102

Flower, P. J. 1996, ApJ, 469, 355

Fressin, F., Guillot, T., Morello, V., & Pont, F. 2007, A&A, 475, 729

Fressin, F., Torres, G., Charbonneau, D., et al. 2013, ApJ, 766, 81

Fressin, F., Torres, G., Rowe, J. F., et al. 2012, Nature, 482, 195

Fuhrmann, K., Pfeiffer, M. J., & Bernkopf, J. 1997, A&A, 326, 1081

Ghezzi, L., Cunha, K., Schuler, S. C., & Smith, V. V. 2010a, ApJ, 725, 721

Ghezzi, L., Cunha, K., Smith, V. V., et al. 2010b, ApJ, 720, 1290

Gilliland, R. L. & Baliunas, S. L. 1987, ApJ, 314, 766

Goldreich, P. & Ward, W. R. 1973, ApJ, 183, 1051

Gomes da Silva, J., Santos, N. C., Bonfils, X., et al. 2012, A&A, 541, A9

Gonzalez, G. 1997, MNRAS, 285, 403

Goździewski, K. & Maciejewski, A. J. 2001, ApJ, 563, L81

Gray, D. F. 2008, The Observation and Analysis of Stellar Photospheres

Gustafsson, B., Edvardsson, B., Eriksson, K., et al. 2008, A&A, 486, 951

Haisch, Jr., K. E., Lada, E. A., & Lada, C. J. 2001, ApJ, 553, L153

Han, C., Udalski, A., Choi, J.-Y., et al. 2013, ApJ, 762, L28

Han, I., Black, D. C., & Gatewood, G. 2001, ApJ, 548, L57

Hartman, J. D., Bakos, G. Á., Béky, B., et al. 2012, AJ, 144, 139

Hekker, S. & Meléndez, J. 2007, A&A, 475, 1003

Hellier, C., Anderson, D. R., Collier Cameron, A., et al. 2013, ArXiv e-prints

Ho, S. & Turner, E. L. 2011, ApJ, 739, 26

Hogerheijde, M. 1998, PhD thesis, Department of Astronomy, University of California, Campbell Hall, Berkeley, CA 94720, USA ¡EMAIL¿michiel@strw.leidenuniv.nl¡/EMAIL¿

Huber, D., Chaplin, W. J., Christensen-Dalsgaard, J., et al. 2013, ApJ, 767, 127

Ida, S. & Lin, D. N. C. 2004, ApJ, 616, 567

Ida, S. & Lin, D. N. C. 2005, ApJ, 626, 1045

Ida, S. & Makino, J. 1993, Icarus, 106, 210

Johnson, J. A., Aller, K. M., Howard, A. W., & Crepp, J. R. 2010, PASP, 122, 905

Johnson, J. A., Morton, T. D., & Wright, J. T. 2013, ApJ, 763, 53

Kalas, P., Graham, J. R., Fitzgerald, M. P., & Clampin, M. 2013, ApJ, 775, 56

Kass, R. E. & Raftery, A. E. 1995, Journal of the American Statistical Association, 90, pp. 773

Kokubo, E. & Ida, S. 1998, Icarus, 131, 171

Kretke, K. A. & Lin, D. N. C. 2007, ApJ, 664, L55

Kurucz, R. 1993, ATLAS9 Stellar Atmosphere Programs and 2 km/s grid. Kurucz CD-ROM No. 13. Cambridge, Mass.: Smithsonian Astrophysical Observatory, 1993., 13

Lagrange, A.-M., Bonnefoy, M., Chauvin, G., et al. 2010, Science, 329, 57

Laws, C., Gonzalez, G., Walker, K. M., et al. 2003, AJ, 125, 2664

Léger, A., Rouan, D., Schneider, J., et al. 2009, A&A, 506, 287

Lin, D. N. C., Bodenheimer, P., & Richardson, D. C. 1996, Nature, 380, 606

Lloyd, J. P. 2011, ApJ, 739, L49

Lloyd, J. P. 2013, ApJ, 774, L2

Lopez, S. & Jenkins, J. S. 2012, ApJ, 756, 177

Lovis, C. & Fischer, D. 2011, Radial Velocity Techniques for Exoplanets, ed. S. Seager, 27–53

Lovis, C. & Mayor, M. 2007, A&A, 472, 657

Luhman, K. L. 2012, ARA&A, 50, 65

Maldonado, J., Villaver, E., & Eiroa, C. 2013, A&A, 554, A84

Marcy, G. W., Butler, R. P., Fischer, D., et al. 2001, ApJ, 556, 296

Marley, M. S., Fortney, J. J., Hubickyj, O., Bodenheimer, P., & Lissauer, J. J. 2007, ApJ, 655, 541

Marois, C., Macintosh, B., Barman, T., et al. 2008, Science, 322, 1348

Matsuo, T., Shibai, H., Ootsubo, T., & Tamura, M. 2007, ApJ, 662, 1282

Matzner, C. D. & Levin, Y. 2005, ApJ, 628, 817

Mayer, L., Quinn, T., Wadsley, J., & Stadel, J. 2002, Science, 298, 1756

Mayor, M., Marmier, M., Lovis, C., et al. 2011, ArXiv e-prints, 1109.2497

Mayor, M. & Queloz, D. 1995, Nature, 378, 355

Meru, F. & Bate, M. R. 2010, MNRAS, 406, 2279

Montalto, M., Gregorio, J., Boué, G., et al. 2012, MNRAS, 427, 2757

Morbidelli, A., Lunine, J. I., O'Brien, D. P., Raymond, S. N., & Walsh, K. J. 2012, Annual Review of Earth and Planetary Sciences, 40, 251

Mordasini, C. 2013, ArXiv e-prints

Mordasini, C., Alibert, Y., Benz, W., Klahr, H., & Henning, T. 2012a, A&A, 541, A97

Mordasini, C., Alibert, Y., Benz, W., & Naef, D. 2009, A&A, 501, 1161

Mordasini, C., Alibert, Y., Georgy, C., et al. 2012b, A&A, 547, A112

Mortier, A., Santos, N. C., Sousa, S., et al. 2013a, A&A, 551, A112

Mortier, A., Santos, N. C., Sousa, S. G., et al. 2013b, A&A, 557, A70

Mortier, A., Santos, N. C., Sousa, S. G., et al. 2013c, A&A, 558, A106

Mortier, A., Santos, N. C., Sozzetti, A., et al. 2012, A&A, 543, A45

Morton, T. D. & Johnson, J. A. 2011, ApJ, 738, 170

Moutou, C., Deleuil, M., Guillot, T., et al. 2013, ArXiv e-prints

Moutou, C., Hébrard, G., Bouchy, F., et al. 2009, A&A, 498, L5

Naef, D., Mayor, M., Lo Curto, G., et al. 2010, A&A, 523, A15

Nardetto, N., Stoekl, A., Bersier, D., & Barnes, T. G. 2008, A&A, 489, 1255

Neves, V., Bonfils, X., Santos, N. C., et al. 2012, A&A, 538, A25

Oshagh, M., Boisse, I., Boué, G., et al. 2013, A&A, 549, A35

Pasquini, L., Döllinger, M. P., Weiss, A., et al. 2007, A&A, 473, 979

Pepe, F., Mayor, M., Galland, F., et al. 2002a, A&A, 388, 632

Pepe, F., Mayor, M., Rupprecht, G., et al. 2002b, The Messenger, 110, 9

Pepe, F. A., Cristiani, S., Rebolo Lopez, R., et al. 2010, in Society of Photo-Optical Instrumentation Engineers (SPIE) Conference Series, Vol. 7735, Society of Photo-Optical Instrumentation Engineers (SPIE) Conference Series

Perryman, M. A. C., de Boer, K. S., Gilmore, G., et al. 2001, A&A, 369, 339

Pierens, A. & Nelson, R. P. 2013, A&A, 556, A134

Pollack, J. B., Hubickyj, O., Bodenheimer, P., et al. 1996, Icarus, 124, 62

Press, W. H., Teukolsky, S. A., Vetterling, W. T., & Flannery, B. P. 1992, Numerical recipes in FORTRAN. The art of scientific computing

Queloz, D., Henry, G. W., Sivan, J. P., et al. 2001, A&A, 379, 279

Queloz, D., Mayor, M., Naef, D., et al. 2000, in From Extrasolar Planets to Cosmology: The VLT Opening Symposium, ed. J. Bergeron & A. Renzini, 548

Rafikov, R. R. 2005, ApJ, 621, L69

Recio-Blanco, A., Bijaoui, A., & de Laverny, P. 2006, MNRAS, 370, 141

Reffert, S. & Quirrenbach, A. 2011, A&A, 527, A140

Rice, W. K. M. & Armitage, P. J. 2003, ApJ, 598, L55

Robertson, H. P. 1937, MNRAS, 97, 423

Robertson, P., Endl, M., Cochran, W. D., et al. 2012, ApJ, 749, 39

Rogers, P. D. & Wadsley, J. 2012, MNRAS, 423, 1896

Safronov, V. S. & Zvjagina, E. V. 1969, Icarus, 10, 109

Santerne, A., Díaz, R. F., Moutou, C., et al. 2012, A&A, 545, A76

Santos, N. C., Israelian, G., & Mayor, M. 2001, A&A, 373, 1019

Santos, N. C., Israelian, G., & Mayor, M. 2004, A&A, 415, 1153

Santos, N. C., Mayor, M., Bonfils, X., et al. 2011, A&A, 526, A112+

Santos, N. C., Sousa, S. G., Mortier, A., et al. 2013, A&A, 556, A150

Scargle, J. D. 1982, ApJ, 263, 835

Schneider, J., Dedieu, C., Le Sidaner, P., Savalle, R., & Zolotukhin, I. 2011, A&A, 532, A79

Shu, F. H., Adams, F. C., & Lizano, S. 1987, ARA&A, 25, 23

Sing, D. K., Désert, J.-M., Lecavelier Des Etangs, A., et al. 2009, A&A, 505, 891

Sneden, C. A. 1973, PhD thesis, The University of Texas at Austin.

Sousa, S. G., Santos, N. C., Israelian, G., Mayor, M., & Monteiro, M. J. P. F. G. 2007, A&A, 469, 783

Sousa, S. G., Santos, N. C., Israelian, G., Mayor, M., & Udry, S. 2011, A&A, 533, A141+

Sousa, S. G., Santos, N. C., Mayor, M., et al. 2008, A&A, 487, 373

Southworth, J. 2008, MNRAS, 386, 1644

Sozzetti, A. 2010, in EAS Publications Series, Vol. 42, EAS Publications Series, ed. K. Gożdziewski, A. Niedzielski, & J. Schneider, 55–77

Sozzetti, A., Torres, G., Latham, D. W., et al. 2009, ApJ, 697, 544

Sumi, T., Bennett, D. P., Bond, I. A., et al. 2010, ApJ, 710, 1641

Supulver, K. D., Bridges, F. G., Tiscareno, S., Lievore, J., & Lin, D. N. C. 1997, Icarus, 129, 539

Swain, M., Deroo, P., Tinetti, G., et al. 2013, Icarus, 225, 432

Szűcs, L., Apai, D., Pascucci, I., & Dullemond, C. P. 2010, ApJ, 720, 1668

Takeda, Y., Sato, B., & Murata, D. 2008, PASJ, 60, 781

Torres, G., Andersen, J., & Giménez, A. 2010, A&A Rev., 18, 67

Torres, G., Fischer, D. A., Sozzetti, A., et al. 2012, ApJ, 757, 161

Traub, W. A. & Oppenheimer, B. R. 2011, Direct Imaging of Exoplanets, ed. S. Seager, 111–156

Triaud, A. H. M. J., Anderson, D. R., Collier Cameron, A., et al. 2013, A&A, 551, A80

Triaud, A. H. M. J., Collier Cameron, A., Queloz, D., et al. 2010, A&A, 524, A25

Tsantaki, M., Sousa, S. G., Adibekyan, V. Z., et al. 2013, A&A, 555, A150

Udry, S. & Santos, N. C. 2007, ARA&A, 45, 397

Valenti, J. A. & Piskunov, N. 1996, A&AS, 118, 595

van Leeuwen, F. 2007, A&A, 474, 653

Vogt, S. S., Allen, S. L., Bigelow, B. C., et al. 1994, in Society of Photo-Optical Instrumentation Engineers (SPIE) Conference Series, Vol. 2198, Society of Photo-Optical Instrumentation Engineers (SPIE) Conference Series, ed. D. L. Crawford & E. R. Craine, 362–+

Weidenschilling, S. J. 1977, MNRAS, 180, 57

Weidenschilling, S. J. 1997, Icarus, 127, 290

Wetherill, G. W. & Stewart, G. R. 1989, Icarus, 77, 330

Williams, J. P. & Cieza, L. A. 2011, ARA&A, 49, 67

Winn, J. N. 2011, Exoplanet Transits and Occultations, ed. S. Seager, 55–77

Wolszczan, A. & Frail, D. A. 1992, Nature, 355, 145

Zechmeister, M. & Kürster, M. 2009, A&A, 496, 577

Zieliński, P., Niedzielski, A., Adamów, M., & Wolszczan, A. 2010, in EAS Publications Series, Vol. 42, EAS Publications Series, ed. K. Gożdziewski, A. Niedzielski, & J. Schneider, 201–205

Appendix A

Methods used for this work

This work has made use of several techniques that I will detail here.

A.1 General Lomb-Scargle periodogram

As explained in 1.1, exoplanets can be detected by using radial velocity data of a star. A planet will create a periodic signal in the data. This periodic signal can be found with the help of frequency analysis. When data is evenly sampled, a frequency analysis is relatively simple (using a Fourier transform). However, in astronomy, and thus also in radial velocity data, the measurements are unevenly sampled. Another method must thus be applied.

The Lomb-Scargle periodogram (Scargle 1982) is therefore used for the frequency analysis of unevenly sampled data (time series). This method is equivalent to a least-squares fitting of sine waves (also called a modified Fourier analysis). However, the original concept of the periodogram did not take into account measurement errors. By using weighted sums, this problem was solved by Gilliland & Baliunas (1987). Additionally, the data was assumed to have no offset (the mean of the data and the mean of the sinewave were both assumed zero). Zechmeister & Kürster (2009) generalized the concept of the periodogram to fit a full sine wave fit, including an offset and weights: the general Lomb-Scargle periodogram (GLS). Thanks to this generalisation, periodic signals coming from planets on eccentric orbits rather than circular orbits, can also be explored.

In a GLS periodogram, a power is plotted as a function of frequency (or period). This power measures how much a fit to the measurements improves by using a sinusoid instead of a constant. Peaks in a periodogram can thus be signs of periodic signals in the data with (or close to) that particular frequency. The power is calculated as:

$$p(\omega) = \frac{\chi^2_{cte} - \chi^2_{sin}(\omega)}{\chi^2_{cte}}$$

where χ^2_{cte} and χ^2_{sin} are the chi-squared values of a constant and a sinusoidal fit, respectively.

Suppose you have measurements y_i with errors σ_i, measured on times t_i. The constant that is used to compare with sinusoidal fits is the weighted mean of the data $\bar{y}$. As weights w_i, the normalized errors are used. Measurements with small error bars will be more important for the fit than data with large error bars.

$$\bar{y} = \sum w_i y_i \qquad \text{with } w_i = \frac{1}{\sigma_i^2 \sum(1/\sigma_i^2)}$$

For the sinusoidal, there are two options. If you consider the periodic signal in the data to come from a planet on a circular orbit, the fitted model will be described by:

$$y(t) = K\cos(\omega t - \varphi) + \gamma = a\cos\omega t + b\sin\omega t + c$$

with $a = K\cos\varphi$, $b = K\sin\varphi$ and $c = \gamma$. Here, K is the RV amplitude, φ the phase, γ the constant system RV and ω the frequency, which is related to the period P: $\omega = \frac{2\pi}{P}$. If an eccentric (Keplerian) orbit is assumed for the planet, a similar sine function will be fitted:

$$y(t) = a\cos\nu(t) + b\sin\nu(t) + c$$

with $a = K\cos\varpi$, $b = -K\sin\varpi$ and $c = Ke\cos\varpi + \gamma$. Here, K is the RV amplitude, e the eccentricity, ϖ the longitude of periastron, γ the constant system RV and $\nu(t)$ the true anomaly. This true anomaly can be found by

$$\tan\frac{\nu}{2} = \sqrt{\frac{1+e}{1-e}}\tan\frac{E}{2}$$

with E the eccentric anomaly which in turn can be found by solving Kepler's equation:

$$E - e\sin E = 2\pi\frac{t - T_0}{P}$$

with P the period and T_0 the time of periastron passage.

The chi-squared values used in the calculation of the periodogram power are then expressed as

$$\chi^2_{sin}(\omega) = \sum \frac{[y_i - y(t_i)]^2}{\sigma_i^2} \qquad \chi^2_{cte} = \sum \frac{[y_i - \bar{y}]^2}{\sigma_i^2}$$

A.2 Bootstrapping

One important part of statistical analysis of data is quantifying the significance of the results. In the case of a GLS periodogram, for example, it is not just important to find peaks in the powerspectrum, but also to understand how significant this peak is and thus how probable the periodic signal in the data. Herefor, I have used a bootstrapping method, which is a widely used resampling method.

Multiple time series of radial velocities (with their error bars) are made by shuffling the original radial velocities while preserving the original times. This shuffling is done with repetition. On each of these shuffled series, a GLS is performed to determine the highest peak in the periodogram. These peaks can then be used to determine the percentage of bootstrapped periodograms with maximum peaks above the one observed in the GLS from the real data and thus determine a probability that the real peak comes from a planetary signal and not just noise. Obviously, it is important to have enough shuffled time series (like 10^4 depending on the probability precision you want to achieve).

The same procedure also allows us to derive a false alarm probability (FAP) level in the data. This is the power a peak should have in order to have a FAP% probability that the peak is created by chance instead of a planetary signal. Using this FAP level, planetary detection limits can be calculated, inherent to the data. For each frequency (period), a fake planetary signal can be added to the data, considering the data as noise. With these new time series, a GLS can be performed. The mass of the fake planet (and thus the amplitude of the periodic signal) can be raised until the peak in the data reaches the FAP level. This allows you to determine detection limits in the data based on planetary mass and period.

A.3 Binomial distribution

Planet frequencies in this work are calculated either through a parametric approach (see section A.4) or through a binning approach. The latter makes use of a binomial distribution. This is a discrete probability distribution of the number of successes n (in this case the existence of a planet) in N independent experiments, each with a probability f_p. This distribution

is a special case of the Poisson distribution. The probability of finding n planet detections in a sample of N stars can thus be calculated as a function of the true planet frequency f_p:

$$P(f_p; n, N) = \frac{N!}{n!(N-n)!} f_p^n (1-f_p)^{N-n} \quad ,$$

This distribution is asymmetric. To compute error bars on the probability, one can measure the range in f_p that covers 68% of the integrated probability function (or does not cover 16% at each end of the distribution). This is equivalent to the 1-sigma error bars for a Gaussian distribution.

A.4 Bayes factors

Another way of calculating planet frequencies is through a parametric approach. A functional form $f([Fe/H], M)$ to express planet frequency as a function of metallicity and/or stellar mass is chosen with a set of parameters X. For the data d, a binary result is valid: a star does have a detectable planet or it does not. Then, Bayes theorem says that

$$P(X|d)P(d) = P(d|X)P(X)$$

In this case $P(d)$ is always a constant, so that term can be left out. Now, assume you have N stars in your sample of which H stars are orbited by a planet. Then you can write $P(d|X)$ as

$$P(d|X) = \prod_i^N P(d_i|X)$$

For a planet host it holds that $P(d_i|X) = f([Fe/H]_i, M_i)$ with $[Fe/H]_i$ and M_i the metallicity and mass of that star, while for a star without a planet, the probability will be $1 - f([Fe/H]_i, M_i)$. To make the calculations easier, the equations can be converted to log-space:

$$\begin{aligned} L = \log P(X|d) &\propto \log P(d|X) + \log P(X) \\ &= \sum_i^H \log f(M_i, F_i) + \sum_j^{N-H} \log[1 - f(M_j, F_j)] + \log P(X) \end{aligned}$$

Since the mass and metallicity of a star are also measured quantities, they are in fact described by a probability distribution function (pdf) $p([Fe/H]_i, M_i)$. That means that the planet frequency function for one star is actually calculated by

$$f([Fe/H]_i, M_i) = \int\int p([Fe/H]_i, M_i) f([Fe/H], M) d[Fe/H] dM$$

This pdf can be approximated by a product of Gaussians with means $([Fe/H]_i, M_i)$ and standard deviations $(\sigma_{[Fe/H]_i}, \sigma_{M_i})$:

$$p([Fe/H]_i, M_i) = \exp\left[-\frac{(M - M_i)^2}{2\sigma_{M_i}^2} - \frac{([Fe/H] - [Fe/H]_i)^2}{2\sigma_{[Fe/H]_i}^2}\right]$$

The only probability left to determine now is the probability of the parameters (prior probability) $P(X)$. This value depends on the assumptions. The most easy assumption is a uniform prior, where each set of parameters has the same chance of happening. In this specific case $P(X)$ would be a constant and thus left out of the equation. Other priors can be chosen obviously.

To find the best set of parameters X for a given functional form, L needs to be maximized. This maximum can be found by numerically evaluating L. Minimizing algorithms are not preferred as the parameterspace usually has many local maxima and an initial guess is not always available.

Different functional forms can be evaluated by using the Bayesfactor as described in Kass & Raftery (1995). When testing two functional forms f and g, the Bayesfactor is expressed as

$$B_{fg} = \frac{P(d|f)}{P(d|g)} = \frac{\int P(d|X_f) P(X_f) dX_f}{\int P(d|X_g) P(X_g) dX_g}$$

with X_f, X_g the set of parameters for f and g, respectively. The integration limits are the limits of the parameterspace. In the case of a uniform parameter distribution in a discrete parameter space (e.g. when you use a grid to search for the maximum L), this probability can be calculated as

$$P(d|f) = \frac{\sum P(d|X)}{length(X)}$$

where $length(X)$ is the amount of possible combinations of the parameters. According to Kass & Raftery (1995), the following rules apply to the Bayesfactors:

B_{fg}	Evidence in favor of f
1 to 3	Not worth more than a bare mention
3 to 20	Positive
20 to 150	Strong
>150	Very strong

Appendix B

Publications relevant to this thesis

- *'The frequency of giant planets around metal-poor stars'*

  Mortier, A.; Santos, N. C.; Sozzetti, A.; Mayor, M.; Latham, D.; Bonfils,X.; Udry, S. 2012, A&A, Volume 543, id.A45

- *'A new analysis of the WASP-3 system: no evidence for an additional companion'*

  Montalto, M., Gregorio, J., Boué, G., **Mortier A.**, et al. 2012, MNRAS Volume 427, Issue 4, pp. 2757-2771

- *'On the functional form of the metallicity-giant planet correlation'*

  Mortier, A.; Santos, N. C.; Sousa, S. G.; Israelian, G.; Mayor, M.; Udry, S. 2013, A&A, Volume 551, id.A112

- *'Deriving precise parameters for cool solar-type stars. Optimizing the iron line list'*

  Tsantaki, M., Sousa, S. G., Adibekyan, V. Z., Santos, N. C.; **Mortier, A.**; Israelian, G. 2013, A&A, Volume 555, id.A150

- *'SWEETCat: A catalogue of parameters for Stars With ExoplanETs'*

  Santos, N. C., Sousa, S. G., **Mortier, A.**, et al. 2013, A&A, Volume 556, id.A150

- *'New and updated stellar parameters for 71 evolved planet hosts. On the metallicity giant planet connection.'*

  Mortier, A.; Santos, N.C.; Sousa, S.G., et al. 2013, A&A, Volume 557, id.A70

- *'Atmospheric Parameters of 169 F, G, K and M-type Stars in the Kepler Field'*

  Molenda-Żakowicz, J., Sousa, S. G., Frasca, A., et al., including **Mortier, A.** 2013, MNRAS Volume 434, Issue 2, p.1422-1434

- *'New and updated stellar parameters for 90 transit hosts. The effect of the surface gravity.'*

  Mortier, A.; Santos, N.C.; Sousa, S.G, et al. 2013, A&A, Volume 558, id.A106

- *'Orbital and physical properties of planets and their hosts: further insights on planet formation and evolution.*

  Adibekyan, V. Zh.; Figueira, P.; Santos, N. C.; **Mortier, A.**; Mordasini, C.; Delgado Mena, E.; Sousa, S. G.; Correia, A. C. M.; and Israelian, G. 2013, accepted to A&A, arXiv preprint: 1311.2417

- *'Li depletion in solar analogues with exoplanets. Extending the sample'*

  Delgado Mena, E., Israelian, G., González Hernández, J. I., Sousa, S. G., **Mortier, A.**, et al. 2013, accepted to A&A, arXiv preprint: 1311.6414

- *'The PLATO 2.0 Mission'*

  Rauer, H.; Catala, C.; Aerts, C, et al. including **Mortier, A.** 2013, submitted to Experimental Astronomy, preprint arXiv:1310.0696

- *'On the mass estimation for FGK stars: comparison of the methods'*

  Pinheiro, F. J. G.; Fernandes, J. M.; Cunha, M. S. et al. including **Mortier, A.** 2013, submitted to MNRAS